AD

19262

UNCLASSIFIED

MOLECULAR MOTION IN ORGANOSILOXANE COMPOUNDS

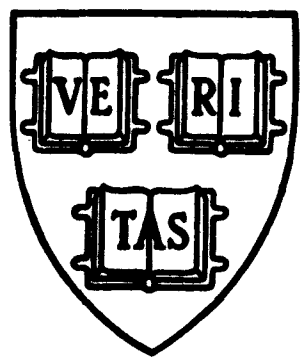

HARVARD UNIVERSITY
DEPARTMENT OF CHEMISTRY
CAMBRIDGE 38, MASSACHUSETTS

OFFICE OF NAVAL RESEARCH

Contract N5 ori-07650-NR052-278

ORGANIC DERIVATIVES OF SILICON AND GERMANIUM

FINAL REPORT:

MOLECULAR MOTION IN ORGANOSILANES AND SILICONES

Hugh G. LeClair
James C. Sternberg
Eugene G. Rochow

September 30, 1953

PREFACE

The contract terminated by the issuance of this report has helped to support two projects concerned with the structure of organosiloxanes (silicones) and the related organogermanium compounds. Progress on the organogermanium problem has been reported in the previous annual report, and later in three articles (J. Am. Chem. Soc., 74, 4363 (1952), J. Organic Chem. 18, 303 (1953), and Naturwissenschaften 40, 142 (1953).

Results on the other project, the investigation of the structure of silicones by studying molecular motion in representative organosilicon compounds, have not been published nor given in detail in the earlier reports. A complete account of the purposes, the plan of attack, the results, and the various conclusions is best obtained from the thesis presented to the faculty of the Graduate School of Arts and Sciences by Hugh G. LeClair. For this reason, the principal portions of this thesis are incorporated in this report, and a summary will be found on pages 137 to 140.

During part of the past year Dr. James C. Sternberg was associated with this project, and contributed much to the analysis of line shapes and widths. He left the project on August 1 to join the staff of instruction at Michigan State University at Lansing.

Dr. Hugh G. LeClair, who built the apparatus described herein and obtained most of the experimental data, left the project on September 1 to take a position with the Du Pont Company at Buffalo, New York.

ABSTRACT

MOLECULAR MOTION IN ORGANOSILOXANE COMPOUNDS

The question of molecular motion in the solid state of organosilicon compounds has been investigated by means of the technique of nuclear magnetic resonance absorption. The theory of the line shape and second moment to be expected for a triangular configuration of nuclei has been extended to include several types of molecular rotation or tunneling.

A radiofrequency spectrometer and permanent magnet have been constructed for use in this research. The operation of the spectrometer is described and its applicability to other types of problems has been discussed. It is found that the fixed magnetic field and variable frequency technique used in this investigation has the advantages of simplicity of operation, automatic recording of data, and avoidance of the problems associated with field regulation of electromagnets. The additions to the existing equipment which would be required for other types of investigations are mentioned, and the need for an oscillator circuit which can operate stably at very low levels is pointed out in connection with the possible investigation of pure organic compounds at low temperatures.

The results of the investigations of organosilicon compounds are as follows:

(1) The methylchlorosilanes exhibit rotation or tunneling of the methyl groups about the C-Si bond at 77°K. Both the line shapes and the second moments indicate there is also some low-frequency

motion of the molecule as a whole. The latter effect is attributed to the near-spherical symmetry of these molecules.

(2) Methoxytrichlorosilane exhibits rotation or tunneling of the methyl group about the C-O bond, but there is little or no motion of the molecule as a whole at 77°K.

(3) Hexamethyldisiloxane exhibits the usual rotation or tunneling of the methyl groups. The low second moment indicates that there is an additional motion of the molecule which may be low-frequency rotation as in the methylchlorosilanes.

(4) The cyclic siloxanes exhibit rotation of the methyl groups at 77°K. The cyclic trimer and tetramer also show an anomalous abrupt increase in the line width and second moment at higher temperatures. The cause of this unusual behavior is tentatively suggested to be due to rotational oscillation of the methyl groups of the type postulated by the Roth-Harker theory.

(5) Silicone rubber shows the usual rotation of the methyl groups at 77°K. The line width decreases abruptly at 164°K to about one-half the low temperature value, and decreases more gradually until it is essentially a liquid-like line at 210°K. The decrease in line width indicates that above 164°K the motion of the protons becomes quite rapid and random. The existence of such motion can be considered as evidence in favor of the Roth-Harker theory, but does not rule out the existence of coiling and uncoiling of the polymer chains.

It is indicated that there is reason for considerable further study of the question of molecular motion in the organosiloxanes.

TABLE OF CONTENTS

INDEX OF FIGURES

Part IV (Continued) Page

INDEX OF TABLES

I. INTRODUCTION

A. General Statement of the Problem.

The popularity of the silicones in both industrial and consumer applications can be ascribed to their physical properties, which are unique in many respects. These properties must have their explanation in terms of their underlying molecular structure; therefore the elucidation of the molecular structure and its relation to the physical properties has become a subject of considerable practical as well as theoretical importance. The purpose of this research has been to apply the method of nuclear magnetic resonance absorption to the study of some dimethylsiloxane compounds, single molecules and polymers; and specifically to investigate the nature of their internal motion, if any.

B. The Structure of the Silicones - Facts and Theories. (R1)

The dimethylsiloxane polymers (silicones) consist of silicon and oxygen atoms linked alternately into long chains, networks, or rings, with organic substituents attached to the silicon atoms in sufficient numbers to make the silicon tetravalent, as shown below.

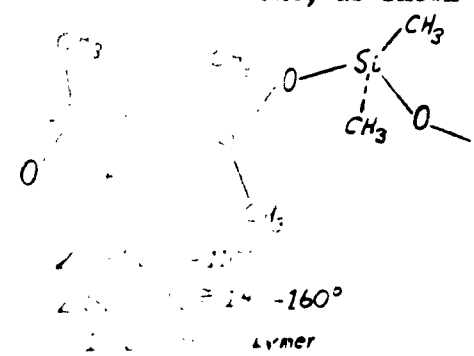

-160°

ymer

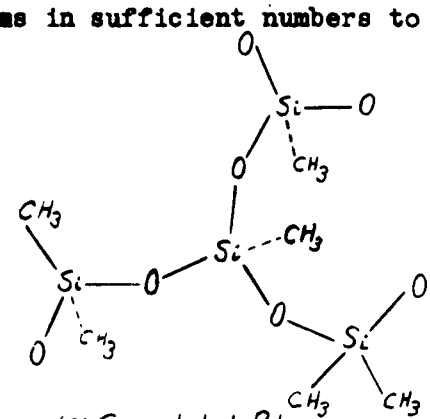

(2) Cross-linked Polymer

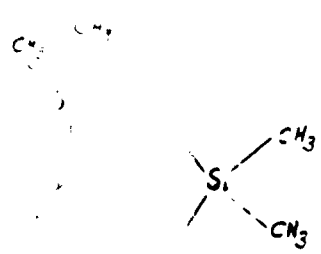

Cyc Polymer

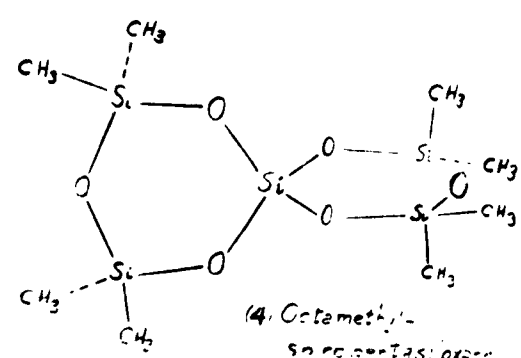

(4) Octameth

The most common substituents in the commercial polymers are methyl groups, although ethyl and phenyl groups are also used in some applications.

A consideration of the structural formulas makes certain properties of the silicones, such as their heat resistance, seem logical, especially when we recall the great strength of the silicon-oxygen bond. However, many other properties are not so readily explained; properties such as the abnormally low boiling points, high molar volumes, small temperature coefficients of viscosity, high compressibility, and the inherently low tensile strength of silicone rubber for a given molecular weight. These properties, when considered as a group, lead to one definite conclusion: that the intermolecular attraction of the silicone polymers is unusually low. Two hypotheses have been advanced to explain this behavior.

Roth and Harker, on the basis of their x-ray diffraction studies on octamethylspiropentasiloxane (formula 4, Figure 1), postulate that the Si-O-Si bond angle is easily deformed, thus allowing the methyl groups to undergo considerable motion. In the long chain polymers, this would allow considerable rotation about the Si-O bonds. The methyl groups would then occupy an effective volume much larger than their actual volume, their rapid motion preventing the close approach of neighboring molecules, and thereby decreasing the intermolecular attraction The easy deformation of the Si-O-Si bond angle is attributed to the high ionic character of the Si-O bond (51% by electronegativity values or the infrared spectra (R1, p. 113-4)) which would result in a decrease in the directional character of the bond. Since this hypothesis considers the presence of siloxane linkages to be the fundamental cause of the low intermolecular attraction, it is significant that replacement of the oxygen atoms by $-CH_2-$ groups changes the properties of the resulting substances (silmethylenes) towards those expected for pure organic compounds (B1, S1).

The theory advanced by Pauling (P1) is that the silicone chains are able to coil and uncoil as the temperature decreases or increases. At low temperatures, the molecules are tightly coiled into spheres, and there is little interference to flow. As the temperature is increased the chains begin to uncoil and snarl, and the resultant interference to flow will at least partially compensate for the effect of increased thermal agitation.

Fox, Taylor, and Zisman (F1) have used this hypothesis to explain the results of their studies of thin silicone films on water. They conclude that the chains are able to coil and uncoil reversibly with changes in temperature, and that the coils will contain six to seven - $(CH_3)_2SiO$ - units per turn. This agrees with the unit of flow deduced from viscosity measurements (R1, p.111-2). They conclude that the compactness of the coils will be limited by steric hindrance, so that the methyl silicones will have the most compact chains. Their explanation of the ease with which the silicone chains coil is also on steric grounds. They feel that the larger size of the Si atom compared to carbon facilitates the coiling process.

Both these theories have been subjected to some criticism. Pauling has pointed out that there is reason to doubt Roth and Harker's interpretation of their x-ray diffraction studies mentioned above. He states (P2):

"Roth and Harker carried out their calculations with use for the methyl group of the x-ray scattering factor for the fluorine atom...It has been found that the scattering factor for the carbon atom, as given by theoretical calculations, serves well for the carbon atom in the methyl group, except that a small correction is needed at very small diffraction angles. The scattering factor for the fluorine atom is between 1.5 and 2 times as great as that for the carbon atom, and it is accordingly not surprising that Roth and Harker were unable to get satisfactory agreement between observed and calculated intensities without making some

additional correction. The correction that they introduced was that of using a temperature factor corresponding to an abnormally great libration of a methyl group. This temperature factor cuts down the scattering factor for fluorine to approximately the correct value for the carbon atom. In other words, the electron distribution for a fluorine atom with a large temperature coefficient is just about correct for a methyl group with a normal temperature coefficient.....

"The foregoing statements would not, or course, be justified if Roth and Harker had been required to assign an abnormal motion to the methyl group only in the transverse directions, with a normal temperature coefficient in the directions along the bonds. However, they themselves state (R3) 'Within the limits of the available data, the correction could probably be represented as a specific temperature factor applied to the CH_3 groups, that is, exp $(-B_{CH_3}$ $(\sin \theta/\lambda)^2)$, but this would seem incorrect since it implies abnormally large amplitudes for silicone methyl stretching vibrations.' Thus an isotropic temperature coefficient correction for the fluorine scattering factors would, according to Roth and Harker, agree with their data. This isotropic temperature correction multiplied into the fluorine scattering factor gives, however, just the correct scattering factor for the methyl group.....Roth and Harker have not presented evidence to show that there is an abnormally great librational motion of the methyl groups relative to the siloxane nucleus in the pentasiloxane molecule....."

When considering the Pauling hypothesis, it should first be pointed out that the viscosities of the silicone oils vary not only with temperature but also with the length of the chain (R1, p.86). The Pauling hypothesis would require that the temperature coefficient for the uncoiling process be of the precise value necessary to reduce the effect of thermal agitation to that required by the experimental data. This would mean that this temperature coefficient would also have to vary in a regular fashion with the length of the chain.

Such a situation would be highly coincidental. Furthermore, his hypothesis apparently does not offer a satisfactory explanation for the high molar volume. Pauling states (P2): "The low intermolecular attraction is, I think, not due to an abnormally large distance between the surface groups of the molecules. If molecules are coiled into a globular shape, there will result a lower intermolecular attraction than if they have an extended shape." However, the reported values for the molar volumes seem high (R1, p.110-1) and are nearly the same for both the linear polymers and for the cyclic compounds for which no coiling process is apparent.

The explanation of the properties of the silicones in terms of their structure is thus still in some doubt, and it is felt that the situation can be at least partially clarified by the method about to be described.

C. The Application of Nuclear Magnetic Resonance Absorption.

The theory of this technique will be described in considerable detail in the next section. Inasmuch as the method is relatively new, the discussion given there has been written on the assumption that the material covered is totally unfamiliar to the reader, and has been made as nearly self-contained as possible. The remainder of this section will give only a very brief outline of the nature of the phenomenon.

Nuclei which possess a magnetic moment will, when placed in a magnetic field, go into one of several possible energy levels whose separation depends on the magnitude of the field and of the magnetic moment of the nucleus. According to the Bohr postulate there will be a certain frequency associated with the energy difference between these levels, and an oscillating field of this frequency irradiating these nuclei will cause them to undergo transitions between the possible energy states. In this process energy will be absorbed from the irradiating field, and the character of the absorption curve as a function of frequency is determined by the atomic configurations in the sample. More important to this

research is the fact that the character of the absorption is extremely sensitive to translational or rotational motion of the nuclei in the sample. Rotation or tunneling at frequencies far too low to affect the specific heat of the material causes pronounced changes in the width and shape of the absorption line.

The application of this technique to the problem of the silicones should be apparent. If the type of motion postulated by Roth and Harker actually occurs, it will certainly affect the nature of the absorption lines obtained from silicone samples. The method is particularly valuable in connection with these materials because the protons of the methyl groups are the only nuclei (other than Si^{29}, relative abundance 4.7%) which have nuclear magnetic moments other than zero.

II. THE THEORY OF NUCLEAR MAGNETIC RESONANCE ABSORPTION AS AS IT APPLIES TO THIS INVESTIGATION

A. The Microscopic Viewpoint.

1. The nuclear magnetic dipole in a field - classical picture. (R3)

Let us consider the nucleus as a spherical, charged particle. Classical theory predicts that any motion of the electrical charge will give rise to a magnetic field; therefore it is not unreasonable to assume that any magnetic properties which a nucleus may have are due to circulation of the nuclear charges within the nucleus itself. We now postulate that the nucleus is spinning about some given axis. It will then have angular momentum, which we will designate $\vec{P}$, the magnitude and direction of this vector denoting the magnitude of the angular momentum and the direction of the axis about which the spin occurs. This spin and the circulation of the charge of the particle will give rise to a magnetic field. If we assume that the particle is a spherical shell with its mass m and charge q distributed uniformly over the surface of the shell this field turns out to be identical with that produced by a small bar magnet whose magnetic moment $\vec{\mu}$, is given by:

(1-1) $$\vec{\mu} = \frac{q}{2mc}\vec{P}$$ c = velocity of light

It is not surprising that the magnetic moments of actual nuclei do not agree with the predictions of this simple picture. However, the disagreement is found to be only one of magnitude and possibly the sign of the constant relating $\vec{\mu}$ and $\vec{P}$. We may therefore rewrite equation (1-1) as:

(1-2) $$\vec{\mu} = \gamma \frac{q}{2mc}\vec{P} = g\mu_0\left(\frac{1}{\hbar}\right)\vec{P}$$

(1-3) $$\mu_0 = \frac{q\hbar}{2mc} = 5.0483 \cdot 10^{-24}\ \text{erg/gauss}$$

In these equations, e represents the electronic or proton charge in e.s.u., M the proton mass in grams, and g is a constant, sometimes referred to as the gyromagnetic ratio, which must be determined empirically. We have also introduced the nuclear magneton μ_0, since nuclear magnetic moments are usually expressed in units of this quantity. Despite the fact that equation (1-2) utilizes the proton mass and charge it is valid for all nuclei, any dependence of the magnetic moment on the mass and charge of other nuclei being incorporated into the factor g.

Now if this nuclear magnet be placed in a magnetic field $\vec{H}_o$, the field will exert a torque on the magnet,

(1-4) $\vec{L} = \vec{\mu} \times \vec{H}_o$

This torque tends to pull the magnet into alignment with the field. However, the fact that the nucleus is spinning an additional interaction which causes the following result. Newton's law of rotational motion states that the rate of change of angular momentum of a body, $\frac{d\vec{P}}{dt}$, is equal to the torque applied. The angular momentum of the nucleus is of course due to its spin. Thus, from equations (1-2) and (1-4):

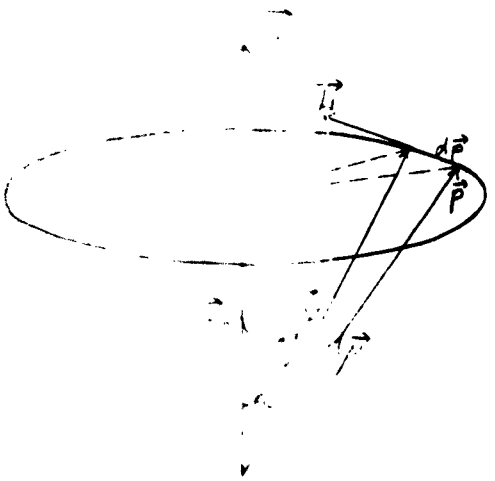

Figure 2

(1-5) $\frac{d\vec{p}}{dt} = \vec{L} = \vec{\mu} \times \vec{H}_0 = -\left(\frac{g\mu_n}{\hbar}\right) \vec{H}_0 \times \vec{p}$

Equation (1-5) is that of a vector $\vec{p}$, of constant magnitude precessing about an axis collinear with $\vec{H}_0$, with an angular velocity $\vec{\omega}_0$, given by:

(1-6) $\vec{\omega}_0 = -\left(\frac{g\mu_n}{\hbar}\right) \vec{H}_0$

$\vec{\omega}_0$ is known as the Larmor precession frequency.

The potential energy of this nuclear magnet in the presence of the magnetic field is expressed, except for an additive constant, by:

(1-7) $U = \vec{\mu} \cdot \vec{H}_0 = \mu_H H_0$

This is in agreement with our expectation that the energy of the nucleus will be at a minimum when the nuclear magnet is aligned with the field and at a minimum when the nuclear magnet and the field are opposed. We have also learned frome equation (1-5) that the torque produced by the field on a nuclear magnet gives rise only to a precession of $\vec{\mu}$ around $\vec{H}_0$, without any change in the orientation (expressed by θ) of $\vec{\mu}$ with respect to $\vec{H}_0$. We should therefore expect the energy of the nucleus in the field to be determined by the orientation which it had at the instant the field was applied; in other words, all values of U from $-\mu H_0$ to $+\mu H_0$ should be equally probable.

2. <u>The restrictions of the quantum theory</u>. We have seen that, classically there is a continuous spectrum of energies which a nucleus could have in a magnetic field. If this were true, there could be no resonance absorption. In this and the following section we shall point out the effect of quantum theory on the results of the previous section, deferring the more detailed quantum treatment to a later section.

According to quantum theory, the angular momentum of a particle is restricted to certain definite values, which are expressible in terms of the

quantity $\hbar$. Furthermore, the projection of $\vec{p}$ on a specified exis is also quantized. We will select as this axis the direction of the field $\vec{H}_o$. The maximum value of the component of $\vec{p}$ along $\vec{H}_o$ is the quantity known as the nuclear spin I, defined by:

$$(2\text{-}1) \qquad (p_H)_{max} = I\hbar$$

I may have either integral or half-integral values and will have a single characteristic value for a particular nuclear species. The permitted values for p_H are given by:

$$(2\text{-}2) \qquad p_H = m\hbar \qquad m = I, I-1, I-2, \cdots, -I+1, -I.$$

so that there are $2I+1$ possible values for p_H. Because of the proportionality of $\vec{\mu}$ and $\vec{p}$ the possible values of μ_H will also be restricted. Combining equations (2-2) and (1-2) we find that

$$(2\text{-}3) \qquad \mu_H = g\mu_o m$$

and from equation (1-7)

$$(2\text{-}4) \qquad U_m = -g\mu_o H_o m \qquad (m = I, I-1, \cdots, -I)$$

Thus the quantum theory predicts the existence of discrete values of the potential energy of the nucleus in a magnetic field. These energy levels are equally spaced, with a separation

$$(2\text{-}5) \qquad \Delta U = U_m - U_{m-1} = g\mu_o H_o$$

3 Resonance Absorption. According to the Bohr postulate, transitions between two states separated by energy ΔU will be accompanied by emission or absorption of radiation at a frequency determined by the relation

Classically we found that the energy spectrum was continuous. Under such conditions, ΔU and ω would also be continuous. However, the quantum theory predicts discrete energy levels, and therefore discrete values for ΔU. These values are further limited by the selection rules governing transitions between the energy levels U_m, which state that only transitions in which $\Delta m = \pm 1$ are permitted. Since the energy levels are equally spaced, ΔU, and hence ω, will actually be restricted to a single value. This is the resonance condition. From equations (2-5) and (3-1) we find that the resonance frequency is

$$\omega_o = \frac{g \mu_o H_o}{\hbar} \tag{3-2}$$

which on comparison with equation (1-6) proves to be identical with the Larmor precession frequency.

The actual values of ω are seen to depend on the external field H_o, and on g, a constant for the particular nuclear species under consideration. In general, the field strengths attainable in the laboratory will not exceed 10,000 gauss, and the values of g usually fall in the range from 0.5-6. The resonance frequencies of most nuclei will thus lie in the region from one to fifty megacycles, which is in the ordinary radiofrequency range. As a result the techniques and equipment used to detect resonance absorption are usually quite similar to those employed in commercial and amateur radio work.

4. The effect of a precessing magnetic field. We have found that a nucleus in a magnetic field $\vec{H_o}$, will undergo precession due to the combined action of its own spin and the torque produced by the interaction of $\vec{H_o}$ and the nuclear magnetic moment $\vec{\mu}$.

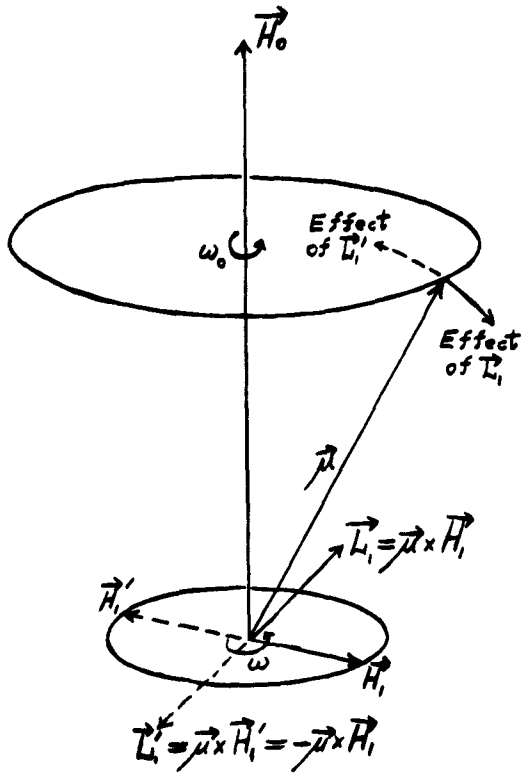

Figure 3

Let us now apply a small magnetic field $\vec{H}_1$, rotating with angular frequency ω in the plane perpendicular to $\vec{H}_0$. The torque produced by $\vec{H}_1$, tends to tip the vector $\vec{\mu}$, as shown in Figure 3. However, if ω differs appreciably from ω_0, the Larmor frequency, the relative orientation of $\vec{H}_1$ and ω will change with time. When $\vec{H}_1$ has the orientation $\vec{H}_1' = -\vec{H}_1$, the torque which it exerts on $\vec{\mu}$ will be opposite to that which it exerted previously. Thus the time average effect of $\vec{L}_1$ will be zero.

If $\omega = \omega_0$, $\vec{\mu}$ and $\vec{H}_1$ will always retain the same relative orientation, and the torque exerted by $\vec{L}_1$ will always act in the same direction. The probability that it will tip $\vec{\mu}$ into a new orientation with respect to will now be appreciable. The new orientation will have to be one of those permitted by the quantum conditions imposed on μ_H so that the energy absorbed or emitted when the transition takes place will fulfill the resonance conditions discussed previously.

We have considered the small field $\vec{H}_1$, as rotating about $\vec{H}_0$. This is not practicable experimentally. However, we can easily apply an alternating magnetic field simply by placing the sample inside a solenoid through which a current is passing. Let us assume that the axis of this coil lies along the x-axis. The field produced by the coil will be:

$$(4\text{-}1) \qquad \begin{cases} H_x = H_1 \cos \omega t \\ H_y = 0 \\ H_z = 0 \end{cases}$$

However this can also be expressed as the sum of two fields

$$(4\text{-}2)\qquad \begin{cases} H_x^a = \tfrac{1}{2}H_1 \cos\omega t \\ H_y^a = \tfrac{1}{2}H_1 \sin\omega t \\ H_z^a = 0 \end{cases} \qquad \begin{cases} H_x^b = \tfrac{1}{2}H_1 \cos\omega t \\ H_y^b = -\tfrac{1}{2}H_1 \sin\omega t \\ H_z^b = 0 \end{cases}$$

Each of these two fields rotates about the z-axis, but in opposite directions. When $\omega = \omega_0$, one of these two fields will rotate in the same direction as and will be capable of inducing transitions. The other will rotate in the wrong direction and will be ineffective. Thus the oscillating field will produce a rotating or circularly polarized field whose effective magnitude will be $\frac{1}{2}H_1$, but whose frequency of rotation will be the same as the frequency of oscillation of the applied field.

5. A more detailed quantum-mechanical treatment. In our previous discussion we have made several assumptions concerning the quantum restrictions on the classical description of the magnetic properties of the nucleus. In order to justify these assumptions and particularly to derive the probabilities of transitions between the energy levels, we must consider the quantum-mechanical description of our system.

The wave function $\Psi(t)$, which is an accurate representation of our system must of course satisfy the time-dependent Schrödinger equation

$$(5\text{-}1)\qquad \mathcal{H}(t)\,\Psi(t) = i\hbar\frac{\partial}{\partial t}\Psi(t)$$

where $\mathcal{H}$ is the Hamiltonian operator. We are considering only the energy of interaction of the nuclear magnetic moment with an external magnetic field; we will assume that all other factors such as translational energy or electronic magnetic moments are absent, or are such as to add only a constant term. In this case the Hamiltonian operator is simply:

$$(5\text{-}2)\qquad \mathcal{H}(t) = -\vec{\mu}\cdot\vec{H}(t)\ .$$

where

(5-3) $\vec{\mu} = g\mu_0 \vec{I}$

$\vec{I}$ is the spin angular momentum vector operator which can be seen from equation (1-2) to be related to the ordinary angular momentum operator by the relation $\vec{I} = (1/\hbar)\vec{p}$.

We shall assume that our magnetic field is composed of a strong constant field H_0, and a small time-dependent field in the plane perpendicular to the strong field. Thus in Cartesian coordinates

(5-4) $\vec{H}(t) = H_x(t)\hat{i} + H_y(t)\hat{j} + H_0\hat{k}$

Then, from equation (5-2)

(5-5) $\mathcal{H}(t) = -g\mu_0(H_x I_x + H_y I_y + H_0 I_z)$

where I_x, I_y, and I_z are the spin operators for the components of the total spin $\vec{I}$. Now let us briefly recall some of the properties of angular momentum operators (E-1), and consider first the operator $\vec{I}\cdot\vec{I} = |\vec{I}|^2$ This operator will commute with each of the operators I_x, I_y, and I_z, although these operators will not commute with each other. It will thus be possible to find a set of eigenfunctions ψ_m, which will be eigenfunctions of both $|\vec{I}|^2$ and I_z. Assuming these functions are known, we may write:

$|\vec{I}|^2\psi_m = I(I+1)\psi_m$ (I is integral or half-integral)

(5-6) $I_z\psi_m = m\psi_m \quad (m = I, I-1, \cdots, -I)$

Returning to our original problem, we may treat this by perturbation theory by separating our Hamiltonian into a time-independent part $\mathcal{H}^0$ and a time-dependent perturbation $\mathcal{H}'$, so that:

$\mathcal{H}^0 = -g\mu_0 H_0 I_z$

(5-7) $\mathcal{H}' = -g\mu_0(H_x I_x + H_y I_y)$

Since $\mathcal{H}^\circ$ is independent of time it will have a solution of the form

(5-8) $$\mathcal{H}^\circ \psi_m = E_m \psi_m$$

where E_m is the energy of the various eigenstates of the system. From equations (5-6), (5-7), and (5-8), we find:

(5-9) $$E_m = -g\mu_o H_o m \quad (-I \leq m \leq I)$$

which agrees with equation (2-4). These are the energy levels for the unperturbed system with the set of eigenfunctions ψ_m which are independent of time

Under the influence of the small perturbing field, a nucleus which was originally in one of the states represented by a particular ψ_m may undergo transitions to some other state ψ_m'. The wave function $\Psi(t)$, which describes the whole system may be expanded in terms of any complete set of eigenfunctions, and for this purpose we shall select the set ψ_m for the unperturbed energy levels, incorporating the time dependence into the coefficients of the individual ψ_m's. We will assume that $\Psi(t)$ is normalized, as are the unperturbed eigenfunctions. Since the latter functions are also orthogonal, we have the relations:

(5-10) $$\Psi(t) = \sum_{m=-I}^{I} C_m(t)\, \psi_m$$

(5-11) $$(\psi_m^*, \psi_{m'}) = \delta_{m,m'}$$

(5-12) $$\sum_{m=-I}^{I} C_m^* C_m = 1$$

Thus the product $C_m^* C_m$ represents the probability that the nucleus will be in the state m at time t. In order to evaluate the constants C_m we must consider the effect of the perturbation $\mathcal{H}'$. Substituting equation (5-10) into (5-1) and using equations (5-7) and (5-8), we find:

(5-13) $$\sum_m C_m E_m \psi_m + \sum_m C_m \mathcal{H}' \psi_m = i\hbar \sum_m \frac{\partial C_m}{\partial t} \psi_m$$

This may be reduced to a set of simultaneous equations by multiplying equation (5-13) by each ψ_m in turn and using equation (5-11). Thus

$$C_m E_m - q\mu_0 \sum_{m'} \left[C_{m'} (\psi_m, \{H_x I_x + H_y I_y\} \psi_{m'}) \right] = i\hbar \frac{dC_m}{dt} \tag{5-14}$$

I_x and I_y individually do not have the functions ψ_m as eigenfunctions. However, it can be shown that (E-1):

$$(I_x + iI_y)\psi_m = \left[(I+m+1)(I-m)\right]^{1/2} \psi_{m+1}$$

$$(I_x - iI_y)\psi_m = \left[(I+m)(I-m+1)\right]^{1/2} \psi_{m-1} \tag{5-15}$$

Therefore:

$$I_x \psi_m = \frac{1}{2}\left\{ \left[(I+m+1)(I-m)\right]^{1/2} \psi_{m+1} + \left[(I+m)(I-m+1)\right]^{1/2} \psi_{m-1} \right\}$$

$$I_y \psi_m = -\frac{1}{2} i \left\{ \left[(I+m+1)(I-m)\right]^{1/2} \psi_{m+1} - \left[(I+m)(I-m+1)\right]^{1/2} \psi_{m-1} \right\} \tag{5-16}$$

It is now possible to evaluate the functions $(\psi_m, \mathcal{H}' \psi_{m'})$, which become:

$$\begin{aligned} (\psi_m, \mathcal{H}' \psi_{m'}) = {} & \frac{1}{2}(H_x - iH_y)\left[(I+m'+1)(I-m')\right]^{1/2} (\psi_m, \psi_{m'+1}) \\ & + \frac{1}{2}(H_x + iH_y)\left[(I+m')(I-m'+1)\right]^{1/2} (\psi_m, \psi_{m'-1}) \end{aligned} \tag{5-17}$$

Before using these relations which are required in the summation in equation (5-14), we must remember that the ψ_m's are orthonormal. Thus there are only two terms in the summation which do not vanish, those for which $m = m' \pm 1$. We have thus justified the selection rule we previously stated, $\Delta m = \pm 1$.

Equation (5-14) now takes the form:

$$\begin{aligned} i\hbar \frac{dC_m}{dt} = {} & C_m E_m - \frac{q\mu_0}{2}(H_x - iH_y)\left[(I+m)(I-m+1)\right]^{1/2} C_{m-1} \\ & - \frac{q\mu_0}{2}(H_x + iH_y)\left[(I+m+1)(I-m)\right]^{1/2} C_{m+1} \end{aligned} \tag{5-18}$$

H_x and H_y may be replaced by their equivalents from equation (4-2b), to yield:

$$\begin{aligned} i\hbar \frac{dC_m}{dt} = {} & C_m E_m \\ & - \frac{q\mu_0 H_1}{4}\left\{ e^{i\omega t}\left[(I+m)(I-m+1)\right]^{1/2} C_{m-1} + e^{-i\omega t}\left[(I+m+1)(I-m)\right]^{1/2} C_{m+1} \right\} \end{aligned} \tag{5-19}$$

We now have a set of simultaneous first order differential equations involving the coefficients C_m. Since we shall be concerned only with nuclei whose spin is $\frac{1}{2}$, we shall solve the equations (5-19) only for this special case. However, the solutions for $I > \frac{1}{2}$ can be obtained from this case by the method of Majorana (M-1). When $I = \frac{1}{2}$, m can have only the values $\pm \frac{1}{2}$. Thus we will have only two equations:

$$i\hbar \frac{dC_{\frac{1}{2}}}{dt} = C_{\frac{1}{2}} E_{\frac{1}{2}} - \frac{g\mu_0 H_1}{4} e^{i\omega t} C_{-\frac{1}{2}}$$

(5-20)

$$i\hbar \frac{dC_{-\frac{1}{2}}}{dt} = C_{-\frac{1}{2}} E_{-\frac{1}{2}} - \frac{g\mu_0 H_1}{4} e^{-i\omega t} C_{\frac{1}{2}}$$

These equations are similar to those obtained by Ramsey (R-4). They may be solved by converting one or the other equation into a second order differential equation (differentiating once more with respect to time), which may be made a function of only one of the C's by proper substitutions from equation (5-20). The resulting equation may then be solved by standard methods and the solution used to find the other C from the proper equation of (5-20). When the arbitrary constants are evaluated in terms of the initial values of the coefficients $C_{\frac{1}{2}}(0)$ and $C_{-\frac{1}{2}}(0)$ (at $t = 0$), the final solutions are:

$$C_{\frac{1}{2}}(t) = \left[\left(\cos\tfrac{1}{2}at + i\cos\theta\sin\tfrac{1}{2}at\right)C_{\frac{1}{2}}(0) - i\left(\sin\theta\sin\tfrac{1}{2}at\right)C_{-\frac{1}{2}}(0)\right] e^{i\left(\frac{\omega}{2} - \frac{E_{-\frac{1}{2}} + E_{\frac{1}{2}}}{2\hbar}\right)t}$$

(5-21)

$$C_{-\frac{1}{2}}(t) = \left[-\left(i\sin\theta\sin\tfrac{1}{2}at\right)C_{\frac{1}{2}}(0) + \left(\cos\tfrac{1}{2}at - i\cos\theta\sin\tfrac{1}{2}at\right)C_{-\frac{1}{2}}(0)\right] e^{i\left(\frac{\omega}{2} - \frac{E_{-\frac{1}{2}} + E_{\frac{1}{2}}}{2\hbar}\right)t}$$

where

$$\sin\theta = -\frac{g\mu_0 H_1}{2\hbar a} \qquad \omega_0 = \frac{E_{-\frac{1}{2}} - E_{\frac{1}{2}}}{\hbar}$$

(5-22)

$$\cos\theta = \frac{\omega_0 - \omega}{a} \qquad a = \left[(\omega_0 - \omega)^2 + \frac{g^2\mu_0^2 H_1^2}{4\hbar^2}\right]^{\frac{1}{2}}$$

We can now show from these equations that the probabilities are the same for the transitions $+\frac{1}{2} \rightarrow -\frac{1}{2}$ and $-\frac{1}{2} \rightarrow +\frac{1}{2}$. Let us assume that initially

the nucleus is in the state $+\frac{1}{2}$; i.e. $C_{+\frac{1}{2}}(0)=1, C_{-\frac{1}{2}}(0)=0$. Then after time t , the probability that the nucleus will be found in the other state, $-\frac{1}{2}$, is given by [illegible] ; the probability that it is still in the state $+\frac{1}{2}$ is $C_{\frac{1}{2}}^{*} C_{\frac{1}{2}}$. Then at time [illegible] ,

$$= \cos^2 \tfrac{1}{2}at + \cos^2\theta \sin^2 \tfrac{1}{2}at$$

(5-23)

$$= \sin^2\theta \sin^2 \tfrac{1}{2}at$$

and [illegible] $C_{-\frac{1}{2}}^{*} C_{-\frac{1}{2}} = 1$, in agreement with equation (5-12). On the other hand, if the nucleus is originally in the state $-\frac{1}{2}$, then [illegible] $C_{-\frac{1}{2}}(0) = 1$, and we find after time t ,

$$= \sin^2\theta \sin^2 \tfrac{1}{2}at = C_{-\frac{1}{2}}^{*} C_{-\frac{1}{2}}$$

(5-24)

$$= \cos^2 \tfrac{1}{2}at + \cos^2\theta \sin^2 \tfrac{1}{2}at = C_{\frac{1}{2}}^{*} C_{\frac{1}{2}}$$

We shall define the symbol $C^{(t)}_{+\frac{1}{2}\rightarrow -\frac{1}{2}}$ as the probability that a nucleus, originally in the state $+\frac{1}{2}$, will after time t be found in the state [illegible] and define $C^{(t)}_{-\frac{1}{2}\rightarrow +\frac{1}{2}}$ similarly. Then equations (5-23) and (5-24) show that

(5-25) [illegible] $= C_{-\frac{1}{2}\rightarrow +\frac{1}{2}} = C = \sin^2\theta \sin^2 \tfrac{1}{2}at$

Replacing [illegible] and a by the values given in equation (5-22),

(5-26) [illegible] $= \dfrac{q^2\mu_0^2 H_1^2}{\hbar^2\left[(\omega_0-\omega)^2 + \frac{q^2\mu_0^2 H_1^2}{4\hbar^2}\right]} \sin^2 \dfrac{t}{2}\left[(\omega_0-\omega)^2 + \dfrac{q^2\mu_0^2 H_1^2}{4\hbar^2}\right]^{\frac{1}{2}}$

We can see from this equation that the probability of a transition taking place will be very small unless $\omega = \omega_0$, confirming the resonant nature of the absorption phenomenon.

The quantum-mechanical treatment has now justified the assumptions made previously. It has also shown that the transition probabilities are equal for either absorption or induced emission in the presence of a radiation field.

In order to obtain a net absorption of energy there must always be an excess of nuclei in the lower energy state. Such a situation can exist only if a relaxation mechanism is available to remove the energy absorbed from the radiation field.

6. Relaxation mechanisms. In the absence of a magnetic field, a sample containing N_o nuclei which have a magnetic moment will have these nuclei distributed equally among the possible spin states. When a strong permanent magnetic field is applied, each spin state will have a different energy due to the coupling of the spin with the field. The new equilibrium number of nuclei for each state will now depend on the Boltzmann factor for that state. For the case of only two energy levels ($I=\frac{1}{2}$),

$$\frac{N_{+\frac{1}{2}}}{N_{-\frac{1}{2}}} = e^{(E_{-\frac{1}{2}} - E_{+\frac{1}{2}})/kT} \qquad N_{+\frac{1}{2}} + N_{-\frac{1}{2}} = N_o \tag{6-1}$$

Before the field was applied, the two states had equal energy, so $N_{+\frac{1}{2}} = N_{-\frac{1}{2}}$ In the presence of the field, this condition of equality would require that the temperature of the spin system be infinite. The spin system must therefore interact with the surrounding lattice in order to "cool down" to the temperature of the lattice.

We have seen that a rotating or oscillating magnetic field at a nucleus will produce transitions. However, we have only considered an externally applied field. It is also possible for fluctuating magnetic fields to be produced by the lattice, by thermal vibrations or rotations of the nuclei in the sample, by Brownian motion in liquids, or by the components of electronic spins or orbital moments if these are present. Such fields will produce transitions, the energy involved being exchanged between the nuclear spin system and the thermal reservoir of the surrounding lattice. It is possible, in principle, to calculate a transition probability for the interactions between the lattice and

the spin system. However, these interactions are providing a thermal mechanism to equalize the temperatures of the lattice and the spins, so it is appropriate to weight the calculated probability with the Boltzmann factor of the final state to which the transition takes place. Let us call the computed transition probability W. Then the total probability of transition is given by:

$$W_{+\frac{1}{2}\rightarrow-\frac{1}{2}} = We^{-E_{-\frac{1}{2}}/kT} = We^{g\mu_0 H_0/2kT}$$

(6-2)

$$W_{-\frac{1}{2}\rightarrow+\frac{1}{2}} = We^{-E_{+\frac{1}{2}}/kT} = We^{-g\mu_0 H_0/2kT}$$

Now let us again consider our nuclear spin system in a magnetic field At equilibrium, in the absence of the weak oscillating field, the number of transitions "up" and "down" must be equal; thus:

$$N_{+\frac{1}{2}} W_{+\frac{1}{2}\rightarrow-\frac{1}{2}} = N_{-\frac{1}{2}} W_{-\frac{1}{2}\rightarrow+\frac{1}{2}} \tag{6-3}$$

If the system is not in equilibrium, it will exchange energy with the lattice in such a manner as to approach equilibrium. Let us call the excess number of nuclei in the lower state η, so that:

$$\eta = N_{+\frac{1}{2}} - N_{-\frac{1}{2}} \tag{6-4}$$

Then we express the approach of η to its equilibrium value by

$$\frac{d\eta}{dt} = 2\left[N_{-\frac{1}{2}} W_{-\frac{1}{2}\rightarrow+\frac{1}{2}} - N_{+\frac{1}{2}} W_{+\frac{1}{2}\rightarrow-\frac{1}{2}}\right] \tag{6-5}$$

the factor 2 being used because η changes by 2 for each transition. The exponents in equation (6-2) are ordinarily very small, so the approximation $e^{x} = 1 + x$ will be extremely good in this case. Using this approximation and substituting the equations (6-2) into (6-5), we obtain:

$$\frac{d\eta}{dt} = 2W(\eta_0 - \eta) \tag{6-6}$$

where $n_0 = \frac{N_0 g \mu_0 H_0}{2kT}$. Then the solution of this equation is:

(6-7) $$n = n_0 [1 - e^{-2Wt}]$$

Thus we learn that equilibrium is established exponentially, with a characteristic time,

(6-8) $$T_1 = \frac{1}{2W}$$

known as the spin-lattice (thermal) relaxation time.

Theroretical calculations of T_1 and their correlation with experimentally observed values have offered a new insight into the nature of the solid state. The details of some of these studies may be found in references (B-2), (B-3), and (W-1). For the purposes of this investigation it will suffice to remember that relaxation mechanisms exist and that the efficiency of these mechanisms as measured by the relaxation time frequently sets a limit on the possibility of detecting nuclear magnetic resonance absorption.

B. The Macroscopic Viewpoint.

1. General. Our previous discussion has been largely microscopic, dealing with the individual nucleus and using the methods and results of quantum mechanics. In actual fact we will be working experimentally with a macroscopic sample containing many nuclei. Furthermore, the experimental technique involves the detection of resonance absorption by its effect on the electrical characteristics of a coil. We must, therefore, relate the quantum-mechanical results obtained previously to the macroscopic experimental conditions, which are best described in terms of classical magnetic theory and electronic circuit theory.

2. The Bloch equations. Let us consider that we have a sample containing N_0 nuclei per unit volume. We shall assume that thermal equilibrium has been established between the nuclear magnetic dipoles and the lattice, in an external

magnetic field, $\vec{H_o}$. The sample will then have a resultant magnetic moment per unit volume $\vec{M_o}$, given by:

$$\vec{M_o} = \chi_o \vec{H_o} \tag{2-1}$$

where χ_o is the nuclear magnetic susceptibility per unit volume (Curie susceptibility. The value of χ_o can be derived in terms of the quantities used in part A (P-3). For nuclei of spin $I = \frac{1}{2}$,

$$\chi_o = \frac{\gamma^2 \mu_o^2 N_o}{4kT} \tag{2-2}$$

This static susceptibility of the nuclear magnetism is extremely small, more than 1,000 times smaller than the ever-present diamagnetic susceptibility due to the electron shells of the atoms. We shall see, however, that when resonance absorption occurs, the susceptibility will be increased by several orders of magnitude.

Let us now apply a radiation field which rotates about the permanent field in the manner already discussed. The total applied magnetic field will have the components

$$\begin{aligned} H_x &= \tfrac{1}{2} H_1 \cos \omega t \\ H_y &= -\tfrac{1}{2} H_1 \sin \omega t \\ H_z &= H_o \end{aligned} \tag{2-3}$$

We have already seen that for a single particle of magnetic moment $\vec{\mu}$, the torque applied by the field can be expressed as

$$\vec{L} = \vec{\mu} \times \vec{H} \tag{2-4}$$

and, from equations (1-2) and (1-5), part A,

$$\frac{d\vec{\mu}}{dt} = \frac{\gamma \mu_o}{\hbar} [\vec{\mu} \times \vec{H}] \tag{2-5}$$

It is a fact that the quantum-mechanical expectation value for the time derivative of an operator (in this case, $\vec{\mu}$) follows the classical equations of motion. Therefore, we are allowed to carry the expression (2-5) over to the macroscopic case unchanged; and the magnetic polarization $\vec{M}$, which is the sum of all the individual moments, fits the equation

$$\frac{d\vec{M}}{dt} = \frac{g\mu_0}{\hbar}\left[\vec{M}\times\vec{H}\right] \tag{2-6}$$

This equation describes the effect of the externally applied field on the polarization. We must also consider other interactions, the first of which is that of spin-lattice relaxation. As pointed out above, this is an interaction which affects the total energy of the spin system. Remembering that the energy depends only upon the component of the polarization in the direction of the strong field (equation (1-7), part A), we may write for the total energy,

$$E = -M_z H_0 \tag{2-7}$$

where M_z is the z-component of the polarization. At equilibrium, this has the value $M_0 = \chi_0 H_0$ (equation (2-i)). If at any time $M_z \neq M_0$, it will approach this value exponentially with the characteristic relaxation time T_1, as we have seen. Thus as a result of thermal perturbations alone,

$$\left(\frac{\partial M_z}{\partial t}\right) = \frac{M_0 - M_z}{T_1} \tag{2-8}$$

the partial indicating that this is only one of the interactions affecting M_z.

We must also consider the factors other than the external field that affect M_x and M_y. Such factors can be classed as spin-spin interactions and strong field inhomogeneity. In order to describe the effect of these factors, let us assume that at a particular instant in time all the nuclear moments are lined up in phase (parallel) as they precess about the strong field

axis. If the field were perfectly homogeneous and each spin could be considered as independent of all the others, all the spins would precess at exactly the same frequency, and M_x and M_y would have large constant values. However, if the field is somewhat inhomogeneous the nuclei in different parts of the sample will have slightly different Larmor frequencies and will precess at slightly different rates. Furthermore, each nuclear moment produces its own small magnetic field which will add to the strong field at the location of neighboring nuclei, and this will have the same effect as inhomogeneity in the field. Finally, two neighboring nuclei which have the same Larmor frequency will each produce at the other nucleus a precessing field at the Larmor frequency which may cause both nuclei to undergo a transition at the same time, leaving the total spin energy unchanged. The final result of all these effects is to destroy the existing phase relationships between the various nuclear spins, while leaving the total spin energy unchanged. Thus these processes will have no effect on M_z, but they will affect M_x and M_y, reducing the latter components to zero in the absence of the radiation field. By analogy to the previously discussed effect of spin-lattice interactions on M_z, Bloch (B-4) expresses the disorienting effect of spin-spin interactions and field inhomogeneity on M_x and M_y as an exponential decay relationship:

$$(2\text{-}9) \qquad \left(\frac{\partial M_x}{\partial t}\right) = -\frac{M_x}{T_2} \qquad\qquad \left(\frac{\partial M_y}{\partial t}\right) = -\frac{M_y}{T_2}$$

where the partials have the same significance as in (2-8), and T_2 is the characteristic time associated with the disorientation process.

Combining equations (2-6), (2-8), and (2-9), Bloch obtained the following set of differential equations for the components of $\vec{M}$ (B-4).

$$(2\text{-}10) \qquad \begin{aligned} \frac{dM_x}{dt} &= \frac{g\mu_0}{\hbar}\left[M_y H_z - M_z H_y\right] - \frac{M_x}{T_2} \\ \frac{dM_y}{dt} &= \frac{g\mu_0}{\hbar}\left[M_z H_x - M_x H_z\right] - \frac{M_y}{T_2} \\ \frac{dM_z}{dt} &= \frac{g\mu_0}{\hbar}\left[M_x H_y - M_y H_x\right] + \frac{M_0 - M_z}{T_1} \end{aligned}$$

The solution of these equations which we will use is given by Pake (P-3). He finds for a particular solution:

$$M_x = \tfrac{1}{2}\chi_0 \omega_0 T_2 \frac{T_2(\omega_0-\omega)(H_1\cos\omega t) + (H_1 \sin\omega t)}{1 + T_2^2(\omega_0-\omega)^2 + \frac{\gamma^2\mu_0^2}{4\hbar^2} H_1^2 T_1 T_2}$$

$$M_y = \tfrac{1}{2}\chi_0 \omega_0 T_2 \frac{(H_1\cos\omega t) - T_2(\omega_0-\omega)(H_1 \sin\omega t)}{1 + T_2(\omega_0-\omega)^2 + \frac{\gamma^2\mu_0^2}{4\hbar^2} H_1^2 T_1 T_2} \qquad (2\text{-}11)$$

$$M_y = \chi_0 H_0 \frac{1 + T_2^2(\omega_0-\omega)^2}{1 + T_2(\omega_0-\omega)^2 + \frac{\gamma^2\mu_0^2}{4\hbar^2} H_1^2 T_1 T_2}$$

In these equations χ_0 is the Curie susceptibility given in equation (2-2), and $\omega_0 (= \frac{\gamma\mu_0}{\hbar} H_c)$ is the Larmor frequency.

3. The complex susceptibility. We have now found a solution for the components of the induced magnetic polarization, $\vec{M}$. However, we will be more interested in the magnetic susceptibility, which is the quantity which appears directly in the expression for the electrical characteristics of a coil.

It is advantageous for many purposes to represent the susceptibility as a complex number.

$$\chi = \chi' - i\chi'' \qquad (3\text{-}1)$$

The applied radiation field, which is actually an oscillating field along the x-axis of our coordinate system, may be represented as the real part of a complex quantity.

$$H_x = H_1 e^{i\omega t} = H_1 \cos\omega t + i H_1 \sin\omega t \qquad (3\text{-}2)$$

Then the observable magnetization will be the real part of the complex product χH_x;

$$M_x = \chi'(H_1\cos\omega t) + \chi''(H_1 \sin\omega t) \qquad (3\text{-}3)$$

Thus, χ'' is proportional to that component of the magnetization which is out-of-phase with the applied field. Comparison of equations (3-3) and (2-11) identifies the real and imaginary parts of the susceptibility as:

$$\chi' = \frac{1}{2}\chi_0 \omega_0 T_2 \qquad \text{(illegible)}$$

(3-4)

$$\chi'' = \frac{1}{2}\chi_0 \omega_0 T_2 \qquad \text{(illegible)}$$

where $S = \frac{e^2 \mu^2 N^2}{4\pi^2}$ (illegible) written as

(3-5) $M_y = \chi_0 H_0$ (illegible)

We may now (illegible) for two general cases, where S is negligible and where $S \ll 1$

$$\chi' = \frac{1}{2}\chi_0 \omega_0 T_2 \qquad \text{(illegible)}$$

(3-6)

$$\chi'' = \frac{1}{2}\chi_0 \omega_0 T_2 \qquad \text{(illegible)}$$

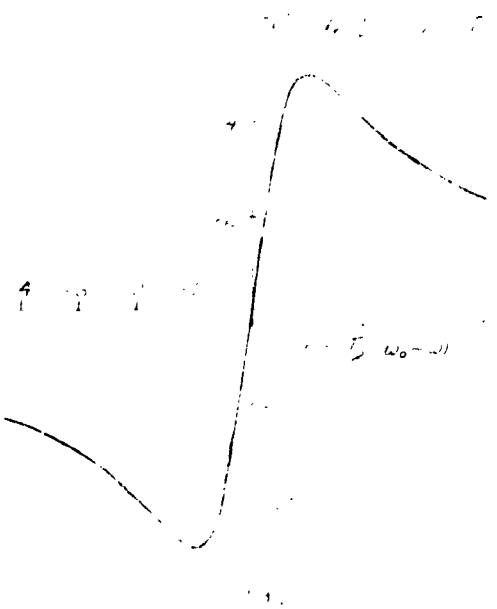

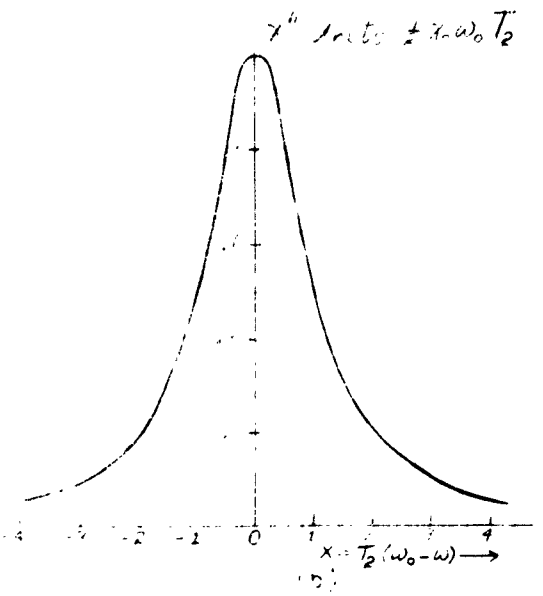

(b)

In Figure 4 we have plotted χ' (the nuclear dispersion) and χ'' (the nuclear absorption) against the dimensionless quantity $a = T_2(\omega_0-\omega)$. The absorption curve illustrates quite clearly the resonant nature of the absorption phenomenon. The half-width of the line (one-half the frequency separation between the points at which the amplitude of χ'' is one-half its maximum value) will be equal to $1/T_2$, because at these points, $T_2^2(\omega_0-\omega)^2=1$. Thus T_2 is a measure of the line width and, as can be seen from equation (3-6), is also a determining factor for the peak amplitude. It can be shown that the area under the curve is a constant for a given χ_0 and ω_0. When spin-spin interactions are small (in liquid or gaseous samples), T_2 will be determined solely by the magnetic field inhomogeneity, which then becomes of considerable importance in attaining good signal strengths or in precision determinations of resonance frequencies.

Now let us consider what happens when S is no longer negligible. This will be the case for long relaxation times (T_1), or fairly strong radiation fields. Consideration of equation (3-4) shows that when S becomes significant, the maximum values of χ' and χ'' are decreased. Furthermore, the width of the absorption curve χ'' is increased, since at one-half maximum intensity, $(\omega_0-\omega) = \frac{\sqrt{1+S}}{T_2}$

M_J will also be decreased when S is increased. If we substitute for χ_0 in equation (3-5) its value from equation (2-2), we find:

$$(3\text{-}7)\qquad M_{J(\omega=\omega_0)} = \frac{g^2\mu_0^2 H_0 N_0}{4kT(1+S)} = \frac{g^2\mu_0^2 H_0 N_0}{4kT_S}$$

where $T_S = T(1+S)$ can be considered to define an effective spin temperature. Thus the effect of too-large radiation fields or inefficient spin-lattice relaxation mechanisms (long T_1) is to increase the temperature of the spin system and reduce the available signal strength. Under these conditions the spin system is said to be saturating, and S will be the measure of the saturation.

4. Comparison of the microscopic and macroscopic viewpoints: the power absorbed by the sample. We can now show that the two approaches we have taken lead to the same expression for the power absorbed by the sample from the radiation field. Pake (P-3) treats the absorption in a manner analogous to the problem of hysteresis losses in a transformer, for which case the power absorbed is

$$P = \frac{\omega}{2\pi} \int_{t=0}^{t=2\pi/\omega} \vec{H} \cdot d\vec{M} \tag{4-1}$$

where the integral represents the power absorbed per cycle of the radiation field. Using the real parts of the complex field and complex induced polarization (equation (3-3)), he evaluates this expression as:

$$P = \frac{1}{2} \omega_0 H_1^2 \chi'' \tag{4-2}$$

where χ'' is given by equation (3-4), and ω_0 replaces ω because it is only in the region around ω_0 that χ'' does not vanish.

Turning again to the results of part A, we have found an expression for the transition probability (equation (5-30)),

$$C^{(t)}_{\frac{1}{2}\to-\frac{1}{2}} = \frac{g^2\mu_0^2 H_1^2}{4\hbar^2} \cdot \frac{\sin^2 \frac{t}{2}\left[(\omega_0-\omega)^2 + \frac{g^2\mu_0^2 H_1^2}{4\hbar^2}\right]^{1/2}}{\left[(\omega_0-\omega)^2 + \frac{g^2\mu_0^2 H_1^2}{4\hbar^2}\right]^{1/2}} \tag{4-3}$$

This expression is identical to that obtained by Bloembergen (B-2, p.25). By considering that the absorption line shape can be described by a function $\phi(\nu)$, such that the line shape is considerably broader than the frequency spectrum of the applied radiation field, Bloembergen was able to derive an expression for the power absorbed, which in our nomenclature becomes:

$$P = \frac{1}{4}\left(\frac{g^2\mu_0^2 H_1^2}{4\hbar^2}\right) g\mu_0 H_0 n \phi(\nu) \tag{4-4}$$

where n is the number of surplus nuclei in the lower state. Neglecting saturation effects, we may replace n by its equilibrium value $n = \frac{g\mu_0 H_0 N_0}{2kT}$. Making the further substitutions of $\omega_0 = \frac{g\mu_0 H_0}{\hbar}$, and χ_0, equation (2-2), we will obtain:

$$(4\text{-}5) \qquad P = \frac{1}{2} H_1^2 \omega_0 \left(\frac{1}{2} \chi_0 \omega_0 \frac{\phi(\nu)}{2}\right)$$

This will be identical with equation (4-2) if we assume that the shape function has the form

$$(4\text{-}6) \qquad \phi(\nu) = \frac{2T_2}{1 + T_2^2(\omega_0 - \omega)^2}$$

which is the shape appropriate to a damped oscillator. Since this shape is frequently encountered both theoretically and experimentally in magnetic resonance absorption studies, we may feel justified in using it here. Thus we find that both the microscopic and macroscopic viewpoints lead to the same expressions for the nuclear susceptibilities.

5. Detection of the absorption: the tuned circuit. We have finally reached the point where we may begin to consider the magnetic resonance absorption in terms of the actual experimental conditions. We have a coil which forms the inductive part of a tuned circuit. The sample is placed in the coil, which is situated so that its axis is at right angles to the direction of the field of a permanent magnet. Let us assume that the circuit is tuned to electrical resonance at all times as the frequency of the applied signal is swept through the Larmor frequency ω_0. We may represent the circuit as shown in Figure 5.

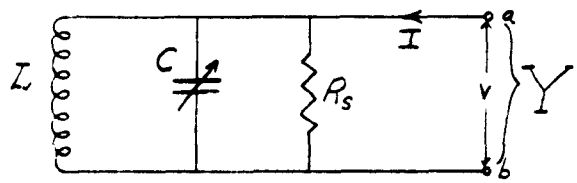

Figure 5

In this circuit, R_S is the equivalent shunt resistance of the tuned circuit, and is composed of the actual resistance of the coil (exclusive of that produced by nuclear magnetic resonance absorption), the resistance of the capacitor and the associated wiring, and the equivalent pure resistive impedance of the resonant circuit formed by L and C. We will assume that the inductance L has the value L_o when all the contributions to it except that of the nuclear susceptibilities are included. Then we may write:

$$L = L_o (1 + 4\pi\xi\chi) \tag{5-1}$$

where ξ is the filling factor representing the fraction of the energy in the coil that is actually stored in the sample. Its value depends on the homogeneity of $\vec{H_1}$ and on the ratio of the volume of the sample to the total volume enclosed by the coil, so it is always less than unity.

The admittance Y, of the resonant circuit is the reciprocal of the impedance and is given by:

$$Y = \frac{1}{R_S} + i\left(\omega C - \frac{1}{\omega L}\right) \tag{5-2}$$

When the circuit is tuned to electrical resonance, $\omega_r C = \frac{1}{\omega_r L}$.
If we replace L by its equivalent expression, equation (5-1), and make use of the fact that $|4\pi\xi\chi| \ll 1$, we may rewrite the admittance at electrical resonance as:

$$Y = \frac{1}{R_S} + i\frac{4\pi\xi\chi}{\omega_r L_o} \tag{5-3}$$

We have already found that χ vanishes except when $\omega_r \cong \omega_o$, so when this condition is not fulfilled the input admittance of the circuit is simply $1/R_S$. When $\omega_r \cong \omega_o$, we must include the effect produced by χ. In this cas

$$Y = \left(\frac{1}{R_S} + \frac{4\pi\xi\chi''}{\omega_o L_o}\right) + i\frac{4\pi\xi\chi'}{\omega_o L_o} \tag{5-4}$$

The imaginary part of the susceptibility, χ'', produces a small change in the input conductance, $G_o = \frac{1}{R_S}$, of the tuned circuit. Thus the experimental problem simply involves the detection of a small increase in the conductance:

$$(5\text{-}5) \qquad \Delta G = \frac{4\pi\xi\chi''}{\omega_o L_o}$$

The effect of χ' is to shift the resonant frequency slightly. It can be shown that this shift is:

$$(5\text{-}6) \qquad \Delta \nu_r = \frac{\Delta\omega_r}{2\pi} = 2\pi\xi\chi'\nu_r \qquad\qquad \nu_r = \frac{1}{2\pi\sqrt{LC}} \text{ cycles/sec.}$$

It is possible to detect either the effects of χ' or χ'' by the proper choice of the experimental conditions. Let us assume that the circuit of Figure 5 is supplied with a constant current I. The voltage developed across the terminals a-b will be:

$$(5\text{-}7) \qquad V = \frac{I}{Y} \cong I R_S \left(1 - i\,\frac{4\pi\xi\chi R_S}{\omega_o L_o}\right)$$

or

$$(5\text{-}8) \qquad V \cong V_o \left[(1 - 4\pi\xi Q_o \chi'') - i\,4\pi\xi Q_o \chi'\right]$$

where $V_o = I R_S$, and $Q_o = \frac{R_S}{\omega_o L_o}$. If the frequency of the applied current is swept through the Larmor frequency with the circuit maintained at electrical resonance at all times, the voltage across the circuit will decrease slightly at and around the Larmor frequency. In actual practice the strong magnetic field is modulated with a low-frequency component which has a magnitude of a few guass. This introduces a periodic variation in the Larmor frequency of the nuclei. The voltage developed across the tuned circuit will vary periodically as the Larmor frequency is swept back and forth through the electrical resonant frequency, and the voltage can be detected and amplified by ordinary electronic methods. If the amplified voltage is then applied to the vertical plates of an oscilloscope, the oscilloscope trace will reproduce the signal appearing across the tuned circuit.

Equation (5-8) shows that around the resonance frequency V will differ from V_0 in amplitude by an amount proportional to χ'' and will differ in phase by an amount proportional to χ'. Each effect is best studied independently, so a way must be found to separate the two. One method frequently used is that of a bridge circuit. The signal from the current source is fed to both halves of the bridge, one containing the sample coil and the other containing a dummy coil, all other components remaining the same. The voltages developed the two tuned circuits are recombined before being amplified. The phases and amplitudes of the two signals can then be adjusted so that the resulting signal is proportional to either χ' or χ'' independently. Such methods are described by Pake (P-3) and Bloembergen (B-2, B-3), and will not be considered further here.

The method used in this research is that first developed by Pound and Knight (P-5). In their radiofrequency spectrometer the sample is placed in the coil of the tank circuit of an oscillator. The oscillation level is kept very low and under this condition it becomes very sensitive to changes in the conductance of the tank circuit. The frequency of the oscillator is varied by changing the capacitance of the tank circuit. The strong magnetic field is modulated in the same manner as was previously mentioned, so the Larmor frequency of the sample nuclei is swept back and forth through the electrical resonance frequency of the oscillator. This yields a periodic variation of the oscillation level, which under ordinary conditions is determined only by χ''.

6. <u>The oscillator as a detector</u>. The oscillator is now serving in a dual capacity, as a power source for the radiation field and also as a detector of nuclear magnetic resonance absorption. A fairly detailed treatment of its operation is thus required, and for this treatment we will follow Watkins'

analysis of the circuits (W-1). The basic circuit of the oscillator is given below:

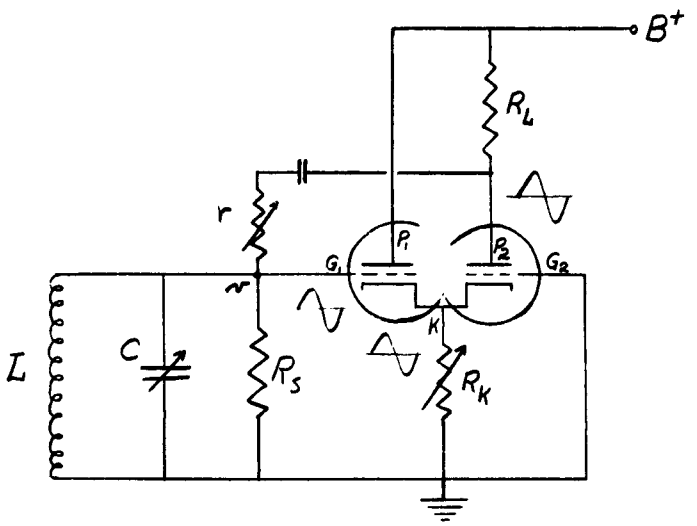

Figure 6.

The operation of the oscillator can be described qualitatively as follows. An oscillating voltage present at G_1 will produce an oscillating voltage across R_K by controlling the current through the first half of the oscillator tube. The voltage at K will be in phase with the applied voltage at G_1. Since the cathode is common to both halves of the tube, and G_2 is kept at ground potential, the voltage at P_2 will also be in phase with G_1, as shown by the waveforms. Thus the voltage fed back through r will be in phase with the voltage already present at G_1 and will sustain the oscillations. By proper adjustment of r and R_K, the feedback is made just sufficient to maintain the oscillations at a very low level.

In order to give a quantitative description of the operation of this circuit, it will first be necessary to transform it into its equivalent

constant current generator circuit. This has been done in two steps, Figure 7.

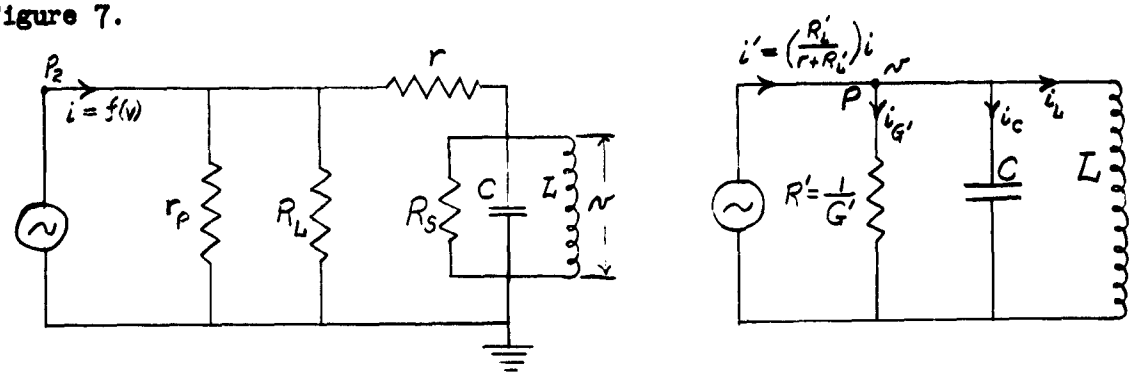

(a) (b)

$i = f(v)$ = the equivalent constant-current generator for the second half of the oscillator tube.

r_p = the internal plate resistance of the second half of the tube, a characteristic of the tube only.

$$R_L' = \frac{r_p R_L}{r_p + R_L} \qquad G' = \frac{1}{R_S} + \frac{1}{r + R_L'}$$

R_S = the equivalent shunt resistance of the tuned circuit.

Figure 7.

Figure 7 (a) is the equivalent circuit of the oscillator as it appears from P_2. We have already pointed out that the current through the second half of the tube will be determined by the potential v, applied to G. It is very difficult to determine an explicit relationship for i because of the complicated nature of the circuit. We shall later assume that it may be represented as a power series in v.

In Figure 7 (b), the equivalent circuit has been further simplified by replacing the original current generator i by another generator i' applied directly across the tuned circuit. The relation between i and i' has then been determined by adjusting the value of i' so that it produces the same current through the tuned circuit as that produced by i in Figure 7 (a).

The differential equation for the oscillator circuit can now be written in terms of the circuit of Figure 7(b). We will express this equation in terms of the total current flowing out of the point P, which must of course be zero. Thus:

(6-1) $$i_C + i_{G'} + i_L - i' = 0$$

or

(6-2) $$C\frac{dv}{dt} + G'v + \frac{1}{L}\int v\,dt - \frac{R_L'}{r+R_L'} f(v) = 0$$

Now let us expand $i = f(v)$ as a power series in v.

(6-3) $$f(v) = a_1 v + a_2 v^2 + a_3 v^3 + \ldots .$$

and use the following substitutions to simplify equation (6-2):

(6-4)
(a) $X = \int v\,dt$
(b) $\frac{1}{LC} = \omega_r^2$
(c) $\frac{1}{C}\left(G' - a_1 \frac{R_L'}{r+R_L'}\right) = K_1$
(d) $\frac{a_2 R_L'}{C(r+R_L')} = K_2$
(e) $\frac{a_3 R_L'}{C(r+R_L')} = K_3$

Equation (6-2) now becomes:

(6-5) $$\ddot{X} + K_1\dot{X} + \omega_r^2 X - K_2\dot{X}^2 - K_3\dot{X}^3 - \ldots = 0$$

In the presence of resonance absorption by the sample, the shunt conductance $G = \frac{1}{R_S}$, will change. Since we are modulating the field at a low frequency, the variation in G will be periodic at the modulation frequency. Let us assume that this variation will be sinusoidal. For broad lines and a modulation amplitude appreciably less than the line width this assumption will be approximately correct. Then:

(6-6) $$G'(t) = G' + \Delta G \cos \omega_m t$$

ΔG will now have not the value given by equation (5-5), but some smaller value, actually one-half the peak-to-peak variation in G over one cycle of the modulation frequency. Insertion of this result into equation (6-5) gives us the final form for the differential equation:

$$(6\text{-}7)\quad \ddot{x} + K_1\left(1 + \frac{\Delta G}{C K_1}\cos \omega_m t\right)\dot{x} + \omega_r^2 x - K_2\dot{x}^2 - K_3\dot{x}^3 - \ldots = 0$$

Watkins assumes that the solution will be of the form:

$$(6\text{-}8)\quad x = [b + a\cos(\omega_m t - \phi)]\cos \omega t$$

where b, a, and ϕ are constants to be evaluated in terms of the experimental conditions. The actual solution of the equation and the evaluation of the constants are quite tedious, so we will give only the final result, as determined by Watkins. He finds that the solution (equation (6-8)) is not rigorously correct but will be highly accurate approximation for the usual conditions of small modulation amplitude and low oscillation levels. Therefore the voltage across the tuned circuit, considering that $\omega_m/\omega_r \ll 1$, can be written as:

$$(6\text{-}9a)\quad v = \dot{x} = [\hat{E}_g + \Delta E_g \cos(\omega_m t - \phi)]\sin \omega_r t$$

$$(6\text{-}9b)\quad \text{where } \hat{E}_g = -\omega_r b$$

$$(6\text{-}9c)\quad \Delta E_g = -\frac{A_1 \cos\phi}{\hat{E}_g}\Delta G$$

$$(6\text{-}9d)\quad \phi = \tan^{-1}\left(\frac{2\omega_m}{\Delta\omega}\right)$$

and

$$(6\text{-}9e)\quad \Delta\omega = A_2 \hat{E}_g^2$$

We have simplified these expressions by including in the constant factors A_1 and A_2 the values of the circuit elements and the coefficients from the power series expansion for $f(v)$, since these terms are held constant at least during the course of an experimental run.

In the equations (6-9), $\hat{E}_g$ is one-half the peak radiofrequency voltage across the tuned circuit when ω_r, the electrical resonance frequency, is unequal to ω_o, the Larmor frequency. It can be seen from equation (6-9b) to be a function of the oscillator frequency, and can thus be expected to vary as the oscillator frequency is swept through the Larmor frequency. This effect can be at least partially compensated by a method which will be described in Part III. We will assume for the present that $\hat{E}_g$ is constant over the range of frequencies within which resonance absorption takes place. For a particular run, the rf amplitude will be determined by adjustment of the proper controls.

ΔE_g represents the amplitude of the modulation which is superimposed on the rf amplitude by the presence of nuclear resonance absorption. It will thus vary at the same frequency as the field modulation, and is proportional to ΔE_g, as we should expect. Equation (6-9c) shows that it is also affected by any variations in $\hat{E}_g$ and ϕ. We have previously assumed that, excluding possible effects caused by resonance absorption, $\hat{E}_g$ will be constant, and from equation (6-9e), ϕ will also be constant over the frequency range covered by the absorption line. However, should $\hat{E}_g$ vary appreciably as the line is traversed, ΔE_g will no longer be a faithful reproduction of the line shape as measured by ΔG. Such a situation is theoretically possible if the absorption line being measured is particularly strong compared to the average rf voltage E_g.

The angle ϕ represents a particularly important and interesting phenomenon from the standpoint of experimental technique. It shows that the amplitude modulation produced by the sample is not necessarily in phase with the applied field modulation. In general there is a phase lag, $0 < \phi \leq 90°$, which is determined by the oscillation level, $\hat{E}_g$ (equations (6-9d and e).

Thus the phase-sensitive detector (discussed in Part III), which must be adjusted to the phase of the absorption-induced modulation, must be readjusted for each new set of experimental conditions. Furthermore, any change in ϕ during the course of a run will produce distortion in the line shape both by its effect on ΔE_g (equation (6-9c)) and its effect on the adjustment of the phase-sensitive detector.

We may summarize the remainder of Watkins conclusions as follows. The sensitivity of the oscillator as a detector of resonance absorption will be decreased from its optimum value by high oscillation levels which reduce the ratio of $\Delta E_g/\Delta G$ (equation (6-9c)). On the other hand very low oscillation levels will reduce $\Delta\omega$, resulting again in lowered sensitivity (by decreasing $\cos\phi$) and in phase shifts which will distort the line shape. Except for these extreme cases the sensitivity of the oscillator is quite good; therefore the signal-to-noise ratio obtainable in this apparatus will be determined by the oscillator circuit alone.

C. Width and Fine Structure of the Absorption Line.

1. General. The width of the absorption line produced by an isolated nucleus in a magnetic field is very small, being determined by the ratio H_1/H_0 which is usually less than 10^{-4}. However, this natural width is usually masked by other factors leading to line broadening. In the samples studied in this investigation only two such sources are encountered under ordinary conditions: field inhomogeneity and spin-spin interactions. The spin-spin interactions predominate when they are present.

In the majority of solids, the nuclei are fixed in space, especially at low temperatures when the thermal energies are small. Under such conditions the field produced at one nucleus by the magnetic moments of neighbor-

ing nuclei will be maximized. These local fields will add to the externally applied field, dispersing the total field by amounts which depend on the nuclear configuration. The observed line shapes will thus be quite broad. If the nuclei are in motion, the local fields will be reduced because they will at least partially average out over a given period of time. The extreme case of nuclear motion will of course be that for which the sample is a liquid or a gas, in which the thermal motion of the molecules is very rapid and completely random. The line width obtained from such samples will be determined solely by field inhomogeneity, all spin-spin interactions averaging out over the period of one cycle of the applied radiation field. However, there is also an intermediate case which normally occurs only in solids. Although translational motion is prohibited, there is the possibility that the nuclei may move about a fixed point. Such motion includes rotation, of the whole molecule or of a particular group about a bond, tunneling, or rotational oscillation. In such cases, the local field will frequently be reduced from that expected for a completely rigid configuration, but it will not necessarily average out to zero. The observed line shape and width will then be intermediate between that obtained from a rigid configuration and the narrow line obtained from liquids. It is interesting to note that the frequency of such motion need not be very great to produce changes in the line shape. Bloembergen (B-2, B-3) states that the line width will be affected by motion of a frequency ν for which $h\nu$ is of the same magnitude as the splitting of the energy levels which is produced by spin-spin interactions. Since the splitting is usually of the order of 10 to 20 guass at the most, the frequency of motion required to cause changes in the line shape is usually less than 80 Kc.

The observed shape and width of the absorption line will depend on the nuclear configuration. For the simple cases of two or three nuclei which are relatively isolated from the other magnetically active nuclei, the line shape

may exhibit fine structure; and the fine structure may give considerable information about the internuclear distances and orientations. However, more complex arrangements of the nuclei will not show fine structure. Furthermore, the existence of fine structure may be masked by the comulative effect of more distant nuclei. It is then necessary to resort to the quantity known as the second moment in order to compare the experimentally observed lines with those predicted by theory. The theoretical second moment can be rigorously calculated from an expression derived by Van Vleck, which will be presented in the next section.

In this investigation we have been dealing primarily with the protons in methyl groups, which form a triangular configuration. The remainder of part C will be devoted to the derivation of the line shapes and second moments to be expected from such a configuration, both for rigid crystalline lattices and for configurations involving certain specific types of motion.

2. The second moment. The second moment of an absorption line is defined as:

$$(2\text{-}1) \quad (\Delta\nu_2)^2 = \frac{\int_{-\infty}^{\infty}(\nu-\nu_0)^2 f(\nu)\,d\nu}{\int_{-\infty}^{\infty} f(\nu)\,d\nu}$$

where ν_0 is the resonant frequency (Larmor frequency) for the external magnetic field, and $f(\nu)$ is a shape function describing the line. The second moment therefore represents a weighted average over the line shape.

The expression given above is that appropriate to the experimental technique of using a fixed magnetic field and a varying radiation frequency. However, most published work on line shapes has been done using a fixed radio-frequency and a varying magnetic field. Since the resonant frequency is linearly proportional to the external field, the results obtained by one technique can easily be expressed in terms of the other through use of the relation $\nu_0 = \frac{g\mu_0 H_0}{h}$. The second moment is then expressed as:

$$(2\text{-}2)\qquad (\Delta H_2)^2 = \frac{\int_{-\infty}^{\infty}(H-H_0)^2 f(H)\,dH}{\int_{-\infty}^{\infty} f(H)\,dH}$$

The second moment of an experimentally observed line can readily be determined by graphical integration. The experimentally recorded curves give the first derivative of the absorption line, in terms of which the second moment can be written (G-1):

$$(2\text{-}3)\qquad (\Delta H_2)^2 = \frac{\iint (H-H_0)^2 f'(H)\,dH\,dH}{\iint f'(H)\,dH\,dH} = \frac{1}{3}\,\frac{\int_{-\infty}^{\infty}(H-H_0)^3 f'(H)\,dH}{\int_{-\infty}^{\infty}(H-H_0) f'(H)\,dH}$$

The values to be reported here were computed by the use of Simpson's rule, and were determined separately over the two halves of the line as a check on the accuracy of the results.

The experimental second moments can be checked against theoretically computed values which are obtainable from a formula of Van Vleck (V-1). His expression is:

$$(2\text{-}4)\qquad (\Delta H_2)^2 = \tfrac{3}{2} I(I+1) N^{-1} g^2 \mu_0^2 \sum_{i>j} (3\cos^2\theta_{ij} - 1)^2 r_{ij}^{-6} + \tfrac{1}{3} N^{-1} \mu_0^2 \sum_j \sum_f I_f (I_f+1) g_f^2 (3\cos^2\theta_{jf} - 1)^2 r_{jf}^{-6}$$

where:

$$(2\text{-}5)\qquad (\Delta \nu_2)^2 = \frac{g^2\mu_0^2}{h^2} (\Delta H_2)^2$$

In these equations, I and g are the nuclear spin and gyromagnetic ratio for the nuclei which are at resonance; I_f and g_f are the nuclear spin and gyromagnetic ratio for other magnetically significant nuclei in the sample; r_{ab} and θ_{ab} are the internuclear distance between nuclei a and b and the angle between this internuclear direction and the external field. N is the number of nuclei at resonance in the molecule or subgroup to which the spin-spin interactions are considered to be confined. We are considering the

protons in methyl groups, and as approximations we shall consider that there is no interaction between protons of different groups or between protons and other magnetically active nuclei in the sample. Thus we are considering an isolated methyl group, for which $I=\frac{1}{2}$, $g=5.585$, $N=3$, and $\mu_0 = 5.049\times10^{-24}$ erg/gauss. Equation (2-4) now becomes:

$$(2\text{-}6)\quad (\Delta H_2)^2 = 298 \sum_{i>j} (3\cos^2\theta_{ij} - 1)^2 r_{ij}^{-6}$$

where r_{ij} is now given in Ångstrom units.

Equation (2-6) may now be used to calculate a theoretical second moment for any assumed configuration of the methyl group. The angle factor permits the determination of the molecular orientation in single crystals, or it may be averaged for crystal powders. However, its chief importance in this investigation is that it permits the determination of motion of the methyl groups, such motion usually causing a decrease in the theoretical second moment when the angle factor is properly averaged over the motion.

3. Fine structure for a triangular configuration of nuclei - quantum-mechanical treatment. The Hamiltonian operator for a system of three identical nuclei is (A-1):

$$(3\text{-}1)\quad \mathcal{H} = g\mu_0 H_0 \sum_{i=1}^{3} I_{zi} + \sum_{i<j} (\vec{I}_i \cdot \vec{I}_j - 3 I_{zi} I_{zj}) A_{ij}$$

where:

$$(3\text{-}2)\quad A_{ij} = \frac{g^2\mu_0^2}{2 r_{ij}^3} (3\cos^2\theta_{ij} - 1)$$

I_{zi} is the spin operator for the z-component of the ith spin: $\vec{I}_i$ and $\vec{I}_j$ are total spin operators; and θ_{ij} is the angle between $\vec{r}_{ij}$, the vector connecting nuclei i and j, and the external field $\vec{H}_0$, along the z-axis. We may treat this problem by perturbation theory, considering the spin-spin interaction term as a perturbation. The wave functions for the unperturbed

energy levels will then be separable into products of three functions, each of which is a function containing the variables for only one of the spins. For nuclei of spin $\frac{1}{2}$, the j-component of the spin may have only two values. We shall designate the two possible wave functions $\alpha(i)$ and $\beta(i)$, where the following operators rules apply.

$$I_{jk}\,\alpha(k) = \tfrac{1}{2}\alpha(k) \qquad I_{jk}\,\beta(k) = -\tfrac{1}{2}\beta(k)$$

(3-3)
$$I_{xk}\,\alpha(k) = \tfrac{1}{2}\beta(k) \qquad I_{xk}\,\beta(k) = \tfrac{1}{2}\alpha(k)$$

$$I_{yk}\,\alpha(k) = \tfrac{i}{2}\beta(k) \qquad I_{yk}\,\beta(k) = -\tfrac{i}{2}\alpha(k)$$

The unperturbed energy levels are then found from:

(3-4) $$\mathcal{H}^{\circ}\psi_m^{\circ} = g\mu_0 H_0 \sum_{k=1}^{3} I_{jk}\,\psi_m^{\circ} = E_m^{\circ}\,\psi_m^{\circ}$$

Therefore:

(3-5) $$E_m^{\circ} = g\mu_0 H_0 m \qquad m = 3/2,\ 1/2,\ -1/2,\ -3/2$$

and the eigenfunctions are:

(3-6)
$$m = 3/2 \qquad \psi_{3/2}^{\circ} = \alpha(1)\alpha(2)\alpha(3)$$

$$m = 1/2 \qquad (\psi_{1/2}^{\circ})_1 = \alpha(1)\alpha(2)\beta(3)$$

$$(\psi_{1/2}^{\circ})_2 = \alpha(1)\beta(2)\alpha(3)$$

$$(\psi_{1/2}^{\circ})_3 = \beta(1)\alpha(2)\alpha(3)$$

with a similar set for $m = -1/2$ and $m = -3/2$.

Application of the perturbation leads to the following matrix for the elements $(\psi_m^{o*}, \mathcal{H}^{(1)}\psi_m^{o})$.

(3-7)
$$\begin{matrix} m = 3/2 \\ m = 1/2 \\ \\ \end{matrix} \begin{pmatrix} -\tfrac{1}{2}(A_{12}+A_{13}+A_{23}) & 0 & 0 & 0 \\ 0 & \tfrac{1}{2}(-A_{12}+A_{13}+A_{23}) & \tfrac{1}{2}A_{23} & \tfrac{1}{2}A_{13} \\ 0 & \tfrac{1}{2}A_{23} & \tfrac{1}{2}(A_{12}-A_{13}+A_{23}) & \tfrac{1}{2}A_{12} \\ 0 & \tfrac{1}{2}A_{13} & \tfrac{1}{2}A_{12} & \tfrac{1}{2}(A_{12}+A_{13}-A_{23}) \end{pmatrix}$$

The matrix for $m = -1/2$ and $m = -3/2$ is identical. The perturbation energies are

obtained by solving the secular equation of the matrix; they are found to be:

$$E^{(1)}_{\pm 3/2} = -2x$$

$$E^{(1)}_{\pm 1/2} = 0,\ x+y,\ x-y \tag{3-8}$$

where:

$$x = \tfrac{1}{4}(A_{12}+A_{13}+A_{23})$$

$$y = \tfrac{1}{4}\left[9(A_{12}^2+A_{13}^2+A_{23}^2) - 6(A_{12}A_{13}+A_{12}A_{23}+A_{13}A_{23})\right]^{1/2} \tag{3-9}$$

The wave functions ψ_m for the perturbed energy levels can also be evaluated, and are expressed as:

$$m = 3/2 \quad \psi_{3/2} = \alpha(1)\alpha(2)\alpha(3)$$

$$m = 1/2 \quad (\psi_{1/2})_j = K_{1j}\alpha(1)\alpha(2)\beta(3) + K_{2j}\alpha(1)\beta(2)\alpha(3) + K_{3j}\beta(1)\alpha(2)\alpha(3) \tag{3-10}$$

where

$$K_{1j} = \frac{(A_{12}-A_{13})(A_{13}-A_{23}) - 2A_{13}(E^{(1)}_{\pm 1/2})_j}{N_j}.$$

$$K_{2j} = \frac{(A_{12}-A_{13})(A_{23}-A_{12}) - 2A_{12}(E^{(1)}_{\pm 1/2})_j}{N_j} \tag{3-11}$$

$$K_{3j} = \frac{(A_{12}-A_{13})^2 + 4A_{23}(E^{(1)}_{\pm 1/2})_j - 4(E^{(1)}_{\pm 1/2})_j^2}{N_j}$$

N_j is a normalization factor determined from the fact that $\sum_{i=1}^{3} K_{ij}^2 = 1$; and $(E^{(1)}_{\pm 1/2})_j$ is given by the values of equation (3-8).

The transition probabilities are proportional to $|(\psi_n^*, I_x\, \psi_m)|^2$, where $I_x = \sum_{k=1}^{3} I_{xk}$. Figure 8 illustrates the energy levels and the allowed transitions for this three-spin system, as determined from the relations given above.

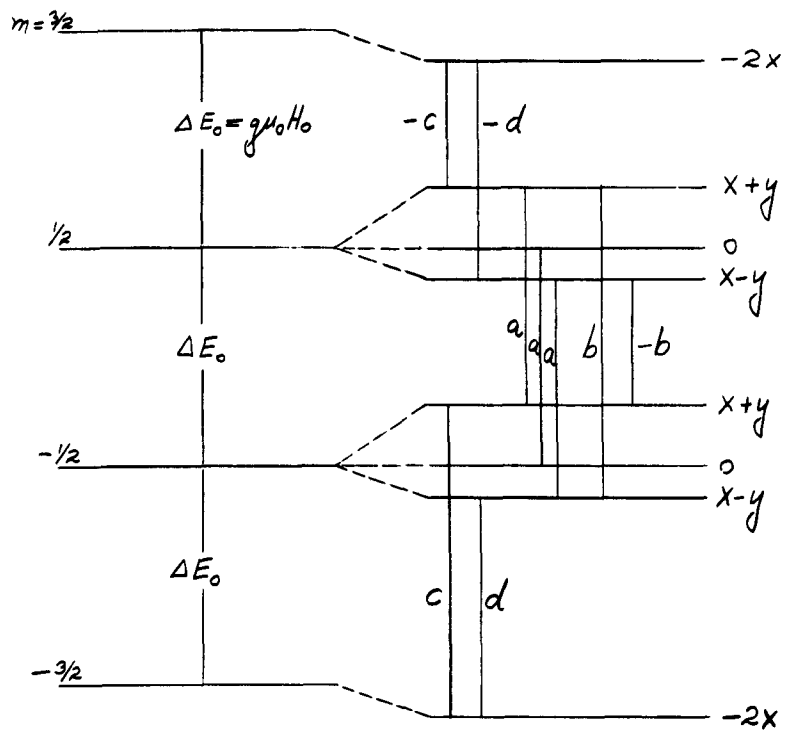

Figure 8.

This energy level diagram is identical with that given by Andrew and Bersohn (A-1). We can see that the single resonance line expected for an isolated nuclear spin will be split into a central line and three pairs of subsidiary lines which will appear at frequency spacings from the central component given by $\Delta\nu = \Delta E/h$. The equivalent spacings in gauss for the fixed-frequency-variable-field technique are given in Table 1, along with the normalized transition probabilities for each pair of fine structure components.

$\Delta\nu \left(= \frac{\Delta E}{h}\right)$	$\Delta H \left(= \frac{h}{g\mu_0}\Delta\nu\right)$	Probability
0	0	$\frac{1}{8}\left(1+3\frac{x^2}{y^2}\right)$
$\pm\frac{2y}{h}$	$\pm\frac{2y}{g\mu_0}$	$\frac{3}{16}\left(1-\frac{x^2}{y^2}\right)$
$\pm\frac{3x+y}{h}$	$\pm\frac{3x+y}{g\mu_0}$	$\frac{1}{8}\left(1+\frac{x}{y}\right)$
$\pm\frac{3x-y}{h}$	$\pm\frac{3x-y}{g\mu_0}$	$\frac{1}{8}\left(1-\frac{x}{y}\right)$

Table I.

Now let us assume that the triangle formed by the nuclei is equilateral, as is the case for a methyl group. The internuclear distances r_{ij} are then identical. If we call this distance R, and make the further substitution of $\mu = \frac{3}{2}\mu_0$ (from the standard definition of $\mu = g\mu_0 I$) and $\alpha = \frac{3}{2}\mu R^{-3}$, we may express X and Y as:

$$X = \mu\alpha\left[\sum_{i>j}(\cos^2\theta_{ij}) - 1\right]$$

$$(3\text{-}12) \qquad Y = \mu\alpha\left[9\sum_{i>j}(\cos^2\theta_{ij})^2 - 6\left(\cos^2\theta_{12}\cos^2\theta_{13} + \cos^2\theta_{12}\cos^2\theta_{23} + \cos^2\theta_{13}\cos^2\theta_{23}\right) - 2\sum_{i<j}(\cos^2\theta_{ij}) + 1\right]^{1/2}$$

For a given value of R, the values of X and Y are seen to be functions of the $\cos^2\theta_{ij}$ only. For single crystals these angle functions will vary with the orientation of the crystal in the field. For rigid groups in polycrystalline material they must be averaged over all possible orientations, and for non-rigid groups they must be averaged over the motion.

4. <u>The line shape and second moment for a rigid equilateral triangle</u>. We wish to determine the line shape and second moment for a rigid nuclear configuration, both for a single crystal and for a polycrystalline material. This may be done directly from equations (3-12) and (2-6) in terms of the functions $\cos^2\theta_{ij}$. However, it is convenient to use the single angle ψ

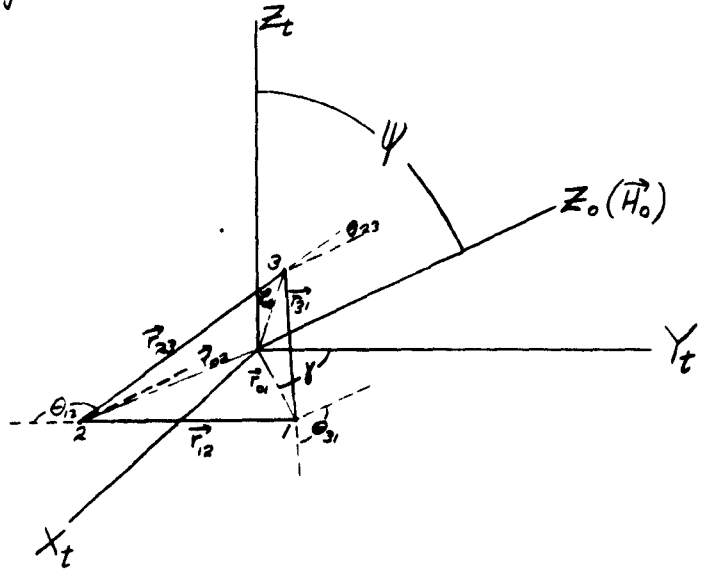

Figure 9.

between the normal to the triangle plane and the strong field , instead of the three angles θ_{ij} . Let us choose a coordinate system X_t-Y_t-Z_t such that the nuclear triangle lies in the X_t-Y_t plane with its center at the origin. The normal to the triangle then lies along Z_t . We will further choose the Y_t axis so that the strong field direction lies in the Y_t-Z_t plane. This is illustrated in Figure 9. The vector $\vec{r}_{ok}$ extends from the origin to the nucleus k . Its magnitude, in terms of the internuclear distance R is equal to $\sqrt{3}R/3$.

If we consider that $\vec{H}_o$ lies along the Z_o -axis of a new coordinate system X_o-Y_o-Z_o , we may consider the transformation from the system X_t-Y_t-Z_t to the new system as a rotation about the X_t axis through the angle ψ . Let us call the unit vectors along the X_t , Y_t , and Z_t axes $\hat{u}_{t1}$, $\hat{u}_{t2}$, and $\hat{u}_{t3}$, respectively. Similarly, $\hat{u}_{o1}$, $\hat{u}_{o2}$, and $\hat{u}_{o3}$ are the unit vectors along X_o , Y_o , and Z_o . Then the relations between the two sets of unit vectors are expressed in terms of a matrix $[M]$, where:

$$(4\text{-}1)\quad [M] = \begin{bmatrix} 1 & 0 & 0 \\ 0 & \cos\psi & -\sin\psi \\ 0 & \sin\psi & \cos\psi \end{bmatrix}$$

and the matrix elements are determined by:

$$(4\text{-}2)\quad \hat{u}_{ok} = \sum_{l=1}^{3} M_{kl}\,\hat{u}_{tl} \quad ; \quad M_{kl} = \hat{u}_{ok}\cdot\hat{u}_{tl}$$

The vectors $\vec{r}_{ij}$ have the form

$$(4\text{-}3)\quad \vec{r}_{ij} = (x_j - x_i)\,\hat{u}_{t1} + (y_j - y_i)\,\hat{u}_{t2}$$

where

$$(4\text{-}4)\quad x_k = \vec{r}_{ok}\cdot\hat{u}_{t1} \qquad y_k = \vec{r}_{ok}\cdot\hat{u}_{t2}$$

In terms of the above relations, the functions $\cos\theta_{ij}$ are expressed as:

$$(4\text{-}5)\quad \cos\theta_{ij} = \frac{\vec{r}_{ij}\cdot\hat{u}_{o3}}{R} = \frac{\sum_{l=1}^{3} M_{3l}\,\vec{r}_{ij}\cdot\hat{u}_{tl}}{R} = \frac{(y_j - y_i)\sin\psi}{R}$$

Evaluation of the components y_k from geometrical considerations in Figure 9 leads to the following set of equations:

$$\cos\theta_{12} = -\tfrac{1}{2}\sin\psi\,(\sin\gamma + \sqrt{3}\cos\gamma)$$

(4-6) $$\cos\theta_{23} = \sin\psi\sin\gamma$$

$$\cos\theta_{31} = \tfrac{1}{2}\sin\psi\,(\sin\gamma - \sqrt{3}\cos\gamma)$$

where γ is the angle giving the azimuth of $\vec{r}_{ok}$ about Y_t . These may now be substituted in equation (3-12), in which case X and y reduce to:

$$X = \mu\alpha\,(\tfrac{1}{2} - \tfrac{3}{2}\cos^2\psi)$$

(4-7) $$y = \mu\alpha\left[\tfrac{27}{4}\sin^4\psi - 3\sin^2\psi + 1\right]^{1/2}$$

Similarly, the expression defining the second moment (equation (2-6)) becomes:

(4-8) $$(\Delta H_2)^2 = \frac{298}{R^6} \times 3\left[\frac{27}{8}\sin^4\psi - 3\sin^2\psi + 1\right] \text{ gauss}^2$$

Equations (4-7) and (4-8) show that the line shape and second moment for an isolated nuclear triangle will vary markedly with the orientation of the triangle in a magnetic field. Thus studies of single crystals should lead to the determination of molecular orientations as well as the internuclear distances, unless the fine structure of the absorption line is masked by the effects of intermolecular broadening.

We shall be concerned with polycrystalline materials in which the orientation of the crystal grains is distributed uniformly over all directions. We must therefore average over ψ for each of the component lines and also in the second moment expression. The fraction of groups for which ψ lies in the range $d\psi$ is $\sin\psi d\psi$ or $d(-\cos\psi)$. For a single crystal line component ΔH , having probability $p(\psi)$ (Table 1), the powder line shape is given by:

(4-9) $$F(\Delta H) = p(\psi)\,\frac{d(-\cos\psi)}{d(\Delta H)}$$

$p(\psi)$ and $\cos\psi$ may be expressed in terms of ΔH through the use of equations (4-7) and the last two columns of Table 1, and $F(\Delta H)$ may then be evaluated for each component line. This has been done by Andrew and Bersohn (A-1), but the expressions they give are not in a convenient form. A slightly different choice of substitutions leads to the following set of functions.

(a) The component line at $\Delta H = 0$ remains unchanged.

(b) The component line at $\Delta H = \frac{4}{3\mu}$ gives:

$$F_1(\Delta H) = -\frac{(\gamma_1 - 1)^2}{24\,\gamma_1(\Delta H)(7+2\gamma_1)^{1/2}} \quad , \quad \alpha > \Delta H > \left(\tfrac{2}{3}\right)^{1/2}\alpha \tag{4-10a}$$

$$F_2(\Delta H) = \frac{(\gamma_1 + 1)^2}{24\,\gamma_1(\Delta H)(7-2\gamma_1)^{1/2}} \quad , \quad \left(\tfrac{2}{3}\right)^{1/2}\alpha < \Delta H < \left(\tfrac{19}{4}\right)^{1/2}\alpha \tag{4-10b}$$

where

$$\gamma_1 = \left[3\left(\frac{\Delta H}{\alpha}\right)^2 - 2\right]^{1/2} \tag{4-11}$$

The dual set of functions with different sets of limits results from the fact that the single crystal line component has double values in the range $\left(\frac{2}{3}\right)^{1/2}\alpha < \Delta H < \alpha$.

(c) For the line component $\Delta H = \frac{3x+4}{2\mu}$

$$F_3(\Delta H) = \frac{\gamma_2 - 1}{12\alpha\,\gamma_2\,\rho_1^{1/2}} \qquad -\alpha < \Delta H < \left(\frac{\sqrt{19}+3}{4}\right)\alpha \tag{4-12}$$

where

$$\gamma_2 = \left[3\left(\frac{\Delta H}{\alpha}\right)^2 + 6\left(\frac{\Delta H}{\alpha}\right) + 4\right]^{1/2} \tag{4-13}$$

$$\rho_1 = 1 - 6\left(\frac{\Delta H}{\alpha}\right) + 2\gamma_2 \tag{4-14}$$

(d) For the line component $\Delta H = \frac{3x-4}{2\mu}$

(4-15) $$F_4(\Delta H) = \frac{\gamma_2 + 1}{12\alpha\,\gamma_2\,\rho_2^{1/2}} \qquad -2\alpha < \Delta H < -\left(\frac{\sqrt{19}-3}{4}\right)\alpha$$

where γ_2 is given by equation (4-13), and:

(4-16) $$\rho_2 = 1 - 6\left(\frac{\Delta H}{\alpha}\right) - 2\gamma_2$$

(e) The functions for the line components $\Delta H = -\frac{y}{\mu}$, $-(3x+y)/2\mu$, $-(3x-y)/2\mu$, are obtained from the above results by replacing ΔH by $-\Delta H$ in the equations above. Each line component has a symmetrical counterpart and the overall line shape is symmetrical about the unperturbed resonance point.

The overall line shape is obtained by taking the sum of all the component lines. The actual spacings between the peaks of the component lines will depend on the internuclear distance R because of its effect on α. Therefore it is convenient to plot $\alpha F(\Delta H)$ vs. $\left(\frac{\Delta H}{\alpha}\right)$. We then obtain a "universal" line shape which is valid for any value of R. This shape is shown in Figure 10.

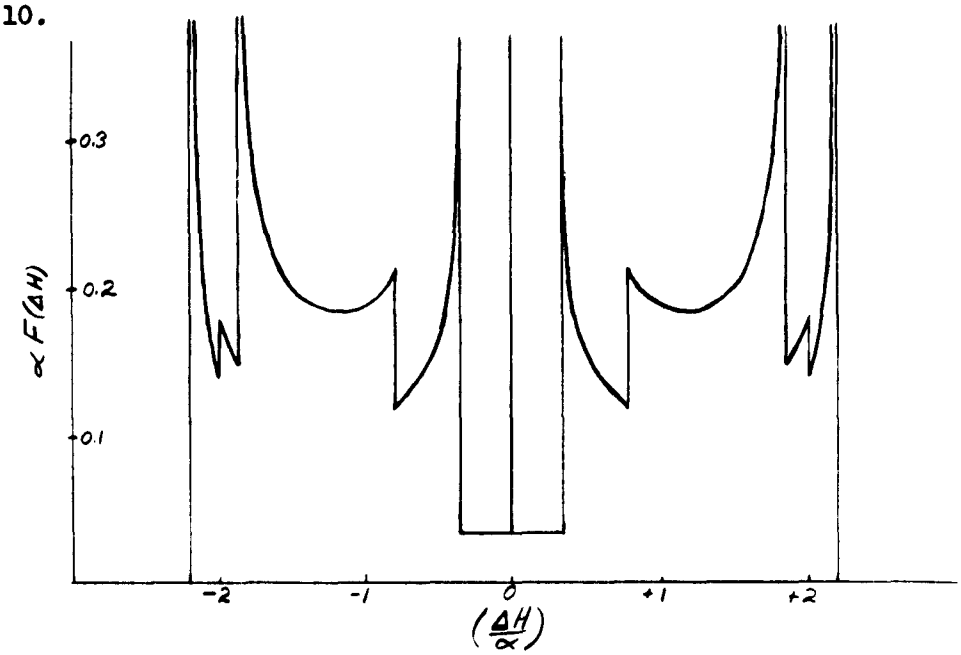

Figure 10

The second moment for a polycrystalline material is obtained by averaging over the function of ψ in brackets in equation (4-8). Thus:

$$(4\text{-}17)\quad \overline{\left[\frac{27}{8}\sin^4\psi - 3\sin^2\psi + 1\right]}^{sphere} = \frac{1}{2}\int_0^{\pi}\left[\frac{27}{8}\sin^4\psi - 3\sin^2\psi + 1\right]\sin\psi\, d\psi = 4/5$$

Substituting this result into equation (4-8) we obtain:

$$(4\text{-}18)\quad \langle \Delta H_2^2 \rangle = \frac{298}{R^6}\left(\frac{12}{5}\right) \text{gauss}^2$$

5. The effects of motion - general relationships. In the previous section, we have considered that the nuclei are fixed in space. However, this assumption may not be valid. We must now consider the effect of motion of the nuclei, which will affect the functions $\cos^2\theta_{ij}$ in equation (2-6) for the second moment and equations (3-12) for X and y. In this section we shall derive expressions for $\cos^2\theta_{ij}$ which may be used to introduce the effects of motions.

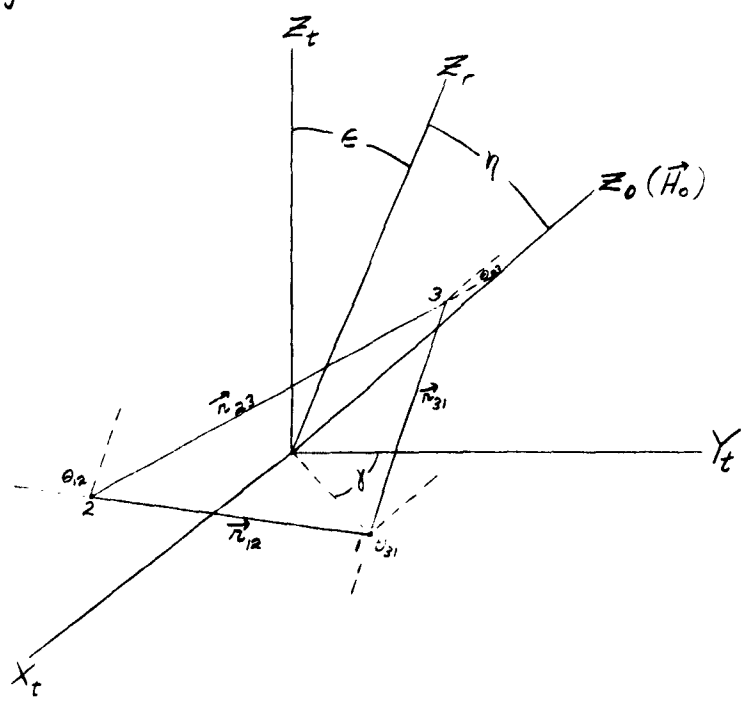

Figure 11.

Let us consider Figure 11. Once again we choose the Z_t axis to be along the normal to the triangle plane so that the nuclei lie in the X_t-Y_t plane with the center of the triangle at the origin. The directions of X_t and Y_t in their plane will be determined later. However, γ as before is the angle between Y_t and the vector $\vec{r}_{01}$. Z_r is the axis about which rotation takes place and may have any orientation with respect to Z_t and Z_o (the external field direction).

The vectors $\vec{r}_{ij}$ are determined by the same relations as before (equations (4-3) and 4-4)), and $\cos\Theta_{ij}$ is given by:

$$\cos\Theta_{ij} = \frac{\vec{r}_{ij}\cdot\hat{u}_{03}}{R} \tag{5-1}$$

where $\hat{u}_{03}$ is the unit vector along Z_o . We must now find the relations between the sets of unit vectors $\hat{u}_{tp}$ and $\hat{u}_{ok}$. This will be done as before in terms of a matrix transformation, this time involving four sets of transformations, as follows:

(a) A rotation through the angle α about the space-fixed axis Z_o to bring the axis X_o (along the axis of the sample coil) to a new position X_a which is perpendicular to both Z_o and Z_r .

$$\hat{u}_{a\ell} = \sum_{k=1}^{3} A_{\ell k}\,\hat{u}_{ok} \qquad A_{\ell k} = \hat{u}_{a\ell}\cdot\hat{u}_{ok} \tag{5-2}$$

$$[A] = \begin{bmatrix} \cos\alpha & \sin\alpha & 0 \\ -\sin\alpha & \cos\alpha & 0 \\ 0 & 0 & 1 \end{bmatrix} \tag{5-3}$$

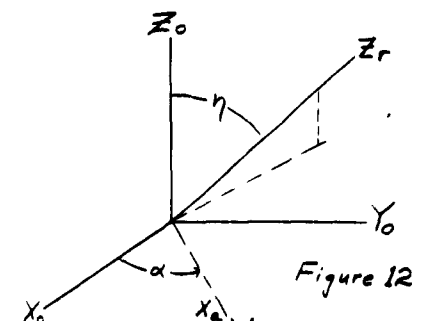

Figure 12

(b) A rotation through the angle η about axis X_a to bring Z_o into coincidence with Z_r .

$$\hat{u}_{rm} = \sum_{l=1}^{3} B_{ml}\,\hat{u}_{al} \tag{5-4}$$

$$B_{ml} = \hat{u}_{rm}\cdot\hat{u}_{al}$$

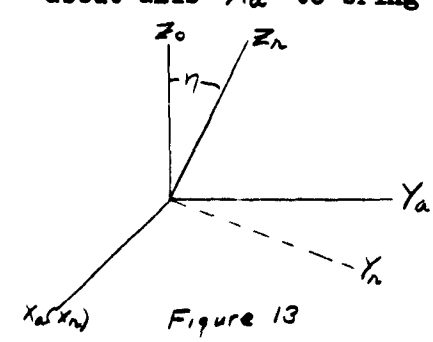

Figure 13

$$(5\text{-}5)\quad [B] = \begin{bmatrix} 1 & 0 & 0 \\ 0 & \cos\eta & \sin\eta \\ 0 & -\sin\eta & \cos\eta \end{bmatrix}$$

(c) Rotation through angle β about the axis Z_r, to bring X_r into position X_b, perpendicular to both Z_r and Z_t.

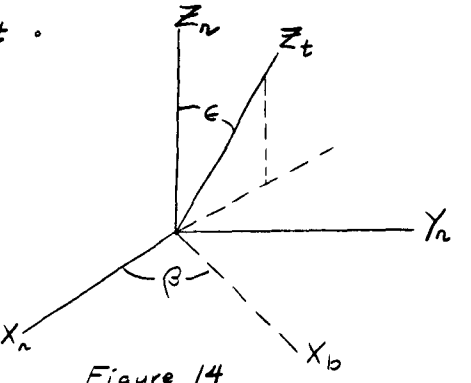

Figure 14

$$(5\text{-}6)\quad \hat{u}_{bn} = \sum_{m=1}^{3} C_{nm}\,\hat{u}_{rm} \;;\; C_{nm} = \hat{u}_{bn}\cdot\hat{u}_{rm}$$

$$(5\text{-}7)\quad [C] = \begin{bmatrix} \cos\beta & \sin\beta & 0 \\ -\sin\beta & \cos\beta & 0 \\ 0 & 0 & 1 \end{bmatrix}$$

(d) Rotation through angle ϵ about X_b to bring Z_r into coincidence with Z_t. Thus X_t is the same as X_b.

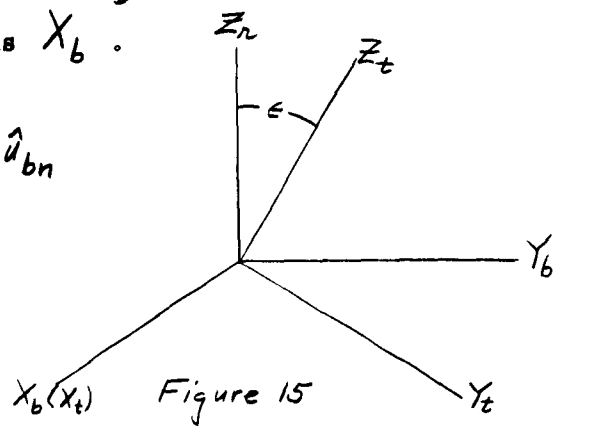

Figure 15

$$(5\text{-}8)\quad \hat{u}_{tp} = \sum_{n=1}^{3} D_{pn}\,\hat{u}_{bn} \;;\; D_{pn} = \hat{u}_{tp}\cdot\hat{u}_{bn}$$

$$(5\text{-}9)\quad [D] = \begin{bmatrix} 1 & 0 & 0 \\ 0 & \cos\epsilon & -\sin\epsilon \\ 0 & \sin\epsilon & \cos\epsilon \end{bmatrix}$$

The overall transformation is now obtained from equations (5-2), (5-4), (5-6), and (5-8).

$$(5\text{-}10)\quad \hat{u}_{tp} = \sum_{k=1}^{3} E_{pk}\,\hat{u}_{ok} \qquad E_{pk} = \sum_{n=1}^{3}\sum_{m=1}^{3}\sum_{l=1}^{3}\sum_{k=1}^{3} D_{pn}\,C_{nm}\,B_{ml}\,A_{lk}$$

and the matrix $[E] = [D][C][B][A]$. Thus:

$$(5\text{-}11)\quad [E] = \begin{bmatrix} \cos\alpha\cos\beta - \sin\alpha\sin\beta\cos\eta & \sin\alpha\cos\beta + \cos\alpha\sin\beta\cos\eta & \sin\beta\sin\eta \\ \sin\epsilon\sin\alpha\sin\eta - \cos\epsilon(\cos\alpha\sin\beta + \sin\alpha\cos\beta\cos\eta & \cos\epsilon(\cos\alpha\cos\beta\cos\eta - \sin\alpha\sin\beta) - \sin\epsilon\cos\alpha\sin\eta & \cos\epsilon\cos\beta\sin\eta + \sin\epsilon\cos\eta \\ \sin\epsilon(\cos\alpha\sin\beta + \sin\alpha\cos\beta\cos\eta) + \cos\epsilon\sin\alpha\sin\eta & \sin\epsilon(\sin\alpha\sin\beta - \cos\alpha\cos\beta\cos\eta) - \cos\epsilon\cos\alpha\sin\eta & \cos\epsilon\cos\eta - \sin\epsilon\cos\beta\sin\eta \end{bmatrix}$$

With the aid of the matrix and equation (4-3), equation (5-1) now becomes:

$$(5\text{-}12)\quad \cos\Theta_{ij} = \frac{(x_j - x_i)}{R} E_{13} + \frac{(y_j - y_i)}{R} E_{23}$$

The factors x_k and y_k may be determined from equation (4-4) in terms of the angle γ, leading finally to the following set of equations.

$$\cos\Theta_{12} = \tfrac{1}{2}\{(\cos\gamma - \sqrt{3}\sin\gamma)\sin\beta\sin\eta - (\sin\gamma + \sqrt{3}\cos\gamma)(\cos\epsilon\cos\beta\sin\eta + \sin\epsilon\cos\eta)\}$$

$$(5\text{-}13)\quad \cos\Theta_{23} = \sin\gamma(\cos\epsilon\cos\beta\sin\eta + \sin\epsilon\cos\eta) - \cos\gamma\sin\beta\sin\eta$$

$$\cos\Theta_{31} = \tfrac{1}{2}\{(\cos\gamma + \sqrt{3}\sin\gamma)\sin\beta\sin\eta - (\sin\gamma - \sqrt{3}\cos\gamma)(\cos\epsilon\cos\beta\sin\eta + \sin\epsilon\cos\eta)\}$$

Both the second moment expression and the equations for X and Y involve $\cos^2\Theta_{ij}$. Therefore the effect of motion on these quantities is determined by averaging $\cos^2\Theta_{ij}$ over the type of motion postulated. We shall do this for several cases in the following section.

6. <u>The effects of motion - specific cases</u>.

Case I. We shall consider first the case of the nuclear triangle rotating about some axis other than its normal. Such a situation could occur for a molecule like CH_3SiCl_3 rotating about any axis through its center of mass. This corresponds to a rotation about the axis Z_r in Figures 11 and 14, and thus means that the angle β is a function of time. We therefore express β as $\beta_0 + \omega t$, and average the functions $\cos^2\Theta_{ij}$ over $t = \frac{2\pi}{\omega}$. In taking this average we need only to know that $\overline{\cos^2\beta}^t = \overline{\sin^2\beta}^t = \frac{1}{2}$, $\overline{\cos\beta}^t = \overline{\sin\beta}^t = \overline{\sin\beta\cos\beta}^t = 0$. Equations (5-13) then yield:

$$\overline{\cos^2\Theta_{12}}^t = \tfrac{1}{8}\left[4(1-\cos^2\eta) - \sin^2\epsilon(1-3\cos^2\eta)(1+2\cos^2\gamma) - 2\sqrt{3}\sin\gamma\cos\gamma\sin^2\epsilon(1-3\cos^2\eta)\right]$$

$$(6\text{-}1)\quad \overline{\cos^2\Theta_{23}}^t = \tfrac{1}{2}\left[(1-\cos^2\eta) - \sin^2\gamma\sin^2\epsilon(1-3\cos^2\eta)\right]$$

$$\overline{\cos^2\Theta_{31}}^t = \tfrac{1}{8}\left[4(1-\cos^2\eta) - \sin^2\epsilon(1-3\cos^2\eta)(1+2\cos^2\gamma) + 2\sqrt{3}\sin\gamma\cos\gamma\sin^2\epsilon(1-3\cos^2\eta)\right]$$

From equation (3-12)

$$X = \mu\alpha\left[\sum_{i<j}\left(\overline{\cos^2\Theta_{ij}}^t\right) - 1\right]$$

$$(6\text{-}2)\quad Y = \mu\alpha\left[9\sum_{i<j}\left(\overline{\cos^2\Theta_{ij}}^t\right)^2 - 6\left(\overline{\cos^2\Theta_{12}}^t\,\overline{\cos^2\Theta_{13}}^t + \overline{\cos^2\Theta_{13}}^t\,\overline{\cos^2\Theta_{23}}^t + \overline{\cos^2\Theta_{12}}^t\,\overline{\cos^2\Theta_{23}}^t\right) - 2\sum_{i<j}\left(\overline{\cos^2\Theta_{ij}}^t\right) + 1\right]^{1/2}$$

and we obtain from equations (6-1) and (6-2):

$$x = \mu \propto (\tfrac{1}{2} - \tfrac{3}{2} \cos^2 \eta)(\tfrac{3}{2}\cos^2\epsilon - \tfrac{1}{2})$$

$$y = \mu \propto (\tfrac{1}{2} - \tfrac{3}{2} \cos^2 \eta)\left[\tfrac{3}{4}\sin^4\epsilon - 3\sin^2\epsilon + 1\right]^{1/2} \tag{6-3}$$

From equation (2-6)

$$\langle \Delta H_i^2 \rangle = \frac{2\gamma^2\hbar^2}{R^6} \sum_{i \neq j} (3\cos^2\theta_{ij} - 1)^2 \tag{6-4}$$

and this becomes:

$$\langle \Delta H_i^2 \rangle = \frac{2\gamma^2\hbar^2}{R^6} \cdot \tfrac{3}{2}(\tfrac{1}{2} - \tfrac{3}{2}\cos^2\eta)\left[\tfrac{3}{4}\sin^4\epsilon - 3\sin^2\epsilon + 1\right] \tag{6-5}$$

It should be remembered that in equations (6-3) and (6-5) η is the angle between the axis of rotation and the direction of the external field, and ϵ is the angle between the axis of rotation and the normal to the nuclear triangle. For any particular sample ϵ will probably have only one value. However, η will vary with the orientation of the crystal in the field when a single crystal is studied. Thus the line shape obtained from a single crystal will be highly anisotropic and in such cases both the molecular orientation and the axis of rotation can be determined in the absence of excessive intermolecular broadening.

If the sample is a crystalline powder the expected line shape can be predicted by averaging over all possible orientations of the angle η. The line shape will then depend only on the angle ϵ and the internuclear distance R. The line shape functions are determined in a manner similar to that used in section 4. Thus:

$$I(\Delta H) = P(\eta) \frac{d(\cos\eta)}{d(\Delta H)} \tag{6-6}$$

Since ϵ is a constant for a particular sample we shall define the functions of ϵ in equations (6-3) as follows:

$$\left(\tfrac{3}{2}\cos^2\epsilon - \tfrac{1}{2}\right) = E_1$$

$$\left[\frac{27}{4}\sin^4\epsilon - 3\sin^2\epsilon + 1\right]^{1/2} = E_2 \tag{6-7}$$

Then from the probability expressions in Table 1, and equations (6-3), (6-6), and (6-7) the line shape functions and their limits become:

(a) The component for $\Delta H = 0$ is unchanged.

(b) The component $\Delta H = \gamma/\mu$ is

$$F_1(\Delta H) = \frac{\sqrt{3}}{16 E_2 \alpha}\left[1 - \left(\frac{E_1}{E_2}\right)^2\right]\left[1 - \frac{2}{E_2}\left(\frac{\Delta H}{\alpha}\right)\right]^{-1/2} \tag{6-8}$$

$$-E_2\alpha < \Delta H < \frac{E_2}{2}\alpha$$

(c) For the component $\Delta H = \frac{3x+y}{2\mu}$

$$F_2(\Delta H) = \frac{1}{4\sqrt{3}(3E_1+E_2)\alpha}\left[1 + \frac{E_1}{E_2}\right]\left[1 - \frac{4}{(3E_1+E_2)}\left(\frac{\Delta H}{\alpha}\right)\right]^{-1/2} \tag{6-9}$$

$$-\frac{(3E_1+E_2)}{2}\alpha < \Delta H < \frac{(3E_1+E_2)}{4}\alpha$$

(d) For the component $\Delta H = \frac{3x-y}{2\mu}$

$$F(\Delta H) = \frac{1}{4\sqrt{3}(3E_1-E_2)}\left[1 - \frac{E_1}{E_2}\right]\left[1 - \frac{4}{(3E_1-E_2)}\left(\frac{\Delta H}{\alpha}\right)\right]^{-1/2} \tag{6-10}$$

$$-\frac{(3E_1-E_2)}{2}\alpha < \Delta H < \frac{(3E_1-E_2)}{4}\alpha$$

(e) The line components $\Delta H = -\gamma/\mu$, $-(3x+y)/2\mu$, $-(3x-y)/2\mu$, are obtained by replacing ΔH by $-\Delta H$ in the equations above.

In general there will still be a central line and three pairs of subsidiary lines. The line separations and probabilities will, however, vary markedly with the angle ϵ . There seems to be no way of drawing a "universal" line shape which will be valid for all values of ϵ . However, an experimentally determined curve can be fitted by trial and error methods by plotting the sum of the functions $F(\Delta H)$, in equations (6-8) to (6-10) for different values of ϵ .

The second moment can be obtained for a crystalline powder by averaging over the angle η in equation (6-5). Thus:

$$(6\text{-}11)\quad \overline{(1/2 - 3/2\cos^2\eta)^2}^{\text{sphere}} = 1/2\int_0^{\pi}(1/2 - 3/2\cos^2\eta)^2 \sin\eta\, d\eta = 1/5$$

and

$$(6\text{-}12)\quad \langle \Delta H_2^2 \rangle = \frac{298}{R^6}\left(\frac{3}{5}\right)\left[\frac{27}{8}\sin^4\epsilon - 3\sin^2\epsilon + 1\right] \text{ gauss}^2.$$

Curves showing the effect of ϵ on the second moment are given in Figure 16. They are symmetrical about $\epsilon = \pi/2$ as one might expect, there being no physical difference between the angle ϵ and $(180 - \epsilon)$. The minimum second moment occurs when $\epsilon = 41° 49'$. The double-valued nature of the second moment function can cause some ambiguity in determinations of the angle ϵ, but the ambiguity should be resolvable from other evidence.

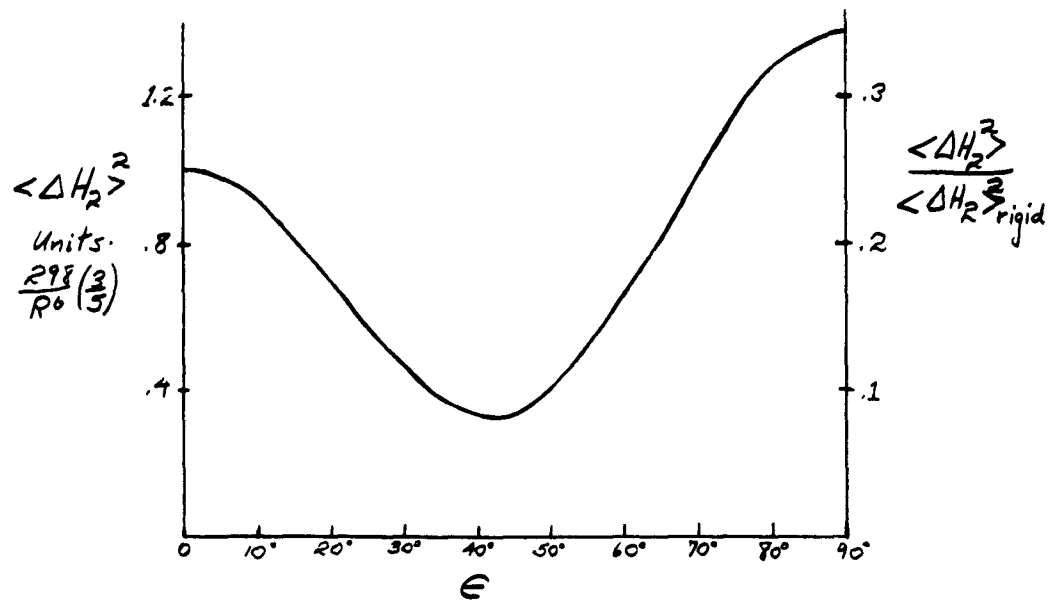

Figure 16

Case II. A particularly interesting case is that of rotation about the normal to the triangle. It corresponds to rotation of a methyl group

about the C-X bond, where X is the atom to which the methyl group is attached. This is actually a special of the one just discussed, that for which $\epsilon = 0$.

From equations (6-3) and (6-5) we find that when $\epsilon = 0$,

$$X = Y = \mu\alpha\left(\tfrac{1}{2} - \tfrac{3}{2}\cos^2\eta\right) \tag{6-13}$$

$$\langle \Delta H_2^2 \rangle = \frac{298}{R^6} \times 3\left(\tfrac{1}{2} - \tfrac{3}{2}\cos^2\eta\right)^2 \tag{6-14}$$

Furthermore, consideration of the probability expressions in Table 1 shows that the line components $\Delta H = \pm Y/\mu$ and $\pm (3X - Y)/2\mu$ vanish leaving only the central peak $\Delta H = 0$, with probability $\frac{1}{2}$, and a pair of lines at $\Delta H = \pm \frac{3X+Y}{2\mu}$, each with probability $\frac{1}{4}$. For a single crystal the spacing between the central and side peaks will vary with the angle η , the total range being given by:

$$\begin{aligned} 0 \le \eta &\le 90^\circ \\ -2\alpha \le \pm \Delta H &\le \alpha \end{aligned} \tag{6-15}$$

The line shape and second moment for a crystalline powder can be found from the previous case. From equations (6-7) we find that for $\epsilon = 0$, $E_1 = E_2 = 1$. Thus the line shape is determined from equation (6-9). For the component $\Delta H = (3X + Y)/2\mu = 2X/\mu$

$$F(\Delta H) = \frac{1}{8\sqrt{3}\alpha}\left[1 - \left(\frac{\Delta H}{\alpha}\right)\right]^{-1/2} \tag{6-16}$$

$$-2\alpha < \Delta H < \alpha$$

The component $\Delta H = -2X/\mu$ is determined as usual by replacing ΔH by $-\Delta H$ in this equation. The entire line shape is shown in Figure 17.

The second moment, as determined from equation (6-12), is:

$$\langle \Delta H_2^2 \rangle = \frac{298}{R^6}\left(\frac{3}{5}\right) \tag{6-17}$$

Comparison with equation (4-18) shows that the second moment is reduced by a factor of 4 from that expected for a rigid configuration.

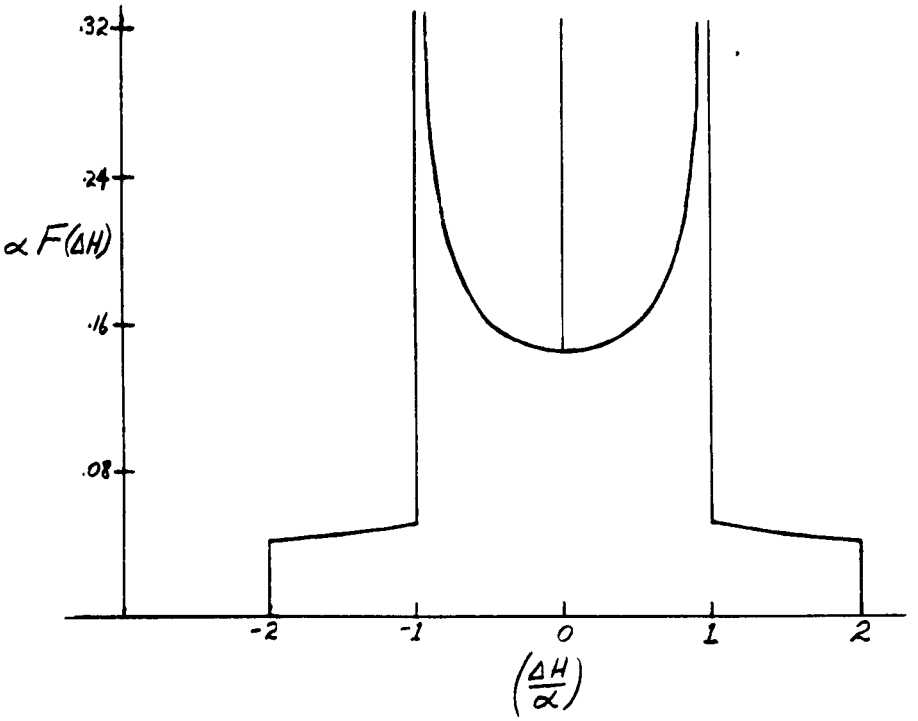

Figure 17

Case III. We shall now consider the effect of rotation about Z_r and Z_t simultaneously, corresponding to rotation of a methyl group about the C-X bond and simultaneous rotation of the whole molecule of which the methyl group is a part.

Equations (6-1) give the functions $\overline{\cos^2\theta_{ij}}^t$ which have been averaged over a rotation about Z_r . For motion about Z_t we must average these functions over a rotation involving the angle γ . The expressions required are $\overline{\cos^2\gamma}^t = \overline{\sin^2\gamma}^t = \frac{1}{2}$, and $\overline{\sin\gamma\cos\gamma}^t = 0$. Thus:

$$(6\text{-}18)\quad \overline{\cos^2\theta_{12}}^{\beta,\gamma} = \overline{\cos^2\theta_{23}}^{\beta,\gamma} = \overline{\cos^2\theta_{31}}^{\beta,\gamma} = \tfrac{1}{2}(1-\cos^2\eta) - \tfrac{1}{4}\sin^2\epsilon\,(1-3\cos^2\eta)$$

Then from equations (6-2)

$$(6\text{-}19)\quad X = Y = \mu\alpha\left(\tfrac{1}{2} - \tfrac{3}{2}\cos^2\eta\right)\left(\tfrac{3}{2}\cos^2\epsilon - \tfrac{1}{2}\right)$$

and from equation (6-4)

$$(6\text{-}20)\quad \langle \Delta H_2^2 \rangle = \frac{298}{R^6} \times 3\left(\tfrac{1}{2} - \tfrac{3}{2}\cos^2\eta\right)^2 \left(\tfrac{3}{2}\cos^2\epsilon - \tfrac{1}{2}\right)^2$$

The usual anisotropy of a single crystal remains. The line shape and second moment for a crystalline powder are determined as before by averaging over η . Since $x = y$, the line shape consists only of the components at $\Delta H = 0$ (probability = $\frac{1}{2}$) and at $\Delta H = \pm \frac{3x+y}{2\mu} = \pm \frac{2x}{\mu}$ (probability = $\frac{1}{4}$ each). For the component $\Delta H = \frac{2x}{\mu}$

$$(6\text{-}21)\quad F(\Delta H) = \frac{1}{8\sqrt{3}\,\alpha E_3}\left[1 - \frac{1}{E_3}\left(\frac{\Delta H}{\alpha}\right)\right]^{-1/2}, \quad -2\alpha E_3 < \Delta H < \alpha E_3$$

where

$$(6\text{-}22)\quad E_3 = \left(\tfrac{3}{2}\cos^2\epsilon - \tfrac{1}{2}\right)$$

The component $\Delta H = -\frac{2x}{\mu}$ is obtained from equation (6-21) by replacing ΔH by $-\Delta H_0$. The line shape will thus be similar in form to that in Figure 17. A "universal" curve could be obtained by plotting $\alpha E_3 F(\Delta H)$ vs. $\frac{\Delta H}{\alpha E_3}$.

The second moment can be obtained from equation (6-20) by averaging $\left(\frac{1}{2} - \frac{3}{2}\cos^2\eta\right)^2$ over a sphere. This has been done in equation (6-11). Introducing this result, we obtain:

$$(6\text{-}23)\quad \langle \Delta H_2^2 \rangle = \frac{298}{R^6}\left(\frac{3}{5}\right)\left(\frac{3}{2}\cos^2\epsilon - \frac{1}{2}\right)^2$$

Curves showing the dependence of the second moment on ϵ are given in Figure 18. When $\epsilon = 0$ the second moment is reduced by a factor of 4 from the rigid lattice value. This is identical with the result of Case II, as it should be, since the physical situation corresponding to $\epsilon = 0$ is that there is rotation only about the C-X bond. When $\epsilon = 90°$ the second moment is reduced by a

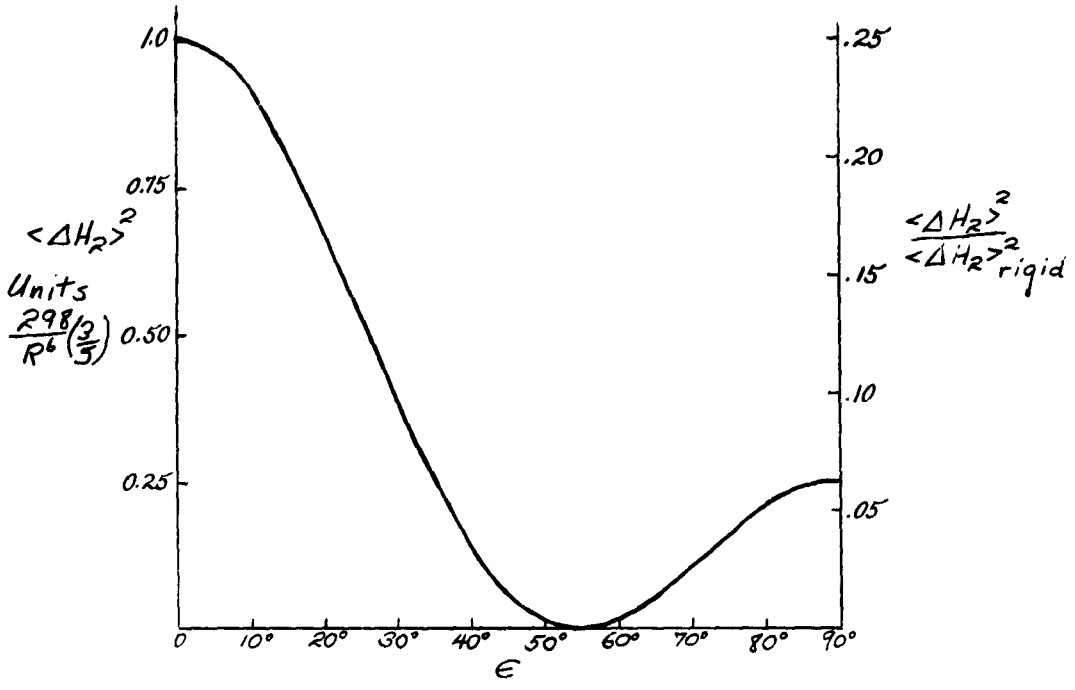

Figure 18

factor of 16 from the rigid lattice value. Most interesting is the situation when $\epsilon = 54°44'$, one-half the tetrahedral angle. For this case, the second moment vanishes, and the line shape should be quite narrow, such as is normally expected from liquid samples.

Case IV: The final case to be considered is that of rotational oscillation of the methyl group. We will consider Z_r as the axis of rotational oscillation in analogy to the previous cases, so we must now replace β by $\beta_0 + K\sin\omega t$, where K is one-half the total angular amplitude of oscillation. The functions $\cos^2\theta_{ij}$ must be averaged over time after this substitution has been made. They may be expressed in terms of Bessels functions through the use of the relations

$$J_n(z) = \frac{1}{\pi}\int_0^{\pi} \cos(n\theta - z\sin\theta)\,d\theta \qquad n = 0, 1, 2, \cdots \tag{6-24}$$

$$\int_c^{2\pi} \sin(z\sin\theta)\,d\theta = 0$$

Each $\cos^2\Theta_{ij}$ then takes the general form:

$$\overline{\cos^2\Theta_{ij}}^t = P_{ij} + Q_{ij} J_0(k) + R_{ij} J_0(k) \tag{6-25}$$

where P_{ij}, Q_{ij}, and R_{ij} are complicated functions of the other angles of the system, γ, ϵ, η, and β_0.

The energy parameters X and y may now be determined by the substitution of the relations (6-25) into equations (6-2), and the final expressions are:

$$\begin{aligned} X = \mu\alpha \Big[& (\tfrac{1}{2} - \tfrac{3}{2}\cos^2\eta)(\tfrac{3}{2}\cos^2\epsilon - \tfrac{1}{2}) \\ & + \tfrac{3}{4}\{J_0(k)\sin 2\eta \sin 2\epsilon \cos\beta_0 - J_0(2k)\sin^2\eta \sin^2\epsilon \cos 2\beta_0\}\Big] \end{aligned}$$

$$\begin{aligned} y = \mu\alpha \Big[& (\tfrac{1}{2} - \tfrac{3}{2}\cos^2\eta)^2 (\tfrac{27}{4}\sin^4\epsilon - 3\sin^2\epsilon + 1) \\ & + \tfrac{9}{2}\sin^4\eta\,(\tfrac{3}{8}\sin^4\epsilon\cos^2 2\beta_0 + \cos^2\epsilon)\, J_0^2(2k) \\ & + 9\sin^2\eta\cos^2\eta\sin^2\epsilon\,\{(1 - 3\sin^2\epsilon)\cos^2\beta_0 + 2\}\, J_0^2(k) \\ & + \tfrac{3}{4}\sin^2\eta\,(\tfrac{3}{2}\cos^2\eta - \tfrac{1}{2})\sin^2\epsilon\,(9\cos^2\epsilon + 5)\cos 2\beta_0\, J_0(2k) \\ & + 6\sin\eta\cos\eta\,(\tfrac{3}{2}\cos^2\eta - \tfrac{1}{2})\sin\epsilon\cos\epsilon\,(\tfrac{9}{2}\sin^2\epsilon - 1)\cos\beta_0\, J_0(k) \\ & + 9\sin^3\eta\cos\eta\sin\epsilon\cos\epsilon\,(2 - \tfrac{3}{2}\sin^2\epsilon\cos 2\beta_0)\cos\beta_0\, J_0(2k) J_0(k)\Big]^{1/2} \end{aligned} \tag{6-26}$$

Unfortunately it does not seem to be possible to obtain general expressions for the line shape components of a crystal powder. However, certain qualitative conclusions may be drawn. For such a sample the single crystal line components must be averaged over β_0 as well as η, and this should lead to a dispersion of each of the peaks of the rigid line shape shown in Figure 10. Thus we may expect to find less evidence of fine structure if the methyl groups are undergoing rotational oscillation.

The overall line width may be expected to decrease at the same time. If the molecule containing the methyl group is rotating or tunneling about some axis, the location of the maxima shown in Figure 10 will be displaced toward the central peak. The amount of such displacement will depend on

the angle ϵ. For example, if $\epsilon = 90°$, each peak will be displaced halfway from its rigid lattice position to the central peak. For the case of rotational oscillation we may thus assume that the maxima will be at some intermediate values as well as being spread out as mentioned above. When the effects of intermolecular broadening are also considered, it seems reasonable to assume that the experimentally determined line shape should be a fairly smooth curve with some possibility of shoulders when the amplitude of oscillation is small. Such curves are indicated qualitatively in Figures 19(a) and (b).

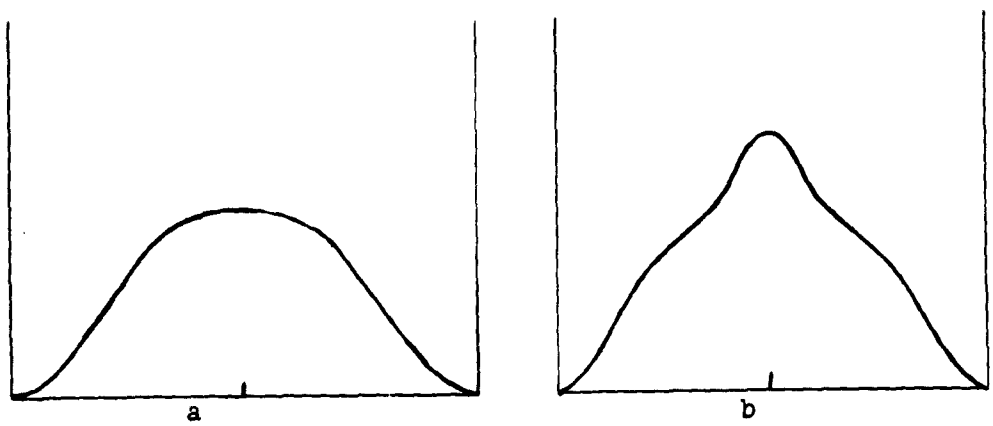

Figure 19

If the methyl group should be rotating about its own axis simultaneously, the same general considerations should apply although the line width will be considerably decreased and the possibility of observing fine structure will be very small.

The second moments to be expected for rotational oscillation are determined by averaging ρ_0 over a circle and η over a sphere in each of the expressions $(3\cos^2\theta_{ij} - 1)^2$, and substituting the resulting expressions in equation (2-6). For rotational oscillation only we obtain:

(6-27) $$\langle \Delta H_R \rangle^2 = \frac{2 \gamma^2 \hbar^2}{R^6}\left(\frac{3}{5}\right)\left[\left(\frac{27}{8}\sin^4\epsilon - 3\sin^2\epsilon + 1\right) - \left(\frac{9}{2}\sin^4\epsilon - 6\sin^2\epsilon\right) J_0^2(k) + \left(\frac{9}{8}\sin^4\epsilon - 3\sin^2\epsilon + 3\right) J_0^2(2k)\right]$$

and for simultaneous rotation of the methyl group about its own axis:

(6-28) $$\langle \Delta H_R \rangle^2 = \frac{2 \gamma^2 \hbar^2}{R^6}\left(\frac{3}{5}\right)\left[\left(\frac{3}{2}\cos^2\epsilon - \frac{1}{2}\right)^2 + \left(3\sin^2\epsilon - 3\sin^4\epsilon\right) J_0^2(k) + \frac{3}{4}\sin^4\epsilon\, J_0^2(2k)\right]$$

The ratios of the second moment for rotational oscillation to that expected for a rigid methyl group have been plotted in Figures 20 and 21 as a function of K, for several values of ϵ.

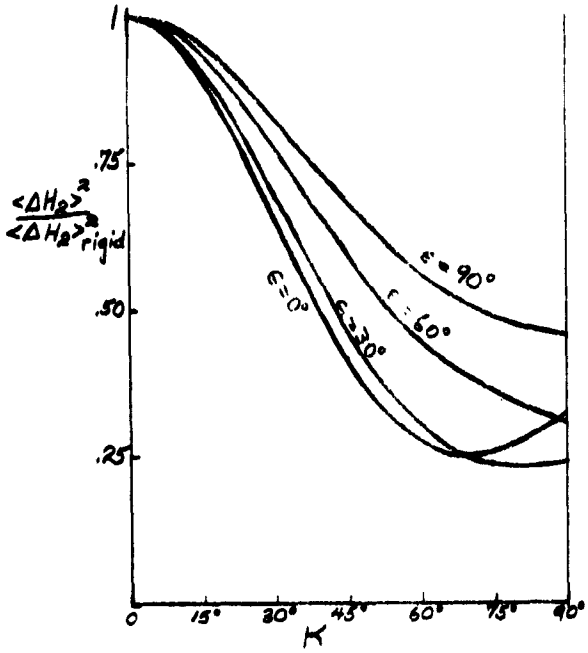

FIGURE 20: ROTATIONAL OSCILLATION ONLY.

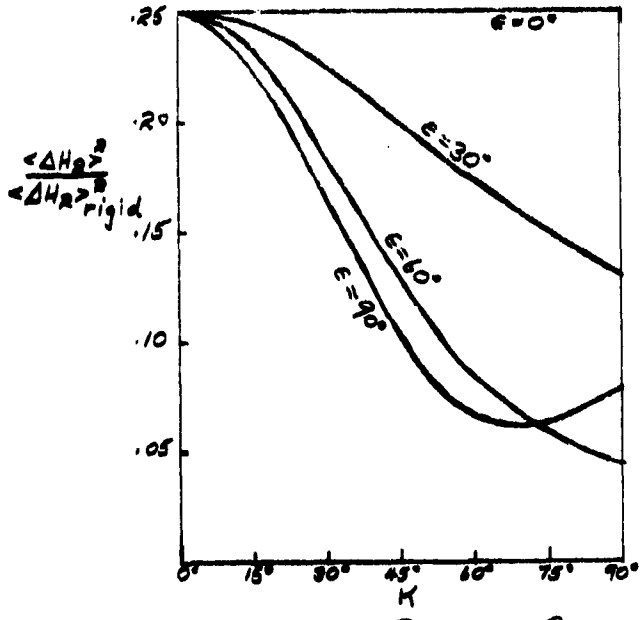

FIGURE 21: ROTATIONAL OSCILLATION PLUS ROTATION OF METHYL GROUP.

7. Comparison of theoretical and experimental line shapes. We have previously assumed that our nuclear triangle was isolated from all other nuclear spins and was in a perfectly homogeneous field. In practice, field inhomogeneity and interactions between the triangular groups impart a finite width to each component line. We shall group all such factors external to the triangular group into one broadening function $S(H - H_0)$, where H is an arbitrary field parameter, and H_0 is defined by $\Delta H = H_0 - H^*$. H^* is the magnitude of the

magnetic field at the center of the absorption line The resultant shape function as a function of the field is thus (P-6):

$$(7\text{-}1) \qquad f_i(H) = \int_{H_o} F_i(H_o - H^*)\, S(H - H_o)\, dH_o$$

This relation holds for each of the components of the line which we have derived above, and also for the overall shape function, since the latter is simply the sum of the individual components.

The broadening function $S(H-H_o)$ cannot be computed directly. However, it is usually assumed to have a gaussian form (P-7) which, though not exact, is a fairly good approximation. Therefore:

$$(7\text{-}2) \qquad S(H-H_o) = e^{-(H-H_o)^2/\beta^2}$$

where β is a parameter expressing the broadening contributions from all sources. If we let $h = \Delta H$, and $m = H - H^*$, and substitute equation (7-2) into equation (7-1), we obtain:

$$(7\text{-}3) \qquad f_i(H) = \int_h e^{-(m-h)^2/\beta^2} F_i(h)\, dh = f_i(m)$$

The expressions derived previously for the various $f_i(h)$ are such that the integration required in equation (7-3) cannot be done analytically. We must therefore perform the integration numerically, and we will find it convenient to express the $F_i(h)$ in a more general form. This will be done only for cases I, II, and III of section 6. The case of a rigid triangle will not be required because the only compound which yields a line shape corresponding to a rigid configuration is 1,1,1-trichloroethane, which has already been investigated (G-2, G-3).

Dr. J. C. Sternberg has shown (S-3) that each component line shape $F_i(h)$ for each of the three cases of rotation to be considered can be expressed in the same general form. Comparison of equations (6-3), (6-13), and (6-19) reveals that the energy parameters X and Y contain the factors $\mu\alpha\,(\tfrac{1}{2} - \tfrac{3}{2}\cos^2\eta)$ in all cases and may also contain a factor which is a function of ϵ alone. Since ϵ is not a variable for a specific compound, any function of ϵ may be considered as a constant when deriving the line shape functions. Accordingly we will define X and Y generally as:

$$X = A\mu\alpha\,(\tfrac{1}{2} - \tfrac{3}{2}\cos^2\eta)$$

(7-4)

$$Y = B\mu\alpha\,(\tfrac{1}{2} - \tfrac{3}{2}\cos^2\eta)$$

For Case I, rotation about an arbitrary axis,

(7-5) $$A = \tfrac{3}{2}\cos^2\epsilon - \tfrac{1}{2} \qquad B = \left[\tfrac{27}{4}\sin^4\epsilon - 3\sin^2\epsilon + 1\right]^{1/2}$$

For Case II, rotation about the normal to the nuclear triangle,

(7-6) $$A = 1 \qquad B = 1$$

For Case III, simultaneous rotation of both the above types,

(7-7) $$A = \tfrac{3}{2}\cos^2\epsilon - \tfrac{1}{2} = B$$

The probability expressions of Table 1 can also be expressed in terms of A and B only, and thus are constants for a particular ϵ. The general expressions for the probabilities are given in Table 2.

Line component	Normalized probability
$h_0 = 0$	$p_0 = \frac{1}{8}(1 + 3A^2/B^2)$
$h_1 = \pm y/\mu$	$p_1 = \frac{3}{16}(1 - A^2/B^2)$
$h_2 = \pm (3x+y)/2\mu$	$p_2 = \frac{1}{8}(1 + A/B)$
$h_3 = \pm (3x-y)/2\mu$	$p_3 = \frac{1}{8}(1 - A/B)$

Table 2.

The line shape functions $F_i(h)$ are determined as before from the equation,

$$(7\text{-}8) \quad F_i(h_i) = p_i \frac{d(-\cos\eta)}{dh_i}$$

and can be shown to have the same general form in every case, which is:

$$(7\text{-}9) \quad \alpha F_i(h_i) = \pm \tfrac{1}{2} p_i \left[3a_i(a_i \mp \tfrac{h}{\alpha})\right]^{-1/2}$$

The factors a_i are functions of ϵ. They are thus constants for a particular sample, but their actual values are different for the different line components. Their values are given in Table 3.

Line component	a_i
$h_1 = \pm y/\mu$	$a_1 = B/2$
$h_2 = \pm (3x+y)/2\mu$	$a_2 = (3A+B)/4$
$h_3 = \pm (3x-y)/2\mu$	$a_3 = (3A-B)/4$

Table 3.

The limits of h/α must be specified for each component and are found to be the same for all. When the positive sign is taken for h/α in

Tables 2 and 3, the limits are $-2a_i \leq h/\alpha \leq a_i$; when the negative sign is chosen the limits are $2a_i \geq h/\alpha \geq -a_i$.

With the exception of the central component F_o , the line components F_i occur in pairs which are mirror images of each other with respect to the axis $h/\alpha = 0$. We shall combine the members of each pair, so that equation (7-9) and the limits will be:

$$\alpha F_i = \tfrac{1}{2} p_i \left[3a_i(a_i - h/\alpha)\right]^{-1/2} \qquad -2a_i \leq h/\alpha \leq 0$$

(7-10)

$$-\tfrac{1}{2} p_i \left[3a_i(a_i + \tfrac{h}{\alpha})\right]^{-1/2} \qquad 2a_i \geq h/\alpha \geq 0$$

If we now make the substitutions $X_1 = -h/\alpha$, $X_2 = h/\alpha$, equation (7-10) takes the form:

$$\alpha F_i = \tfrac{1}{2} p_i \left\{ \left[3a_i(a_i + X_1)\right]^{-1/2} - \left[3a_i(a_i + X_2)\right]^{-1/2} \right\}$$

(7-11)

$$2a_i \geq \begin{matrix} X_1 \\ X_2 \end{matrix} \geq a_i$$

We may now substitute this result in equation (7-3) to obtain:

$$f_i(m) = \tfrac{1}{2} p_i N_i \int_{2a_i}^{-a_i} \left\{ e^{-(m/\alpha + X_1)^2/(\beta/\alpha)^2} \left[3a_i(a_i + X_1)\right]^{-1/2} (-dX_1) \right.$$

(7-12)

$$\left. - e^{-(\frac{m}{\alpha} - X_2)^2/(\beta/\alpha)^2} \left[3a_i(a_i + X_2)\right]^{-1/2} dX_2 \right\}$$

where N_i is a normalization factor. Since the limits are the same for both X_1 and X_2 we may replace them by the single variable X . If we make the further substitution $\omega = \sqrt{\frac{1 + X/a_i}{3}}$, we obtain:

13) $f_i(m) = p_i N_i \int_0^1 \left\{ e^{-[(\frac{m}{\alpha a_i}) + (3\omega^2 - 1)]^2/(\beta/\alpha a_i)^2} + e^{-[(\frac{m}{\alpha a_i}) - (3\omega^2 - 1)]^2/(\beta/\alpha a_i)^2} \right\} d\omega$

The normalization factor remains to be evaluated. This requires the solution of the equation

$$2a_i = \int_{-a_i}^{2a_i} f_i(m)\,dm$$

$$= \int_{-a_i}^{2a_i} \frac{\alpha}{2} P_i N_i \frac{dx}{[3a_i(a_i+x)]^{1/2}} \left[e^{-(\frac{m}{\alpha}+x)^2/(\beta/\alpha)^2} + e^{-(\frac{m}{\alpha}-x)^2/(\beta/\alpha)^2} \right] d(\tfrac{m}{\alpha})$$

Thus:

$$(7\text{-}15)\quad \frac{4}{\alpha N_i} = \int_{-a_i}^{2a_i} \frac{1}{[3a_i(a_i+x)]^{1/2}} \left\{ \int_{-\infty}^{\infty} \left[e^{-(\frac{m}{\alpha}+x)^2/(\beta/\alpha)^2} + e^{-(\frac{m}{\alpha}-x)^2/(\beta/\alpha)^2} \right] d(\tfrac{m}{\alpha}) \right\} dx$$

Each term in the inner integral may be reduced to the standard form

$$(7\text{-}16)\quad 2\int_0^{\infty} e^{-k^2\mu^2}\,d\mu = \frac{\sqrt{\pi}}{k}$$

where $k = \alpha/\beta$, $\mu = \frac{m}{\alpha} \pm x$, and $d\mu = d(\frac{m}{\alpha})$. Therefore:

$$(7\text{-}17)\quad \frac{4}{\alpha N_i} = \int_{-a}^{2a_i} \frac{1}{[3a_i(a_i+x)]^{1/2}} \left(2\frac{\beta}{\alpha}\sqrt{\pi} \right) dx$$

and

$$(7\text{-}18)\quad N_i = \frac{1}{\beta\sqrt{\pi}}$$

Substitution of this result in equation (7-13) with some rearrangement of terms leads to the final equation:

$$(7\text{-}19)\quad \frac{\alpha a_i f_i(m)}{P_i} = \frac{1}{\sqrt{\pi}(\beta/\alpha a_i)} \int_0^{1} \left\{ e^{-[(\frac{m}{\alpha a_i})+(3\omega^2-1)]^2/(\beta/\alpha a_i)^2} + e^{-[(\frac{m}{\alpha a_i})-(3\omega^2-1)]^2/(\beta/\alpha a_i)^2} \right\} d\omega$$

The equation just obtained is particularly convenient in that it yields general results that may be used to determine the line shape

expected for any value of the angle ϵ. It is also in a form which is convenient for numerical integration by the standard quadrature formulas. The right-hand side of equation (7-19) was evaluated for several combinations of $m/\alpha a_i$ and $\beta/\alpha a_i$ on the Whirlwind I computer at the Massachusetts Institute of Technology Digital Computer Laboratory. The data are given in Table 4. The values of $m/\alpha a_i$ for values of $\beta/\alpha a_i$ other than those tabulated directly can be obtained with some loss of precision by direct interpolation or from plots of $\alpha a_i f_i(m)/p_i$ against $\beta/\alpha a_i$ for the selected values of $m/\alpha a_i$.

The actual comparison of experimental and theoretical line shapes can be made with either the absorption lines or their first derivatives. We will compare the derivative curves for two reasons: the derivative curves are more sensitive to the effects of fine structure; also, the experimental results are obtained in the form of the first derivative of the line shape, and it is simpler to determine the derivative of the theoretical line shapes than to carry out the reverse procedure.

The derivative curves $\alpha f_i(m)$ have been determined by the method of Rutledge (M-3), and have been plotted against m/α for comparison with the experimental curves. If we call the tabulated values of Table 4 $I \left(= \frac{\alpha a_i f_i(m)}{p_i}\right.$, and let $\frac{m}{\alpha a_i} = X$, the use of Rutledge's method enables us to determine $\frac{dI}{dX}$. The equations determining the normalized values of the line shape function $\alpha f_i(m)$ vs. m/α are:

$$(7\text{-}20) \quad \alpha f_i(m) = \frac{p_i}{a_i} I \qquad \frac{m}{\alpha} = a_i X$$

and those determining the derivative function $\alpha f_i'(m)$ vs. m/α are:

$x = m/\mu_{ai}$ \ β/μ_{ai}	0.10000	0.20000	0.40000	0.60000	0.80000	1.00000	1.50000	2.00000
0.00000	0.57600	0.58188	0.59968	0.63546	0.65206	0.63922	0.55466	0.46694
0.10000	0.58150	0.58428	0.60340	0.63812	0.65206	0.63804	0.55342	0.46614
0.20000	0.58944	0.59176	0.61494	0.64556	0.65178	0.63446	0.54970	0.46376
0.30000	0.59656	0.60522	0.63508	0.65634	0.65060	0.62832	0.54352	0.45982
0.40000	0.62220	0.62668	0.66402	0.66798	0.64746	0.61938	0.53496	0.45436
0.50000	0.64560	0.66054	0.69970	0.67732	0.64118	0.60736	0.52412	0.44742
0.60000	0.68970	0.71670	0.73590	0.68070	0.63056	0.59202	0.51110	0.43908
0.70000	0.76496	0.80958	0.76170	0.67464	0.61458	0.57318	0.49602	0.42942
0.80000	0.89910	0.92754	0.76374	0.65648	0.59254	0.55076	0.47906	0.41852
0.90000	1.21994	0.97840	0.73150	0.62502	0.56426	0.52486	0.46038	0.40648
1.00000	1.09114	0.84588	0.66308	0.58086	0.53004	0.49568	0.44022	0.39340
1.10000	0.40774	0.57302	0.56768	0.52644	0.49070	0.46366	0.41876	0.37942
1.20000	0.19134	0.33798	0.46234	0.46456	0.44746	0.42934	0.39628	0.36464
1.30000	0.20114	0.22556	0.36458	0.40218	0.40178	0.39338	0.37298	0.34920
1.40000	0.17684	0.19189	0.29572	0.34052	0.35526	0.35656	0.34914	
1.50000	0.18961	0.18322	0.22822	0.28350	0.30938	0.31960	0.32498	0.31684
1.60000	0.17630	0.17814	0.18761	0.23284	0.26546	0.28326	0.30080	
1.70000	0.17213	0.16945	0.15675	0.18910	0.22450	0.24820	0.27680	
1.80000	0.18080	0.14853	0.12967	0.15193	0.18720	0.21498	0.25322	
1.90000	0.11078	0.11059	0.10338	0.12057	0.15395	0.18410	0.23028	
2.00000	0.05655	0.06627	0.07775	0.09420	0.12486	0.15582	0.20814	0.23314
3.00000	0.00000	0.00000	0.00003	0.00131	0.00616	0.01519	0.05345	0.09513

Table 4: Values of $I\left(=\frac{\mu_{ai} f_i(m)}{P_i}\right)$ for several β/μ_{ai}

(7.23) $\alpha f_i'(m) = \frac{P_i}{a_i^2} \frac{dI}{dx} \qquad \mu = a_i x$

... equations are valid only for the side ... The ... function for the central component ... y a ... s let $(m/\alpha)/(\beta/\alpha) = y$ we may plo... versa... y plotting $G\,(= \frac{1}{\pi} e^{-y^2})$ vs ... $(= -\frac{2}{\pi} y e^{-y^2})$ vs. y (Figure 23) ... ... (m) or its derivative αf ... through the use of the relation

$$\frac{P_0}{(\beta/\alpha)} G \qquad \frac{m}{\alpha} = (\beta/\alpha) y$$

$$\alpha \frac{P_0}{(\beta/\alpha)^2}$$

All ... ments will then be plotted to the ... and can be ... ted t... the total line shape or its derive... illustration of the ... s is given in Figures 24 and 25, in which the sensitivity of the ... rative curve to fine structure is q... ...

We ... yet considered the problem of evalu... the broadening parameter β. In principle β can be est... ... from the field ... and from the crystal structure of the ... when this is know... ...ever, the crystal structure of most of the materials studied in t... ...estigation has not been determined. Nevertheless it is possible to ... ...imate β from the line shape or second moment of the experimental ... ...ption lines. Paka (P-6) has indicated that the experimental second ... ...ent determined for a particular sample will be greater

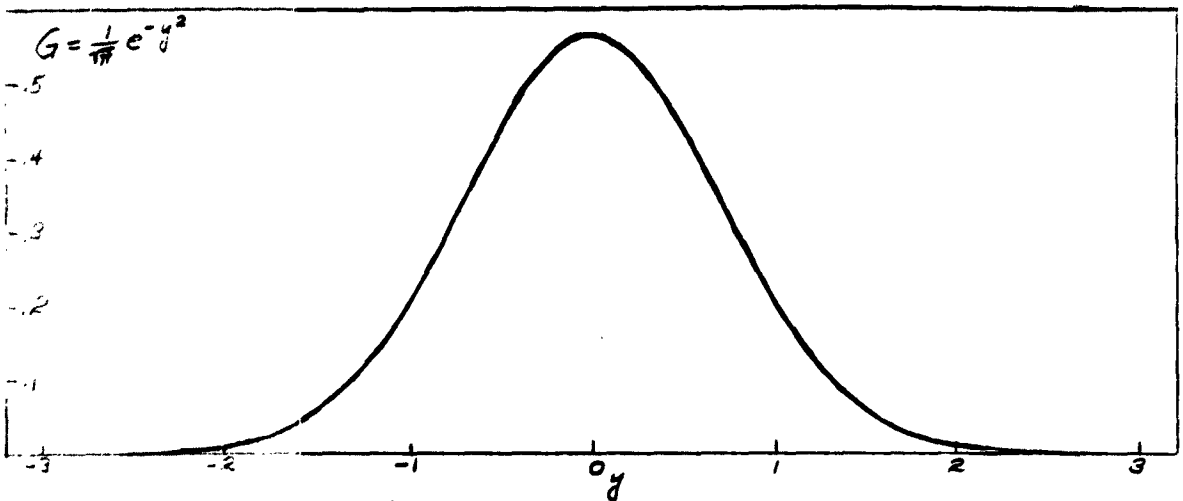

FIGURE 22: "UNIVERSAL" GAUSSIAN FUNCTION

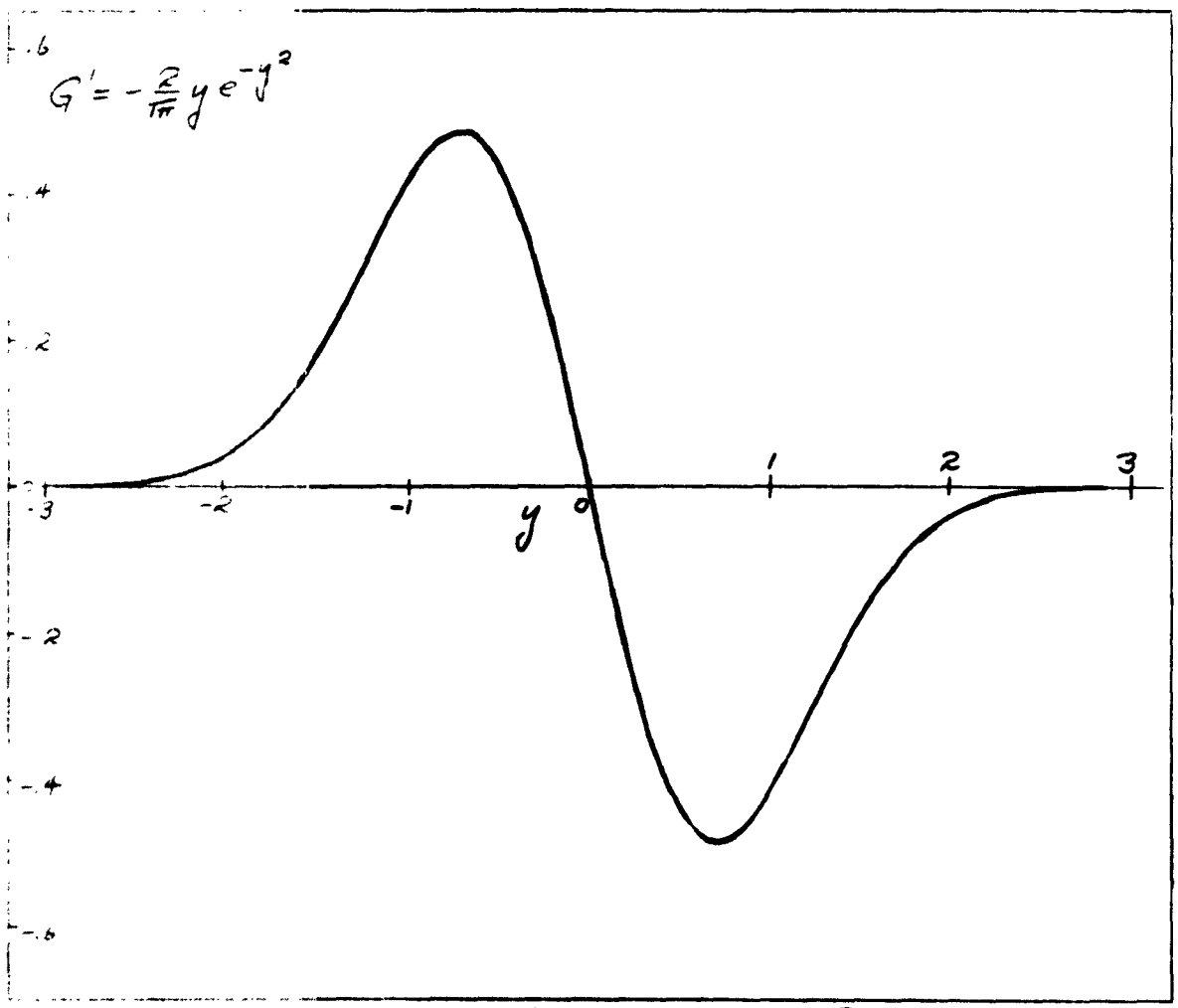

FIGURE 23: "UNIVERSAL" GAUSSIAN FIRST DERIVATIVE FUNCTION

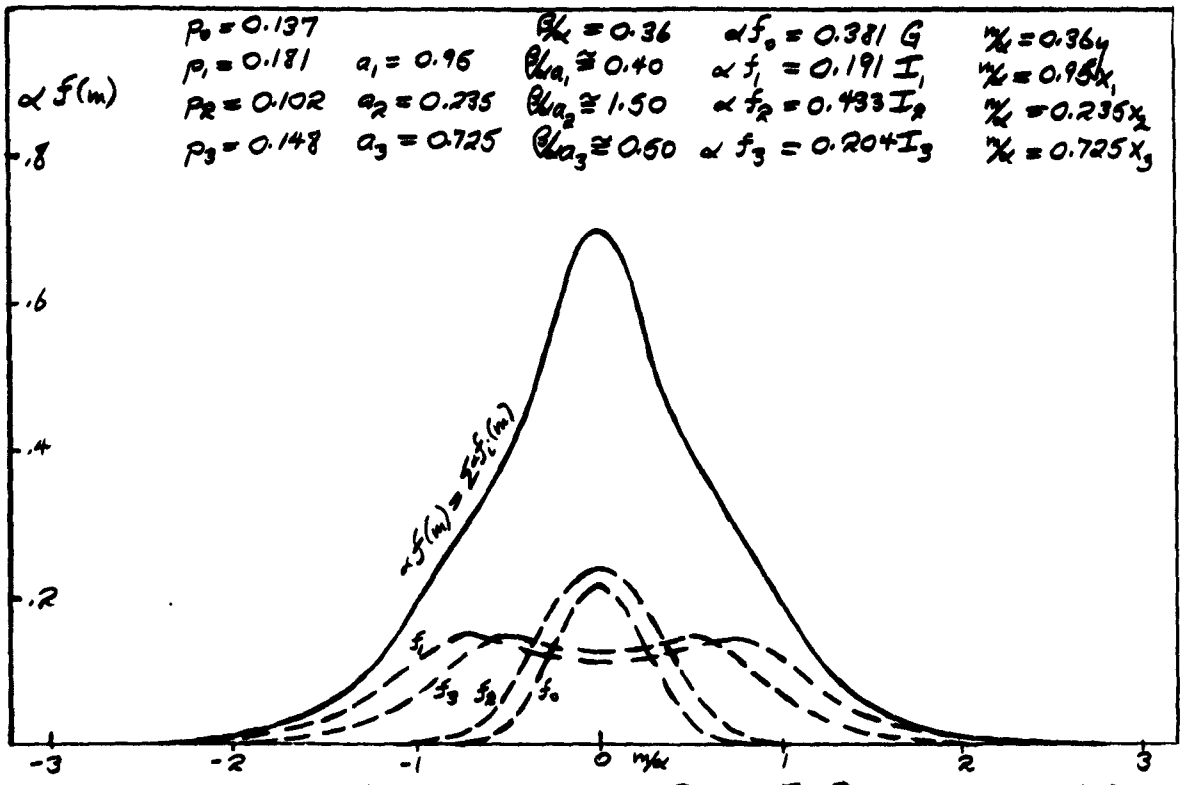

FIGURE 24: LINE SHAPE FOR CASE I ROTATION, $\epsilon = 110°$

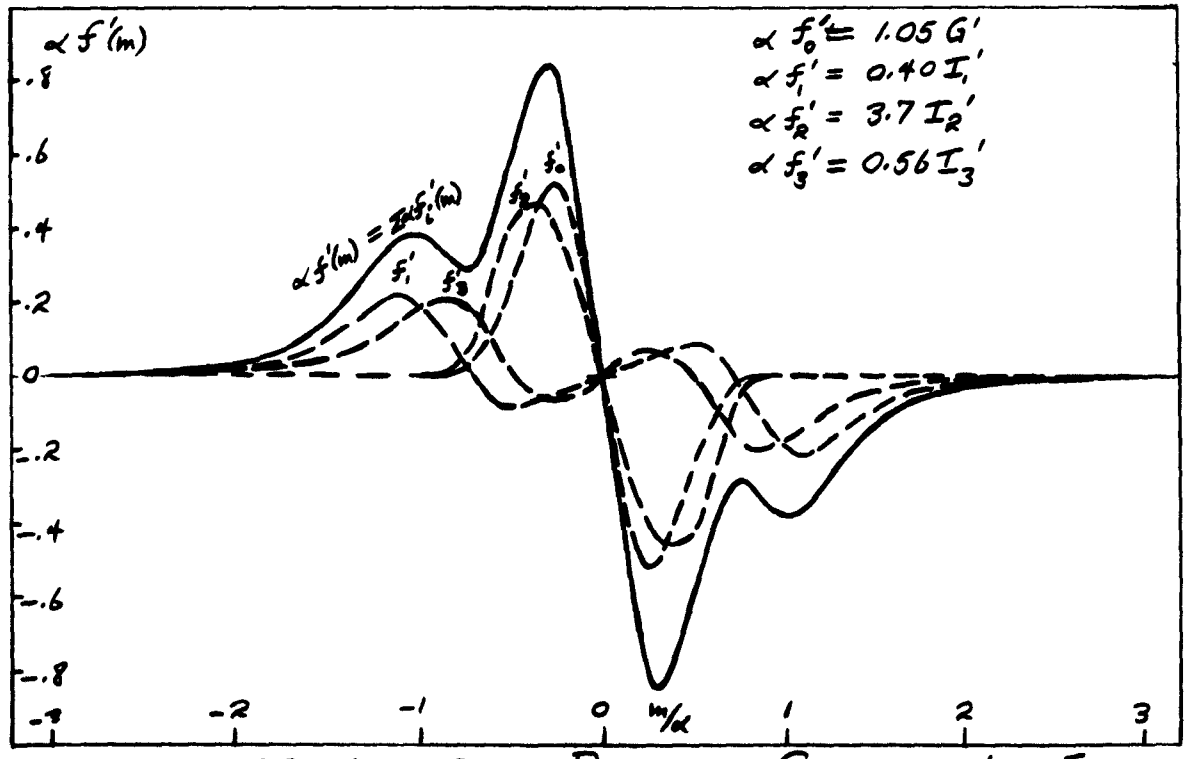

FIGURE 25: LINE SHAPE DERIVATIVE CURVE FOR LINE SHAPE OF FIGURE 24

than the value predicted for an isolated triangular group by an amount which depends on β. The increase in second moment can be expressed as:

$$(7\text{-}24) \quad \langle \Delta H_2^2 \rangle_{EXP} = \langle \Delta H_2^2 \rangle_{THEOR} + \tfrac{1}{2}\beta^2$$

This relation is particularly useful if there is no motion of the protons, or if any existing motion is already known to be of a certain type so that the theoretical second moment can be precisely determined from the equations and curves of section 6. This is not likely to be the case, but the number of possible choices for the theoretical second moment can usually be limited to only a few. The amount of resolution of the fine structure will give some indication of the magnitude of the broadening factor and this in itself may help to select the most likely value of the theoretical second moment.

Direct estimates of the broadening may also be made from the experimental line shape derivative curve. Sternberg (S-3) has shown that by assuming that the central peak of the derivative curve is largely due to the gaussian shape of the central component it is possible to obtain three independent estimates of the magnitude of β, and that these estimates will bracket the true value in many cases. Sternberg's first relation is:

$$(7\text{-}25) \quad \beta \cong \sqrt{2}\, m_p$$

where m_p is the spacing, in gauss, between the center of the line and the peak of the derivative curve. The other two relations require that the experimental line be normalized. However, the normalization factor will have been determined during the process of evaluation of the second moment, since it is the denominator of equation (2-3). In terms

of the normalized derivative curve, the broadening factor is also approximated by:

(7-26) $$\beta^2 \cong \frac{1}{\sqrt{2\pi e}\left(\frac{dy}{dm}\right)_{max}}$$

(7-27) $$\beta^3 \cong -\frac{1}{\sqrt{\pi}\left(\frac{d^2y}{dm^2}\right)_{m=0}}$$

where $(dy/dm)_{max}$ is the peak height of the derivative curve, and $(d^2y/dm^2)_{m=0}$ is the slope of the derivative curve at the center of the line. In the results to be discussed in part IV, the broadening factors have been estimated by at least two of the several methods mentioned here.

III. APPARATUS AND EXPERIMENTAL TECHNIQUE

A. Overall Operation of the Apparatus.

The block diagram of the radiofrequency spectrometer is shown in Figure A. The sample, shown in its normal position in the magnetic field, is connected to the R-F unit by a length of high-frequency coaxial cable. It serves as the inductive part of the oscillator tank circuit, as discussed in part II. The oscillator tuning capacitor is driven by a clock motor coupled through a series of reduction gears, which thus varies the oscillator frequency at a steady rate. The continuous variation of the oscillator frequency, in conjunction with continuous recording of the output signal, has some advantages over the fixed-frequency, variable magnetic field technique. The magnetic field may be produced by a permanent magnet, eliminating the problem of field regulation; the detection of unknown resonances or the observation of resonance lines of different nuclear species is facilitated; and point-by-point plotting of line shapes is eliminated.

The magnetic field is modulated at 280cps. by a current from the modulation unit passing through the modulation coil which is wound around one of the pole pieces of the magnet. Any absorption in the sample thus produces an amplitude modulation of the oscillation level at the coil. This modulated radiofrequency current is amplified and detected, and the audiofrequency component from the detector stage is further amplified before leaving the R-F unit. When the absorption signal is strong, the output from the R-F unit may be applied to the vertical plates of an oscilloscope, as shown by the dashed line in the block diagram, in which case the line shape will be pictured directly.

In most solids, the absorption line is broadened by spin-spin interactions, and the resultant signal is too weak to be observed visually. In such cases the output from the R-F unit is sent to the tuned amplifier in

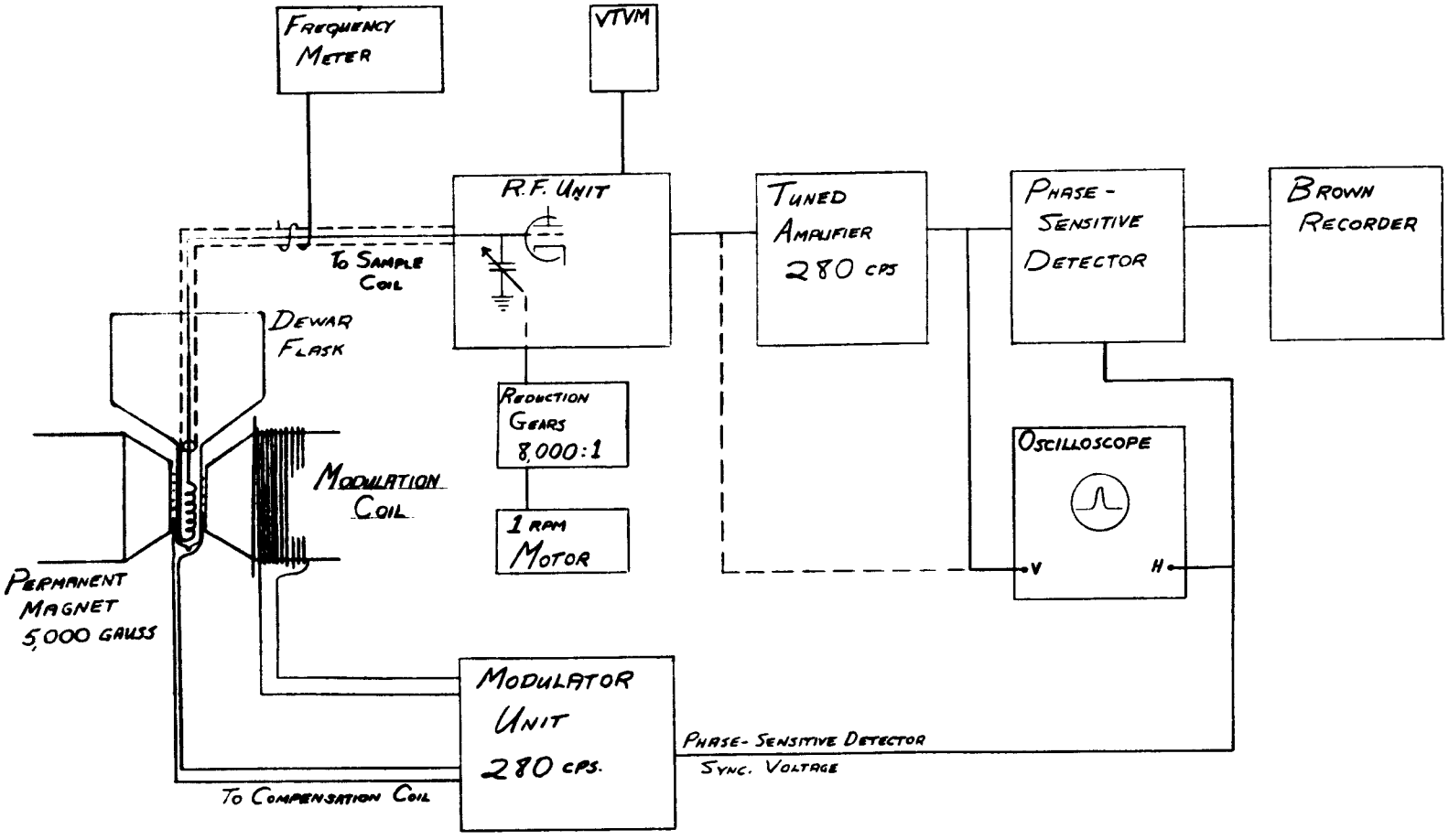

FIGURE A: BLOCK DIAGRAM OF APPARATUS

which only the 280cps component of the signal and a narrow range of noise frequencies in the vicinity of 280cps are amplified. The signal is then sent to the phase-sensitive detector which converts the signal to a DC voltage which is proportional to the first derivative of the absorption line. After being passed through a filter to reduce the noise further, the DC signal is fed to a specially-adapted Brown recorder.

The modulation unit supplies all the 280cps outputs for the spectrometer. These include the modulation current for the magnet mentioned above, the compensation current which serves to balance out any direct coupling between the modulation coil and the sample coil, and a reference voltage to the phase-sensitive detector which is required for the conversion of the applied 280cps signal to a DC output.

B. The R-F Unit.

The R-F unit originally was constructed identical with that described by Pound and Knight (P-5), and differed from the present circuit (Figure B) primarily in having a second tuned circuit between the high-frequency amplifier and the detector. This tuned circuit could be expected to reduce the amount of noise at the output of the R-F unit by narrowing the noise bandwidth. However, it was found that the difficulties involved in tracking this tuned circuit with the oscillator frequency outweighed any advantages it might have, especially since most of the results to be obtained were expected to be broad resonance lines for which the tuned 280cps amplifier would be used. Therefore the tuned circuit was replaced with a second stage of broad-band amplification. The oscillator circuit was later revised also to take advantage of the modifications made by Watkins (W-1). The final form of the circuit is given in Figure B.

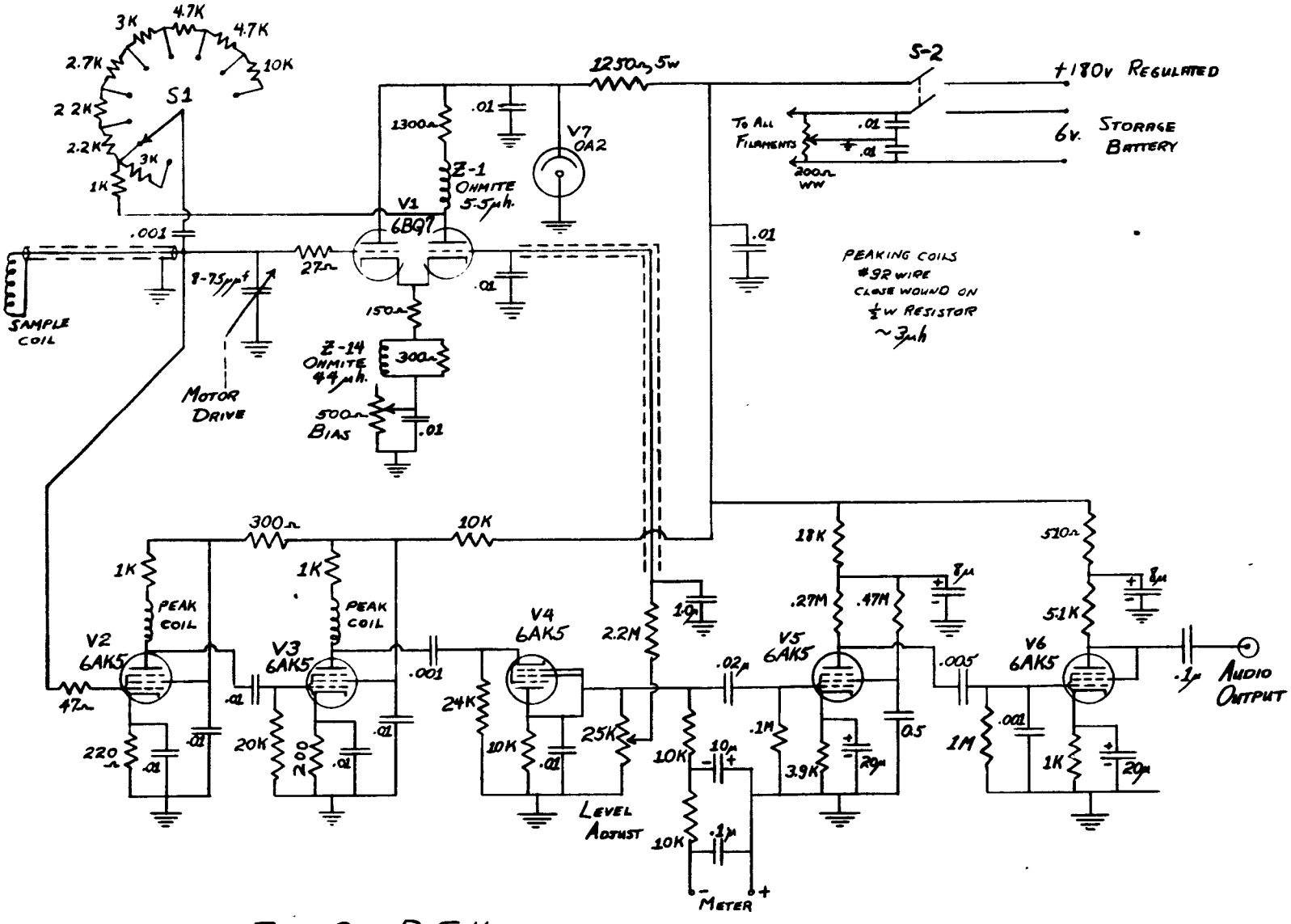

FIGURE B: R.F. UNIT

The oscillator circuit has previously been discussed (part II, B). A 6BQ7 tube is used in place of the 6J6 originally used for the oscillator tube VI. It has proved to be less microphonic than the 6J6, but otherwise has the same characteristics. The tuning capacitor is driven by a Telechron Model 762M220 1rpm motor which is reversible in direction. The revolution rate of the tuning capacitor is reduced 8,000 times by three National Company reducing gears in series, and the resultant rate of sweep of the oscillator frequency is approximately 2.5Kc/sec each minute. The rate of sweep is not quite linear with time, probably because a straight-line-capacity tuning capacitor is used. Use of a straight-line-frequency capacitor therefore is recommended to give a linear frequency scale for the recorded line shape. It should also be pointed out that the mounting for reduction gears should be made as rigid as possible and all couplings between motor, gears, and tuning condenser shaft should be rigid rather than of the flexible type in order to insure that the rotation of the motor shaft is transmitted to the condenser without whip or lag. The coupling between the final reduction gear and the condenser shaft should also be of insulating material such as Bakelite to minimize pickup of either the modulation frequency or stray 60cps voltages.

Certain points concerning the operation of the oscillator itself deserve some further consideration beyond that given in part II, B. The decoupling resistance (controlled by switch S-1) reduces the loading effect of the plate load on the tuned circuit of the oscillator. In principle the value of this resistance should just be equal to the shunt resistance of the tuned circuit (R_s in the earlier discussion). In practice, the largest value which will permit oscillations is selected. The plate load is compensated for loss of gain at high frequencies by the Z-1 Ohmite choke, which has an inductance of 5.5 microhenries.

We previously pointed out that the noise figure of the apparatus will ordinarily be determined solely by the oscillator circuit. Hence, reduction of noise in this circuit is of paramount importance. The use of a 6BQ7 tube for the oscillator was one result of such considerations. Other "tricks of the trade", well known to electronics workers but usually unknown to chemists, are well worth mentioning. These include: (1) all ground connections in the oscillator circuit are made to a common point on the chassis; (2) both filament pins as well as the pins for plate 1 and grid 2 on the oscillator tube socket are by-passed to ground through .01mf capacitors to minimize the effect of stray potentials picked up by the associated wiring; (3) all leads are made as short as possible; (4) the oscillator circuit, including the voltage regulator tube V7, is shielded from the rest of the circuits in the R-F unit; and (5) the B^+, filament, and feedback voltage leads between the oscillator section and the rest of the unit are shielded. As a result, the noise figure of the oscillator circuit compares favorably with those of others which have been observed by the author, although a quantitative determination of the noise figure has not been made. At present, the noise seems largely to be determined by thermal noise developed in the sample coil. This would seem to be the final limit in attempting to reduce the noise level. However, some improvement might still be made by the use of special low-noise deposited metal resistors instead of the usual carbon type. The thermal noise level is decreased when the temperature of the sample and sample coil is lowered. At the same time the signal strength is increased because the Boltzmann factor governing the difference in the populations of the spin energy levels is increased. The overall effect on the observed signal-to-noise ratio is quite marked when the absorption lines for a sample are compared at both room temperature and -196°C. It is thus advantageous to work at temperatures as low as possible when the temperature dependence of the line width is unimportant.

The voltage developed across the oscillator tuned circuit is amplified by a broad-band r-f amplifier composed of V2 and V3. The 47 ohm resistor is used to eliminate parasitic oscillations. The peaking coils reduce the effect of stray capacitance at high frequencies, thus preventing loss of gain. The r-f voltage is detected by V4, a 6AK5 tube connected as a diode, and the audiofrequency signal is further amplified by V5 and V6.

The oscillation level, and thus the magnitude of the radiation field in the sample coil, is controlled by both the Bias and the Level Adjust controls. The Level Adjust control picks up a certain portion of the DC voltage developed by the detector circuit, and feeds it back to the second grid of the oscillator tube. The long (2 second) time constant network formed by the 2.2 Megohm resistor and the 1.0 mf capacitor prevents the 280cps component produced by absorption in the sample from being fed back to the oscillator circuit, so the feedback voltage is responsive only to slow drifts in the oscillation level resulting from changes in the filament voltage or changes in the tube characteristics. In practice, the Bias control is set to allow the Level Adjust control to cover the range of oscillation levels normally used, the latter control being used to make the final adjustment. This arrangement is used because changes in the Bias control cause much greater frequency shifts than corresponding changes in the Level Adjust control.

A vacuum-tube voltmeter is connected at the meter terminals to monitor the r-f level. The oscillation level usually was adjusted to give a meter reading of -0.15 to -0.3 volts, which corresponds to approximately 0.05 to 0.1 volts rms at the tuned circuit. While not necessarily the optimum voltage, this usually gave good signal-to-noise ratios for the absorption lines studied while avoiding saturation effects in all but a few samples.

The plate voltage of 180 volts is supplied from a regulated power supply (Model 25, Lambda Electronics Corporation). The regulation circuit is similar

in overall design to the one employed in the tuned amplifier circuit to be discussed. The output voltage is constant to less than ±1 volt over the course of an experimental run. No 120cps ripple voltage could be detected, but transient surges in the 117 volt line are sometimes passed through to the R-F unit. These are of such short duration that their effect is negligible.

The voltage regulator tube V7 is used to decouple the plate voltage at the oscillator tube from the power supply and the other tubes in the unit, as well as to provide further stabilization of the oscillator plate voltage. A good indication of the sensitivity of the oscillator circuit is given by the fact that a 120cps ripple could be seen in the output from the R-F unit when this was fed directly to the oscilloscope, despite the regulation furnished by both the power supply and V7. However, the effect was small and this ripple voltage was easily removed by the tuned amplifier.

The filaments are supplied from a storage battery. A charger is floated across the battery terminals through a variable one ohm resistor, which is adjusted to keep a 50-100 ma charging current through the battery. The filaments can thus be kept heated at all times with no drain on the battery, and no warmup time is required before using the unit. No 60cps ripple has been observed in the output from the R-F unit that could be attributed to the charger. Both sides of the filament line are bypassed to ground by .01 mf capacitors as they enter the chassis. A 200 ohm potentiometer is connected across the filaments with its center tap grounded. The position of the center tap can be varied to minimize any 60cps pickup in the filament leads. However, this has proved to be unnecessary in this particular unit as no 60cps component can be clearly distinguished from the background noise and the 120cps ripple mentioned above in the output from the R-F unit.

All .01 and .001 mf capacitors in the R-F unit are of ceramic construction, these having the advantage of low high-frequency loss as well as small

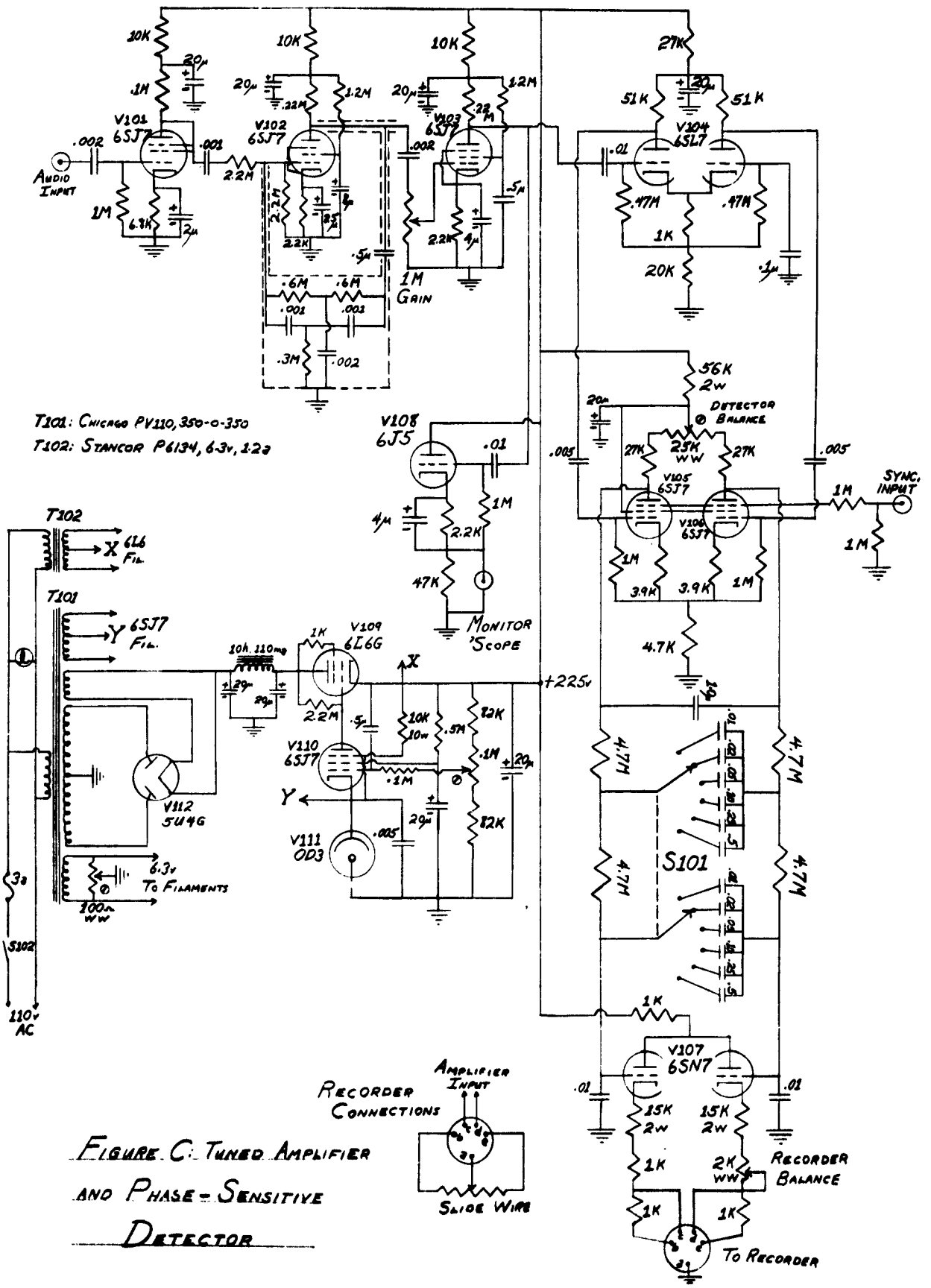

FIGURE C: TUNED AMPLIFIER AND PHASE-SENSITIVE DETECTOR

size. The coaxial cable connecting the sample coil and the oscillator is RG-62/U cable with the center conductor replaced by #22 solid copper wire.

C. The Tuned Amplifier and Phase-Sensitive Detector.

These two units are incorporated into a single chassis. The present form of the circuit (Figure C) is derived from a circuit designed by Mr. L. C. Hedrick for Professor E. Bright Wilson's research group. The input signal from the R-F unit is amplified by V101, a 6SJ7 connected as a triode, and is then sent to the tuned amplifier, V102. This amplifier consists of a normal resistance-coupled pentode amplifier circuit and a twin-T resistance-capacitance network connected between the grid and plate of the amplifier tube.

The twin-T network has an impedance which is frequency sensitive, as we can show from the following considerations. In the network of Figure D-1, each of the two single T networks of which the twin-T is composed can be converted to an equivalent Π network, which is equivalent in that it will give the identical terminal currents and terminal voltages under identical external conditions. The impedances Z_B and Z_E in which we are particularly interested are given in the figure in terms of the actual circuit elements from which they are derived (for derivation, see C-1).

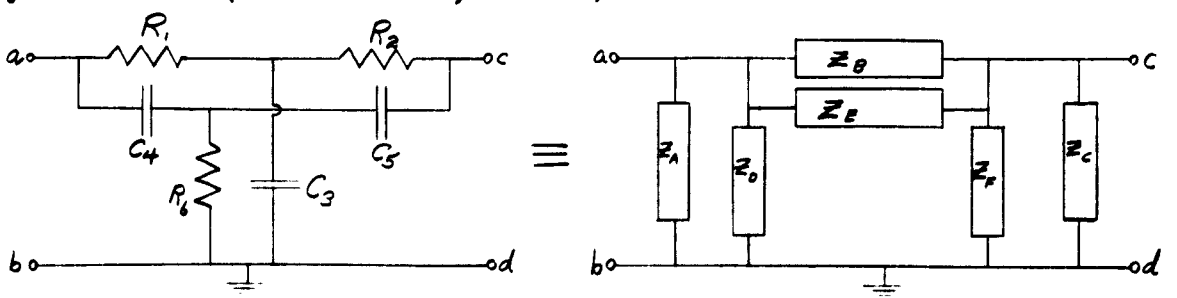

$$Z_B = R_1 + R_2 + j\omega C_3 R_1 R_2$$

$$Z_E = -\frac{1}{\omega^2 C_4 C_5 R_6} - j\frac{1}{\omega}\left(\frac{C_4 + C_5}{C_4 C_5}\right)$$

Figure D

In Figure D-2, we can see that the impedance between points a and c is represented by the parallel combination of Z_B and Z_E, so $Z_{ac} = \frac{Z_B Z_E}{Z_B + Z_E}$. If $Z_B + Z_E = 0$ the impedance from a to c will be infinite; no signal will be transmitted from a-b to c-d. This condition will be fulfilled if both the resistive and reactive parts of Z_B and Z_E, respectively, are equal in magnitude, or:

$$R_1 + R_2 = \frac{1}{\omega^2 C_4 C_5 R_6} \qquad \omega C_3 R_1 R_2 = \frac{1}{\omega}\left(\frac{C_4 + C_5}{C_4 C_5}\right)$$

These relations involve the applied frequency, ω. Thus the values of the components in the twin-T network can be selected so that one desired frequency will be rejected by the network while all other frequencies will be transmitted. Considering the whole circuit of the tuned amplifier, we can now see that the twin-T network will provide considerable degenerative feedback from the plate to the grid of V102, except at the rejection frequency of the network. As a result this stage will amplify only the rejection frequency of the twin-T, which is adjusted to be the same as the modulation frequency. In practice, the components of the twin-T network were chosen to give a rejection frequency as close as possible to the desired 280cps modulation frequency, and the modulation oscillator (to be discussed later) was tuned to the actual rejection frequency, which is approximately 260cps in this unit.

In addition to the high attenuation of the signal there is also produced by the twin-T network a phase shift which is a rapidly varying function of frequency, for frequencies close to the rejection frequency. It is thus very important to minimize thermal drifts in the twin-T network. This is accomplished by using silver-mica capacitors and one watt carbon resistors in the twin-T network, the positive temperature coefficients of the capacitors tending to offset the negative temperature coefficients of the carbon resistors. The network also is mounted in a separate can which plugs into a standard octal socket. This arrangement shields the network from pickup voltages to

which it is quite sensitive, and also provides for easy changes in the network components in case the modulation frequency is changed. As a final precaution, the filament and plate voltages are left on at all times.

One other practical point is worth mentioning. It was found necessary to shield the input and output socket pins to the shield can of the twin-T network in addition to using shielded leads, to eliminate a severe source of pick-up. This was accomplished by improvising a shield of heavy copper braid which was soldered to the chassis as well as to the shield on the input and output leads.

The overall operation of the tuned amplifier has been satisfactory. There has been little drift in the rejection frequency, which has been checked periodically. However, the bandpass characteristics could be improved. A semi-quantitative check has indicated that the bandwidth between the points at which the output voltage is one-half its maximum is approximately 30cps. This does not compare well with the circuit devised by Watkins which has a bandpass of 8cps (W-1). The difference is due, at least in part, to the loading effect of the plate load resistor of V102. The Watkins circuit is designed to keep the twin-T unloaded, and in addition is arranged to make the bias on the tuned amplifier tube self-compensating for aging or changes in the tube characteristics.

The output from the tuned amplifier is further amplified by V103, and the signal is then applied both to the phase-inverter stage of the phase-sensitive detector and to a cathode-follower circuit employing V108, from which the output is connected to the oscilloscope for monitoring and frequency measurement (discussed in section G, below).

The phase-inverter stage V104 converts the input signal into two signals which are identical in amplitude but 180° out of phase with respect

to each other. In brief, its operation is as follows. The input signal, applied to the first grid, produces a voltage at the first plate which is 180° out of phase with respect to the input. The cathode, which is unbypassed and connected directly to the cathode of the second half of the tube, will apply a signal at the second cathode which is in phase with the voltage applied to the first grid. Since the second grid is grounded, the voltage at the second plate will also be in phase with the input voltage and therefore 180° out of phase with respect to the voltage at the first plate. If the plate load resistors for the two plates have the same resistance, the two voltages will have practically the same amplitude, and the balance is improved by the degenerative effect of the cathode circuit.

The two voltages from the phase-inverter are fed to the grids of the phase-sensitive detector tubes, V105 and V106. At the same time, a synchronizing voltage at the modulation frequency is fed to both suppressor grids from a source in the modulation unit. The operation of the circuit is best explained in terms of the diagrams in Figure E. In the absence of a signal from the sample (Figure E-1), the plate current in each tube is controlled by the synchronizing voltage. It can be seen that each tube is cut off during alternate half-cycles but that the average plate current is the same for each tube. This is accomplished by placing the suppressor grids at d-c ground potential in the absence of the synchronizing voltage, and thus about 20 volts negative with respect to the cathode voltages. This is sufficient to cut off the plate currents except during the positive half-cycles of the synchronizing voltage. The tubes therefore are being operated non-linearly, such operation being essential if an output signal is to be obtained.

In Figure E-2 we see the effect of a signal from the sample. The modulation current sweeps the applied magnetic field back and forth over a portion of the line, causing a periodic variation in the oscillation level

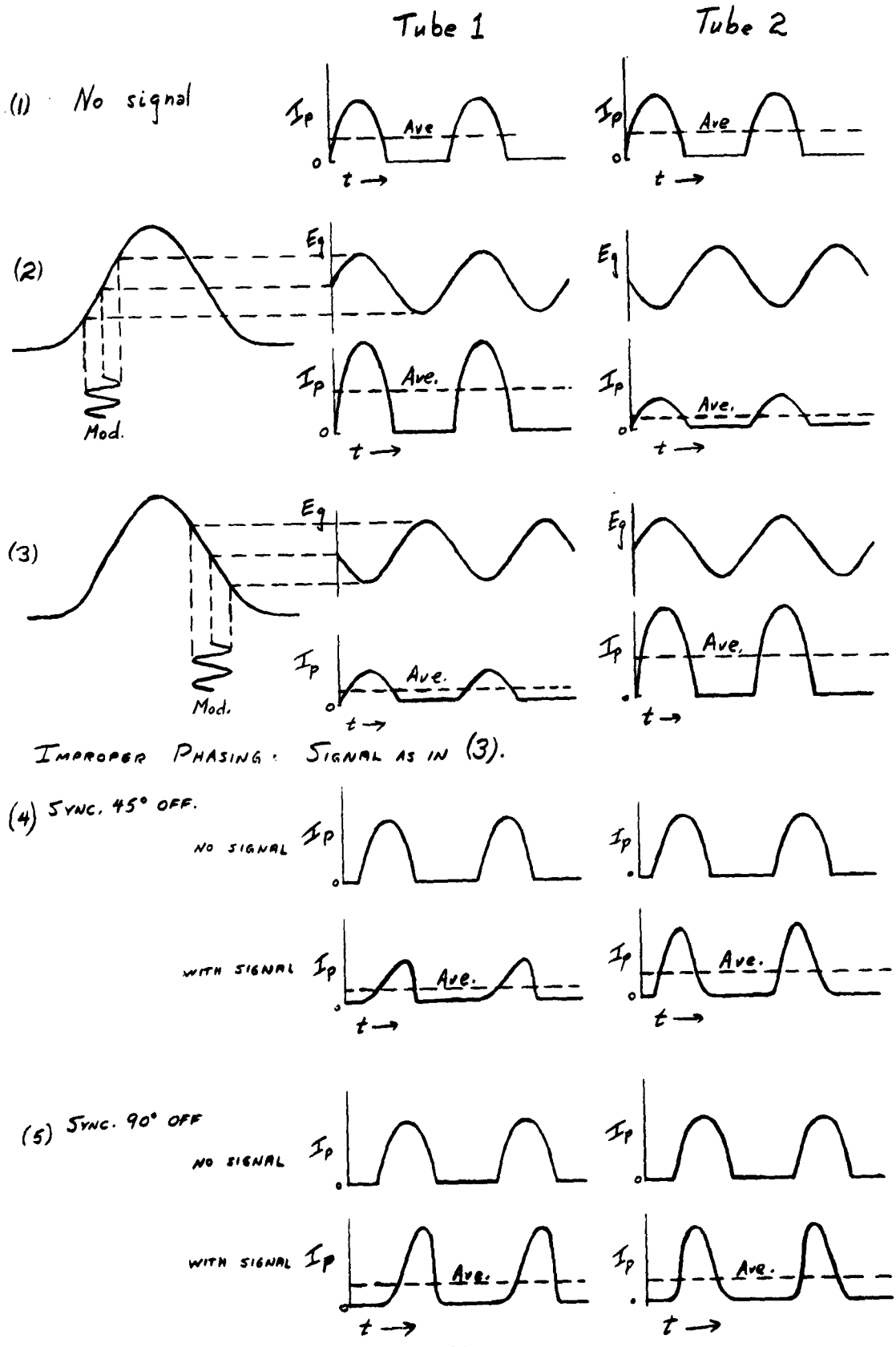
Tube 1
Tube 2
(1) No signal
I_p
Ave
0
t →
(2)
E_g
Mod.
(3)
IMPROPER PHASING. SIGNAL AS IN (3).
(4) SYNC. 45° OFF.
NO SIGNAL
WITH SIGNAL
(5) SYNC. 90° OFF
NO SIGNAL
WITH SIGNAL

FIGURE E.

across the sample coil which appears at the phase-sensitive detector as a pair of alternating voltages applied to the grids of the tubes. If the synchronizing voltage is adjusted so that it is exactly in phase with the signal applied to the grid of tube 1, it will then be 180° out of phase with the signal applied to the other grid. The average plate current through tube 1 will be increased while that through tube 2 will be decreased, as shown in the figure. When the oscillator frequency corresponds to a point on the other side of the resonance line the situation will be that illustrated in Figure E-3. The plate current through tube 1 will be decreased and that through tube 2 will be increased. We can also see from the figures that the signal applied to the grids will be approximately proportional to the slope of the line at the center of the range of field strengths covered by the modulation.

Figures E-4 and E-5 illustrate the effect of improper phasing of the synchronizing voltage. The result of such maladjustment is to reduce the amplitude of the output signal. The phasing control for the synchronizing voltage consists of a resistance-capacitance phase shifting network located in the modulation unit. The phase variation is accomplished by adjusting the setting the oscillator frequency so that it falls at or near one of the points of maximum slope of the absorption line (a maximum point on the recorded curve). The phasing control is then adjusted to give the maximum deflection of the recorder. Further adjustment is not necessary thereafter, as long as the oscillation level is not altered.

In the output from the phase-sensitive detector tubes is a fluctuating direct current. It is filtered by the long time constant network, which also integrates out noise. Switch S101 permits a selection of time constants from .25 to 15 seconds. Longer time constants provide better filtering of noise; however the response of the system to changes in the input signal is slowed

proportionately. Thus the time constant used for a particular run must be less than the length of time required to sweep through the absorption line by a factor of at least five.

The final stage V107 is a d-c amplifier which supplies the current required to drive the recorder. The connections to the recorder are also shown in Figure C. The slide wire potential is supplied from the cathode circuit of V107, eliminating both the battery supply and the automatic balancing circuit in the recorder itself. The recorder operates as a null point indicator. Any voltage difference between the two input terminals is amplified and used to drive the motor which moves the center tap on the slide-wire. Since the center tap is the common ground connection for both the cathode circuits of V107, which are connected to the ends of the slide wire, any change in the position of the center tap will increase the resistance of one cathode circuit at the expense of the other. When the connections to the recorder are properly made the motion of the center tap will be in such a direction as to decrease the voltage difference between the input terminals. When the recorder is at balance (zero potential across the input) it may be unbalanced by either of two means, a change in the potentials at the two grids of V107 or a change in the Recorder Balance control, which is a variable resistance in one of the cathode circuits. The Recorder Balance control is used to bring the recorder pen to midscale when the grids of V107 are temporarily tied together. Then the grids are unshorted and the Detector Balance control is used to return the pen to midscale, thus balancing the phase-sensitive detector tubes against each other in the absence of a signal.

The tubes V109, V110, V111, and V112 and their associated components form an electronically regulated power supply. The principle of operation is as follows. Let us assume that a certain potential exists between the cathode

of V109 (B^+) and ground. If this potential increases for any reason, the potential applied to the grid of V110 will increase because of the increased potential at the center tap of the 100K potentiometer. The cathode of V110 is kept at a constant potential of 150 volts by the voltage regulator tube V111. Therefore an increase in the grid voltage will allow the plate current of V110 to increase. This current must pass through the 1.2 Meg resistor which is connected between the plate of V110 and the output of the power supply filter, and it will therefore increase the potential across this resistor. The end result is to decrease the grid voltage of tube V109 and increase the voltage drop across this tube, compensating for the original increase in the B^+ voltage. The B^+ voltage is adjusted initially by the setting of the 100K potentiometer.

From the nature of the diagrams of Figure E, it can be seen that the phase-sensitive detector could also be designed to feed the signal in phase to both detector tubes and the synchronizing voltage 180° out of phase to the tubes. In principle, either arrangement would be equally satisfactory. In practice, the present arrangement has proved to be superior. The original circuit, which was constructed to feed the synchronizing voltage out of phase to the detector tubes, showed a marked dependence of the recorder balance point on the phasing control of the synchronizing voltage. This was found to be caused by failure of the phase-inverting stage, located under these conditions in the synchronizing voltage circuits, to give a balanced output for all positions of the phasing control. Furthermore, any unbalance in the two voltages fed to the suppressor grids of the detector tubes was increased in the detector tubes themselves. This is probably due to the tube characteristics because no tolerances are specified in the construction of the suppressor grids of most pentod tubes whereas the other tube elements are rigidly controlled in manufacture. The latter consideration has not been significant in the present

circuit, which is based on that of Watkins (W-1), where the suppressor grids are driven in phase. Any existing differences in the two tubes are partially compensated by the common cathode resistor and the remainder is removed by the adjustment of the Detector Balance control.

It has been suggested that this circuit might be improved by using transformer phase-inversion and transformer coupling of the synchronizing voltage with diode detector tubes, in an arrangement which superficially resembles the discriminator circuit of a frequency modulation receiver. Such a system might have the very definite advantage of simplicity of the circuit and balancing arrangements, although the overall gain of the apparatus would be reduced. The decrease in gain would be of no importance, since the available gain of the existing apparatus is several hundred times that needed for the signals thus far detected. The only possible drawback to a transformer-coupled system would be the cost of the transformers as compared to the cost of the components in the existing system.

In summary, it is felt that the present circuit for both the tuned amplifier and the phase-sensitive detector is satisfactory for the present application of the equipment to line shape and line width measurements of proton lines. For studies involving weak absorption signals the bandpass characteristics of the tuned amplifier should be improved, while relaxation time measurements would require a stepwise gain control so that the setting could be reproduced accurately. The details of such modifications can be found in Watkins thesis (W-1).

D. The Modulation Unit.

The modulation unit, Figure F, was originally constructed according to a circuit diagram obtained from Watkins (W-2). The present circuit differs in some details from the original design and these changes will be mentioned

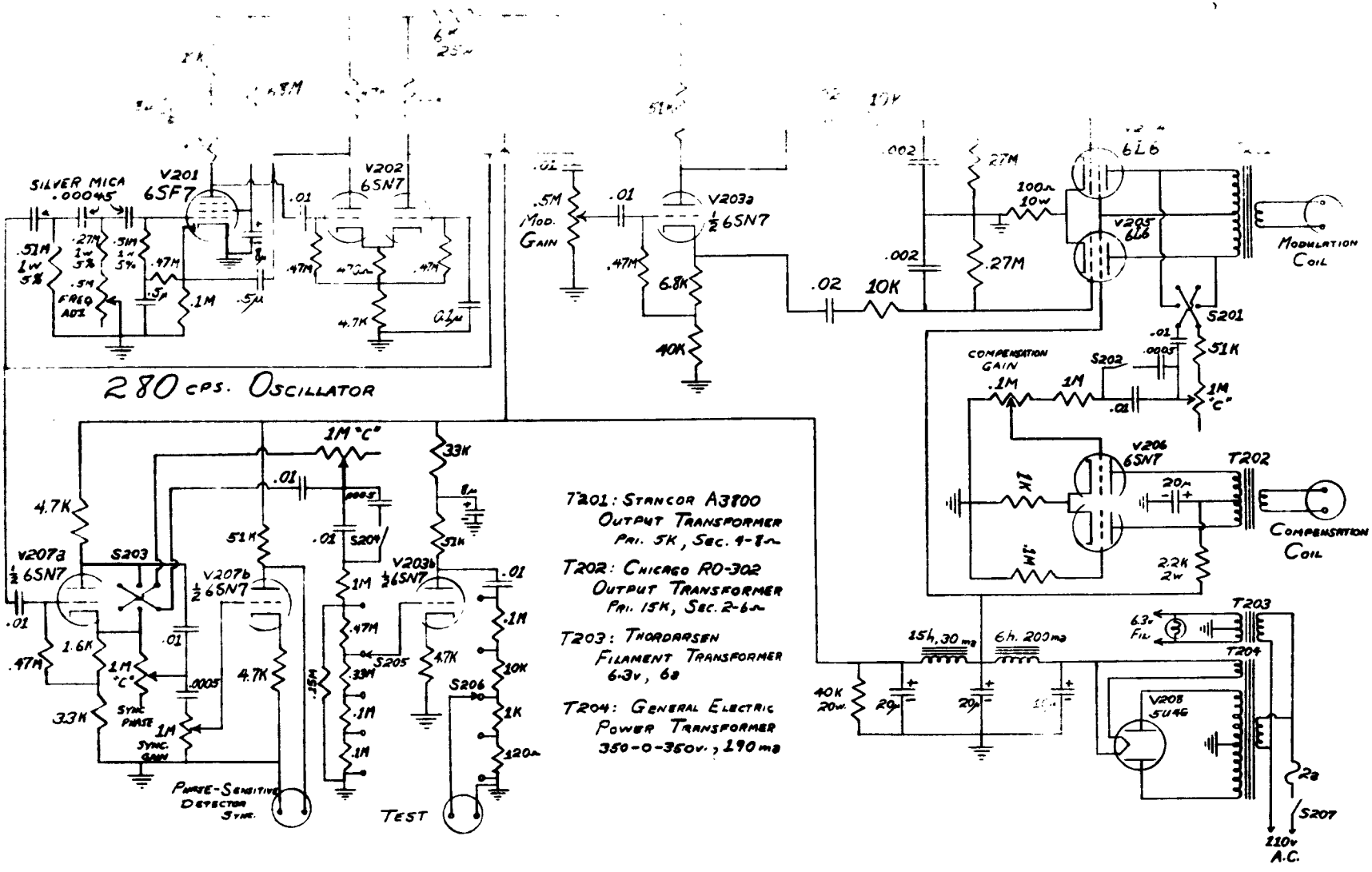

FIGURE F: MODULATOR UNIT

as they appear in the following discussion. Watkins' published circuit (W-1) differs considerably from that of Figure D, primarily in being designed for both sine- and square-wave modulation. The present circuit has no provision for square-wave modulation, so its adaptability for such operation will be discussed at the conclusion of the description of the existing circuits.

The 280cps oscillator circuit consists of tubes V201 and V202. It is a phase-shift oscillator of relatively standard design (see C-1, p. 509), and its operation may be described qualitatively as follows. Assume that a oscillatory signal is present at the control grid of V102. This will produce a signal at the plate that is shifted in phase by 180°. This signal, applied to the first grid of V202 will produce a signal at the second plate of V202 that is in phase with the signal at the first grid because of the common cathode arrangement for the two halves of the tube. Part of the signal from the second plate of V202 is then fed back to the grid of V201 through the three phase shift networks. Each of the networks produces a phase shift of 60°, so the signal arriving at the grid is in phase with the signal which we assumed was present at the beginning, and will sustain the oscillations. The frequency of the oscillator is determined by the phase-shifting network, being inversely proportional to the product of the resistance and capacitance used in a single stage of the network. The frequency can be varied slightly by the Frequency Adjust control, the total variation being restricted to about 40cps for stable operation, which is sufficient to permit tuning of the oscillator frequency to the rejection frequency of the tuned amplifier.

The first half of V202 and the diode of V201 are used to provide amplitude stabilization of the oscillator, an increase in amplitude of the oscillations causing the diode to draw more current and increase the negative bias on the grid of V201. The oscillator circuit thus provides a nearly pure sine-wave output at the second plate of V202, which is stabilized at about 13

volts. The frequency stability is also quite good, the same precautions being taken here as in the tuned amplifier circuit. Silver mica capacitors are used and the power is left on at all times. The tuning network is not mounted in a shielded can, but this would seem to be advisable.

V203a is a phase-inverter stage providing two balanced outputs 180° out of phase to drive the modulation power amplifier tubes in push-pull. The 10K resistors and .002mf capacitors in the grid circuits of the power tubes were added to eliminate spurious oscillations in the power amplification stage.

The power amplifier consists of V204 and V205, a pair of 6L6's operating in push-pull. They are theoretically capable of providing up to 20watts of audio power to drive the modulation coil. The usable output is actually considerably less, being limited by distortion of the output waveform at greater than 50% settings of the Modulation Gain control. The usable power output could probably be increased by better impedance matching between the modulation coil and the output transformer. However, the operation has been satisfactory, providing up to two gauss modulation of the magnetic field.

Part of the power output is fed to a phase-shifting network which supplies the signal for the compensation amplifier, V206. The combination of switches S201, S202, and the 1Meg potentiometer provides a full 360° of phase shift. In conjunction with the Compensation Gain control, they provide for completely variable phase and amplitude of the compensation current which is used to nullify any direct coupling between modulation coil and sample coil. The compensation is necessary at higher modulation amplitudes because such coupling causes serious zero drifts of the recorder trace during the course of a run and may also distort the recorded line shape. The compensation coil is wound around the outside of the Dewar flask and consists of approximately two linear inches of close-wound #22 enameled copper wire in a single layer winding.

The procedure for balancing is straightforward. The modulation amplitude is set at the desired level with no compensation voltage applied. The compensation gain is then set at an arbitrary level and the phasing controls are adjusted to give maximum deflection of the recorder pen in the direction opposite to the deflection caused by the modulation pickup alone. The Compensation Gain control is finally readjusted to give the original balance reading on the recorder. Unlike the phase sensitive detector phasing, the compensation must be readjusted for each run. The sample coil must be moved to change samples, and minute differences in the position of the coil change the coupling between the sample coil and the modulation.

The phasing arrangement for the compensation circuit is one of the least satisfactory parts of the circuit. The principle of deriving the signal for the compensation stage from a point in the modulation circuit following the Modulation Gain control is undoubtedly sound, as it keeps the compensation current approximately proportional to the modulation current without adjustment of the Compensation Gain. However, the present circuit arrangement with the phasing network connected between the plates of the modulation power tubes puts a severe strain on the circuit components. At higher power levels the voltage differential across S201 is several hundred volts, and considerable trouble has been experienced with breakdown of the switch, the .01mf capacitor, and the 1M potentiometer. The 51K resistor was added to reduce the current through the potentiometer when it is nearly shorted, and has alleviated some of the difficulty. However, the modulation current is still affected slightly by changes in the switch positions or the setting of the potentiometer. In addition, there is the inconvenience of manipulating three different controls to obtain the full 360° phase shift. It is therefore recommended that any future modifications of the modulation unit include the replacement of the present phasing arrangement by a magnetic phase shifter which will provide a linear, continuous

phase shift of 360° in one control, even though this might entail the addition of another tube to the existing circuit. One such phase shifter is the Eclipse-Pioneer AY242-53 Autosyn, manufactured by the Bendix Corporation (W-3).

V207a is another phase-inverter stage, similar to V203a. It is driven by a signal from the output of the oscillator section and supplies the phase shifting networks for both the phase sensitive detector synchronizer, V207b, and a test source, V203b. The 1M potentiometer in the cathode circuit of V207a provides about 160° of phase shift for the synchronizing voltage. The Sync. Gain control gives a synchronizing output of up to 50 volts at the plate of V207b, the full output usually being used for the phase sensitive detector.

The phasing network which supplies the test circuit, V203b, is identical to that used in the compensation circuit, and the same considerations apply. The switch S205 in the grid circuit of V203b allows the test output to be attenuated in steps of about two, while S206 attenuates the output by factors of 10. In the present apparatus, this circuit is not used except when the absorption signal is observed visually, in which case it supplies the horizontal sweep of the oscilloscope to give a sweep synchronous with the modulation field. For relaxation time measurements, this circuit supplies the calibrator circuit which is discussed by Watkins (W-1)

The power supply (V208 and the associated filter circuit) is unregulated, and has a capacitor-input filter. The 16mf capacitor at the input of the filter was added to increase the plate voltage of the modulation power tubes and thereby increase the power output. The increased B^+ voltage affected the stability of the oscillator circuit, so the 6K resistor was introduced to lower the oscillator plate voltage to its original value. Under the present operating conditions, the power supply arrangement is satisfactory. Should the distortion in the modulation output be corrected, allowing higher useful modulation output, it is felt that the capacitor-input filter will not have

the necessary voltage stability. The total plate current of the modulation tubes decreases as the audio power output increases, so the B^+ voltage of all tubes will increase. This can cause a change in the oscillator frequency, which has already been observed for settings of the Modulation Gain control just slightly above the normal range of use.

We have already mentioned that Watkins circuit includes provision for square-wave modulation. This is accomplished by taking the sine-wave output from the oscillator and clipping the wave shape before sending the signal to the modulation amplifier stages. Square-wave modulation has the advantage of presenting the actual line shape rather than its first derivative on the recorder trace. However it requires considerably higher modulation amplitudes, greater than the overall line width in gauss, or 10-20 gauss. It also requires a high quality output transformer in the modulation stage to pass all the harmonics which give the square shape to the waveform. The present system is unsuitable for square-wave modulation for two reasons. The output transformer is not of the high quality required, and the modulation coil, which is wound on one of the pole pieces, will not respond properly to a square-wave signal under any conditions. The coil would have to placed in the gap where it would be approximately an air-core coil in order to give the square shape to the modulation field.

In general, the modulation unit seems to be the least satisfactory part of the entire apparatus. Considerable trouble has been encountered periodically in its operation, and the maximum useful modulation field is limited as we have mentioned. It has given satisfactory results for the range of compounds studied in this investigation, but these have for the most part given relatively narrow line shapes. It is felt that the general utility of the apparatus could be improved by a better design of the modulation unit and the modulation coil.

E. The Magnet.

The present apparatus utilizes an Alnico V permanent magnet, the Alnico being supplied on indefinite loan by the Carballoy company. Each pole piece consists of seven discs of Alnico, each six inches in diameter and one inch thick, with a one inch diameter hole in the center. The pole caps are of soft iron and are tapered from six inches to four and one-half inches in a length of one and three-quarter inches. The pole pieces are bolted to the magnet yoke by a one-half inch bolt of stainless steel which extends through the yoke and the center holes of the Alnico discs and into the pole caps. The yoke is made of 4"x7" Armco iron ground flat at the joints, and the whole assembly appears as shown in Figure G.

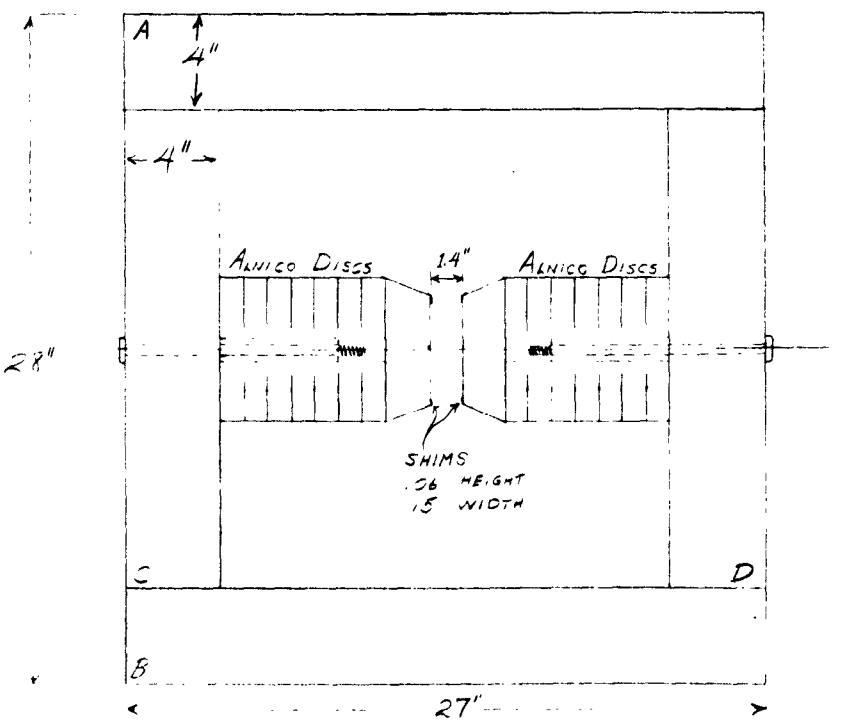

Figure G

The most recent check of the field strength gave 5,052 gauss. However, the field strength varies with temperature, as much as three gauss. Since we will be concerned only with line widths the actual value of the field

is of little importance, but the field inhomogeneity is an important factor. The best spot in the field was determined by trial and error, and was found to give an inhomogeneity over the sample of less than 0.25 gauss. This is too small to affect the line shapes and second moments of the observed samples, so inhomogeneity broadening has been neglected in the calculations of results.

Considerable difficulty was experienced in obtaining the necessary homogeneity of the magnetic field. The Alnico was magnetized at first by a current in excess of 1200 amperes supplied by the cyclotron generator at the Nuclear Physics Laboratory. To protect the generator, the current was interrupted after less than one second. When the proton line was first observed in a sample of water, the inhomogeneity was greater than two gauss over the area of the sample. A discussion with Professor R. V. Pound of the Physics department led to the conclusion that the original magnetizing current had been left on for too short a period to allow eddy currents in the Alnico to die out. There were also indications that the pole faces were not parallel, so that shimming of the pole pieces would be required. It was therefore necessary to demagnetize the Alnico so that the magnet could be dismantled. It was also decided to rewind the magnetizing coils so that a generator in the Department of Chemistry could be used for any subsequent magnetizations or demagnetizations, and to widen the gap from the original 3/4 inches to $1\frac{1}{4}$ inches in order to accommodate a low-temperature thermostat.

The available generator was rated at 120 volts and 80 amperes. Even with the use of a second generator for external excitation of the generator field the maximum current that could be obtained from the generator under overload was about 120 amperes at 105 volts. The coils were wound to meet these limits and to satisfy the requirement for Alnico V of an applied magnetizing force of at least 6,060 ampere-turns per inch. Thus the coils were required to have a minimum of 50 turns per inch. The only wire available under

the restrictions on the purchase of copper in force was #17 solid copper wire. This can be close-wound to give about 18 turns per linear inch in a single layer, so a triple-layer coil was required. However, it was necessary in practice to wind eight such coils and connect them in parallel to reduce the total resistance sufficiently to use the full current output of the generator Coil forms were made of brass sheet and were constructed to fit as snugly as possible over the pole pieces of the magnet. The coils were then wound on the forms and consist of eight individual three layer coils close-wound on top of each other and connected in parallel. The two sets of coils were connected in series during the magnetization process, and the current was applied for a sufficient time for it to reach a steady value. During the magnetization process a set of thin iron plates were placed in the air gap of the magnet to reduce the reluctance of the magnetic circuit, thin sheets being superior to a solid iron block because of the ease of removal from the magnetic field after magnetization.

The pole faces were adjusted for parallelism before the second magnetization. This was done by trial and error, using copper shim stock between the yoke and the pole pieces, and measuring the gap spacing at several points with a set of Johanson blocks. By this method a difference in gap width between the widest and narrowest points of 0.0007 inches was achieved. The final result of this adjustment and proper magnetization procedure was the field strength and inhomogeneity given above, which has proved satisfactory for line shape and line width measurements.

For certain purposes such as "chemical shift" studies (M-2) or determination of natural line widths in liquids the field inhomogeneity of the present magnet is unsatisfactory. It could best be improved by extensive remodeling designed to improve both the parallelism of the pole faces and the alignment of the pole pieces. The most important change would be to mount the pole pieces against pieces A and B of

flat along their entire length, the parallelism of the ground faces will be determined by the relative lengths of pieces C and D, which can be ground to equal length with almost any accuracy desired. The parallelism of the pole faces will then be determined by the accuracy of the grinding of the Alnico discs and the turning of the pole caps. The alignment of the pole pieces can be facilitated by drilling oversized holes for the stainless steel bolts so that the pole pieces can be moved sideways relative to each other. Final adjustment of the parallelism of the pole faces can be done by shimming as before, by rotation of the pole pieces relative to each other, or by a combination of the two; and a tolerance of less than 0.0001 inches should be attainable without excessive difficulty. Under such conditions, the field inhomogeneity should be determined largely by inhomogeneity in the iron of the pole caps and this can be corrected by hand polishing if lower inhomogeneity is required.

F. Gap Units and Low Temperature Arrangements.

The original gap unit, which was used for testing of the apparatus and for a few room temperature measurements, was constructed in a manner identical to that of Watkins (W-1). A similar unit also is discussed and illustrated in the article by Pound and Knight (P-5). Most of the results reported here were obtained with the low-temperature arrangement discussed below, so no further description of the original gap unit will be given here.

The low temperature gap unit is shown in Figure H. The Dewar flask was manufactured by the H. S. Martin company of Evanston, Illinois. An appropriate inner diameter of the stem could be obtained only by using a Pyrex test tube instead of the standard Pyrex tubing. The internal arrangement of the sample coil and thermocouple leads is the final result of a series of trial arrangements. The sample coil must be shielded from the coolant, except when liquid nitrogen is used, since the other coolants either contained hydrogen

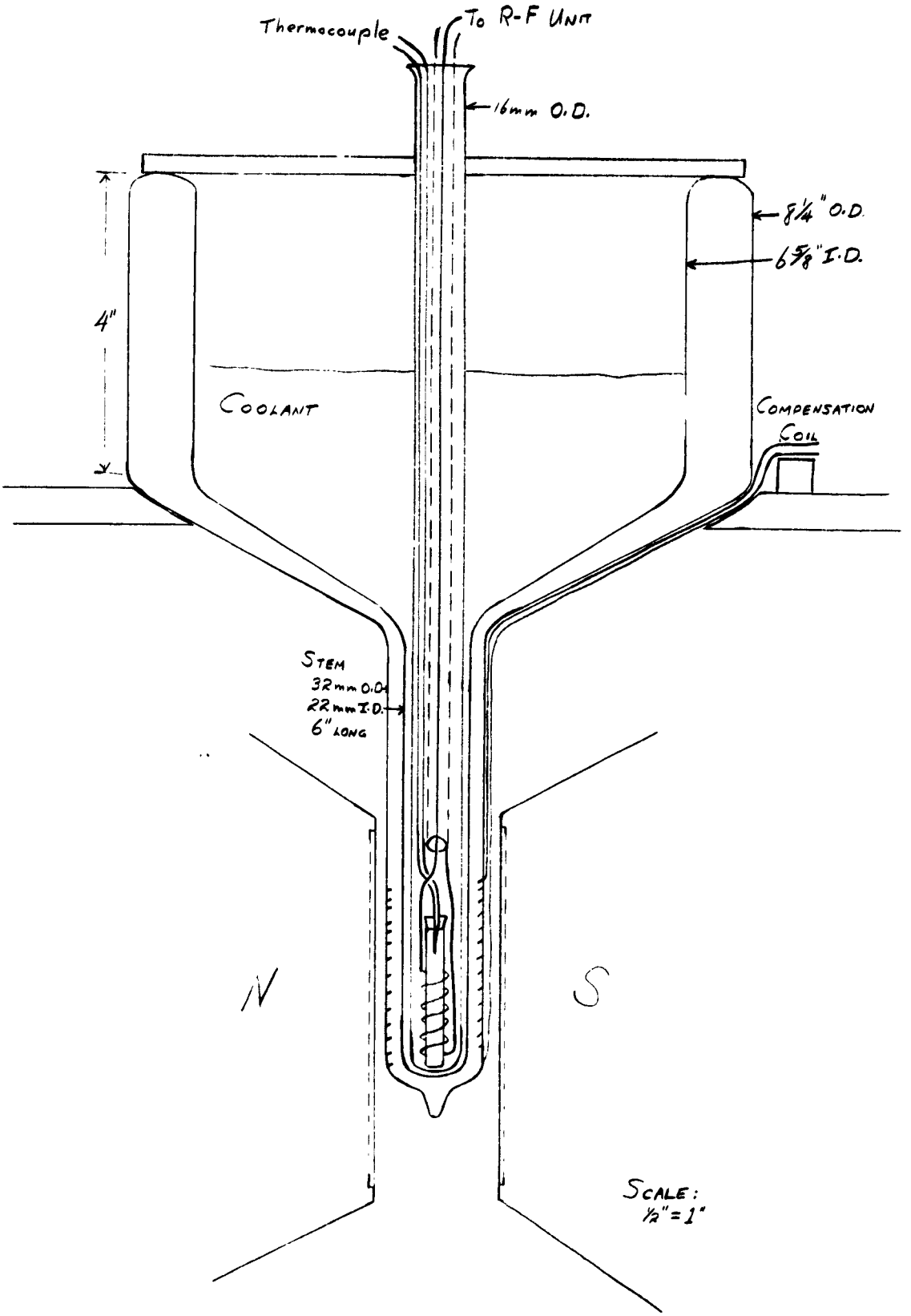
Thermocouple
To R-F Unit
16mm O.D.
8¼" O.D.
6⅝" I.D.
4"
Coolant
Compensation Coil
Stem
32mm O.D.
22mm I.D.
6" long
N
S
Scale:
½" = 1"

FIGURE H

(isopentane) or were polar and would have adverse electrical effects on the coil. It was decided to use a closed system for all low temperature measurements, and glass was chosen in preference to copper to avoid increasing the coil-to-ground capacitance. Attempts to fix the sample coil rigidly to the glass shield and to use a ground-glass joint at the bottom of the tube for replacement of samples failed to give a leakproof system, so the present arrangement was devised. The coil and thermocouple must be withdrawn from the tube in order to change samples, but with careful handling this has been satisfactory.

The sample containers are of two types. The samples which are sensitive to moisture have been sealed into vials made of 6mm Pyrex tubing. Other samples are placed in standard 1/8th dram vials. In the latter case the thermocouple can be embedded in the sample; otherwise it is placed in contact with the glass wall of the sample tube.

The thermocouple is made of chromel-alumel wire and is connected to a Leeds and Northrup student potentiometer. The calibration table for the thermocouple was taken from the literature (W-4), and was checked at both -196°C and -80°C. Temperatures have been read to within one degree, although somewhat better accuracy is possible from the potentiometer. However, there was always some possibility of the existence of temperature differentials between the thermocouple and the sample when these were not in direct contact, so it is felt that readings of more precision than one degree are not significant. It should be pointed out that under normal operating conditions the heat produced by the current circulating in the coil is negligible. The coil has an inductance of about 0.04 microhenries, and a d-c resistance of about 0.01 ohms. The current through the coil is thus about 20 ma and the heat dissipated in the coil is around four microwatts. This is certainly too small to cause any measurable temperature rise in the coil or sample.

G. Miscellaneous.

1. Frequency measurement. The oscillator frequency is measured with a Signal Corps BC-221-B frequency meter which is coupled loosely to the plate of the second r-f amplifier, V-3 (Figure B). This arrangement produces a strong beat signal in the frequency meter output without disturbing the oscillator frequency. A beat signal is also produced in the r-f amplifier and fed through the tuned amplifier to the monitor oscilloscope. This signal has little effect on the phase-sensitive detector because it is strongly attenuated in the tuned amplifier stage except for the brief periods when it has nearly the same frequency as the modulation frequency. However it affords a second check on the frequency and is especially useful when the oscillation level is low and the beat signal in the frequency meter is weak. The instant of zero beat can be observed either in the frequency meter output or on the oscilloscope and the recorder chart can be marked with the aid of a switch which momentarily connects one of the recorder input terminals to ground through a 100K resistor.

The precision of measurement of the absolute frequency is probably not better than $\pm$ 3Kc, because there is no provision made in the meter for calibration of the meter frequency against an absolute standard such as WWV. However, frequency differences can be measured with the precision of the calibration of the meter dial, which is $\pm$ 400cps, corresponding to a difference of 0.1 gauss. The actual precision is probably closer to $\pm$ 0.2 gauss because of other random errors associated with the operation of both the frequency meter and the oscillator unit.

The frequency meter was designed to operate from battery supplies for both the filament and plate voltages. In the present arrangement the filaments are supplied from the same storage battery that supplies the filaments of the R-F unit, but the plate voltage is supplied by a small power supply consisting

of a half-wave rectifier and a capacity-input filter. A-c operation of the filaments was also tried, but proved unsatisfactory because of the large amount of 60cps hum in the meter output.

2. Oscilloscope. The oscilloscope used for monitoring or direct observation of narrow lines is a Heathkit Model O-6. It has proved very satisfactory for the purposes mentioned, especially considering its cost. However, it is not equipped for photographing the trace. A simple arrangement of a metal cone, blackened to avoid reflections, and an Argus C-3 camera equipped with a portrait lens has given fairly good pictures of the oscilloscope trace. However, it is questionable whether a similar arrangement with a movie camera, used to make direct measurements of relaxation times, would be satisfactory.

H. Summary.

The apparatus just described was constructed to study the shapes and widths of proton absorption lines in silicone polymers, and has proved satisfactory for this purposes. There are, however, certain limitations to the utility of the apparatus in its present form. It is not suitable for relaxation time studies either by the direct method or the saturation method. This limitation could be removed by the addition of a calibrator unit (W-1) or a suitable photographing arrangement such as was mentioned above.

Use of the apparatus for the study of electric quadrupole resonances would be possible only after the addition of a high power square wave modulator unit and special sets of sample and modulation coils. Designs for such units can be found in Watkins' thesis (W-1).

We have already mentioned that the present arrangement of the modulation coil, wound around one pole of the magnet, puts a definite limit on the useful modulation amplitude. In order to increase this limit, and also to make possible the use of square-wave modulation, it would be necessary to wind new

modulation coils. It seems that the best arrangement would be to wind them as Helmholtz coils according to Watkins' specifications and tape or shellac them against the pole faces of the magnet. Such coils could be wound with a thickness less than the height of the shims on the pole faces, and therefore would not decrease the space available for the Dewar flask. They would also cause less pickup at the modulation frequency in the sample coil and cable or in the R-F unit. It should be pointed out that the problem of pickup increases as the modulation frequency increases, so it is not as important when a modulation frequency of 30cps is used, as is done by many other investigators.

The final limitation is that imposed by the minimum oscillation level of the oscillator. The saturation factor s (part II) is proportional to the square of the radiation field H_1, and to the product T_1T_2. To avoid saturation effects H_1 must be decreased as T_1T_2 increases, which usually happens as the temperature is reduced in a given sample. It has been observed that water and certain organic liquids, 1,1,1-trichloroethane, t-butyl chloride, and benzene for example, have fairly long relaxation times, so long that saturation effects could not be avoided with this apparatus. At low temperatures these effects were so strong that signals from some solid organic compounds could barely be distinguished from noise. Thus an important experimental problem would be the design of an oscillator which could operate stably at very low levels, while retaining the advantages of variable-frequency-fixed-field operation.

IV. RESULTS AND DISCUSSION

A. Chronology

Our expressed purpose, as stated in the introduction, has been to investigate the question of internal motion in organosiloxane polymers by the application of the nuclear magnetic resonance absorption technique. We hope to obtain evidence which will aid in determining which of the two theories, the Roth-Harker "free-wheeling" theory or the Pauling-Zisman coiling hypothesis best describes the behavior silicones. The materials which have been investigated in this research were chosen with this purpose in mind. However, the development of the problem has led to a choice of samples whose relation to the problem is not always obvious; and it seems to the writer that a brief discussion of this development is in order.

The first materials chosen for study were, obviously, silicone rubber and, less obviously, hexamethylcyclotrisiloxane (cyclic trimer). The latter compound was selected because it is a solid at room temperature, it is easily purified, and especially because it is a cyclic compound and therefore cannot coil according to the Pauling-Zisman hypothesis although it might still show restricted motion of the type postulated by Roth and Harker.

Room temperature studies showed that silicone rubber has a narrow liquid-like line indicating a considerable amount of motion. However, natural rubber also has a narrow resonance line at room temperature, so this fact by itself is of little significance. On the other hand, the cyclic trimer has a broad resonance line at room temperature with no evidence of fine structure in the line shape. This result was unexpected and led to the investigation of other cyclic dimethyl siloxanes.

Upon completion of the low-temperature arrangements, the samples of silicone rubber and the cyclic trimer, tetramer, and pentamer were investigated at 77°K (-196°C). At this temperature all the samples yield practically identical line shapes, broad smooth curves with no evidence of fine structure, and nearly identical second moments. The second moments are about one-half that expected for a rigid lattice, so we may conclude that some motion still persists in these materials even at a temperature which is at least 150 degrees below the melting point, and as much as 260 degrees in the case of the cyclic trimer. Gutowsky (G-1) found that rotation or tunneling of methyl groups in such compounds as methyl and ethyl alcohol, the ethyl halides, acetone, methyl chloroform, and acetonitrile, ceases at temperatures only 100 to 150 degrees below their respective melting points. We thus have an indication of an unusual mobility of the protons in the organosiloxanes. However, the lack of fine structure in the absorption lines makes a determination of the type of motion uncertain.

The uncertainty of any conclusions based on second moment data alone led to the next change in the scope of the investigation. A group of organosilicon compounds were sought which would have structures simple enough to yield good line shape information. It also seemed advisable to investigate some compounds which did not contain Si-O bonds in order to determine whether the siloxane linkage would show any significant effects on the molecular motion. These requirements are fulfilled by the methylchlorosilanes. Two other compounds, methoxytrichlorosilane and hexamethyldisiloxane, were also investigated as the simplest compounds containing siloxane linkages which were or could be made available.

The results obtained from the abovementioned compounds will be discussed below. The contributions of the chlorine nuclei and Si^{29} to the

second moments have been neglected. Their maximum contribution to the rigid lattice second moment would be around 0.1-0.2 gauss^2, and would be considerably less when the methyl group is in motion. In the interpretation of line shapes their contribution is included in the broadening factor β .

The arrows in the center of each derivative curve indicate the modulation width used.

B. The Monomethyl Compounds

1. 1,1,1-trichloroethane (methyl chloroform) has been investigated by Gutowsky and Pake (G-2,G-3). It has been repeated here as a check on the apparatus and also as an illustration of the line shape to be expected from a rigid methyl group. The line shape obtained in this investigation is shown in Figure I superimposed on that obtained by Gutowsky. The comparison between the two sets of data is particularly interesting because the apparatus used was quite different in each case. Gutowsky and Pake used a bridge technique, maintaining a fixed radiofrequency and varying the magnetic field, whereas the present investigation involves the fixed-field variable-frequency technique developed by Pound.

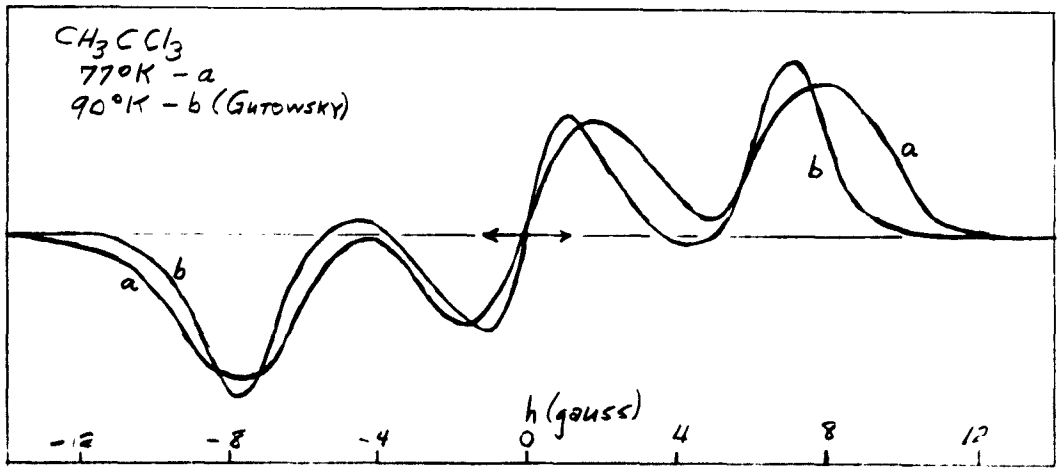

Figure I: Line Shape Derivative Curve for 1,1,1-trichloroethane

Qualitatively the two derivative curves are quite similar. The differences may be accounted for by two factors, the difference in the temperatures of observation, and saturation of the sample in the results obtained in this investigation. Saturation of the sample can be expected to cause some broadening of the line as well as a decrease in amplitude. Both effects were observed, the broadening being apparent from Figure I. The decrease in signal strength made the experimental determination of the line shape extremely difficult. When the oscillation level in the sample coil was set at the same value as that used for the organosilicon compounds, the signal was barely distinguishable from noise. Decreasing the oscillation level to the lowest value obtainable from the apparatus improved the sensitivity but never to a point comparable to that obtained from the silicon-containing samples.

The ease with which the sample of methyl chloroform saturates provides another example of the increased mobility of the organosilicon compounds. Saturation of the sample results, among other things, from long relaxation times; and the relaxation process requires the existence of fluctuating magnetic fields which are the result of vibration or rotation of the atoms in the sample.

The effect of temperature is most noticeable in the central peak, which is markedly broader at 77°K than at 90°K. Second moment data also indicate the residual motion in the sample has been decreased by the drop in temperature. If we assume that the methyl group has the same C-H distance as in methane (1.094 Å, (H-1)) and tetrahedral angles, the proton-proton distance will be 1.79Å, $\alpha = 3.69$ gauss, and the intramolecular second moment is 21.8 gauss^2. The intermolecular contribution to the second moment has been determined by Andrew from the line shape to be

2.1 gauss^2 (A-1), leading to a total second moment of 23.9 gauss^2. Gutowsky obtained an experimental second moment of 18.7 gauss^2, which is significantly less than the theoretical value. The second moment obtained from this investigation at 77°K was 21.7 gauss^2, which though still low is rapidly approaching the value predicted for a rigid methyl group. We may thus assume that methyl chloroform has an essentially rigid lattice at 77°K.

2. Methyltrichlorosilane. The experimental derivative curve, shown in Figure II, illustrates the effect on the line shape of restricted motion of the methyl group. The line shape is compressed by a factor of two in the horizontal direction, and the amplitude of the subsidiary peaks is markedly decreased from that obtained for a rigid methyl group.

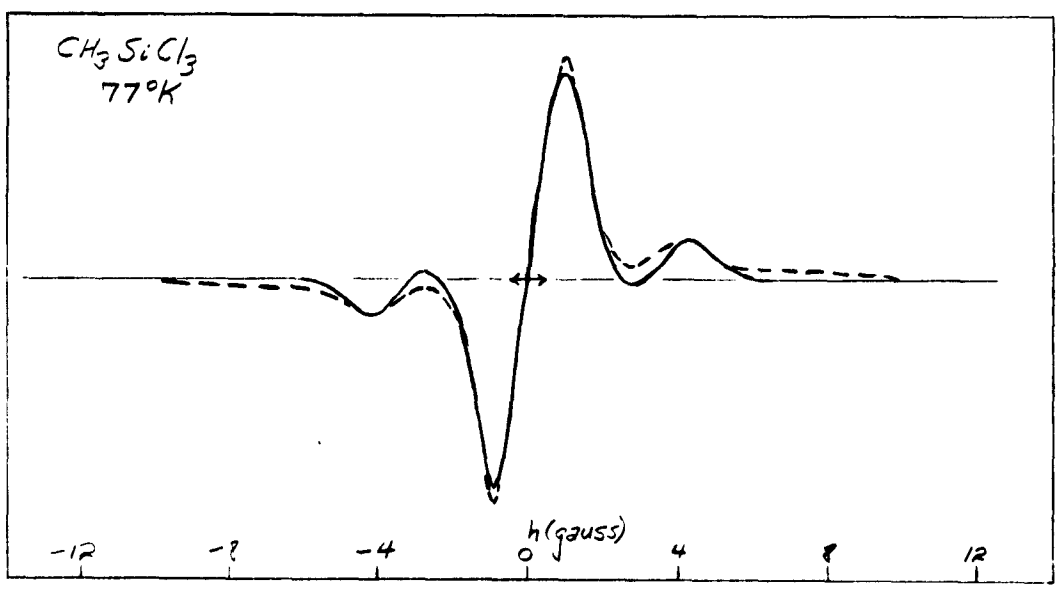

Figure II: Line Shape Derivative Curve for Methyltrichlorosilane

The second moment of the experimental curve is 3.55 gauss^2. If we assume as before that the methyl group has the same configuration as in

methane, we find that the second moment is only 0.163 time the computed intramolecular value for a rigid methyl group, and is less than that predicted for rotation or tunneling of the methyl group about the Si-C bond. This still includes the contribution from intermolecular broadening, which must be subtracted. Estimates of the broadening parameter by the use of equations (7-25) to (7-27), Part II, place the value of β between 1.0 and 1.4 gauss; thus from equation (7-24), Part II, the intramolecular part of the second moment should be 2.6-3.1 gauss^2, and $\langle \Delta H_2 \rangle^2 / \langle \Delta H_2 \rangle^2_{rigid} =$ 0.12-0.14. From Figure 16, Part II, we find that this is consistent with rotation of the molecule about an arbitrary axis with ϵ between 24 and 28 degrees, or between 54 and 57 degrees. Another possibility is obtained from Figure 18, Part II, rotation of the methyl group about the Si-C bond and simultaneous rotation of the molecule about an axis such that ϵ is between 24 and 27 degrees.

It should now be possible to compute theoretical line shapes and their derivatives for the three possibilities just mentioned, for several values of β/α in the range 0.27-0.38; and by comparison with the experimental derivative curve select the most likely values for ϵ and β as well as choose between single and double rotation of the methyl group. Considering the mass of information already obtained from the second moment data and the line shape, it is singularly unfortunate that none of the possibilities mentioned yields a reasonable fit with the experimental curve. In general, the theoretical curves calculated from the estimates made above, deviate from the experimental curve in two ways. They do not exhibit fine structure to an appreciable extent or if the fine structure is noticeable the maxima of the side peaks occur much too close to the central maximum.

Attempts to fit the calculated curves by varying the value of α do not yield any improvement without making drastic assumptions concerning the bond distances and the valence angles of the methyl group. In one case an approximate agreement can be reached if we assume that $\alpha \cong 4.3$ gauss. This would require either that the C-H bond distance be shortened to 1.04Å or that the H-C-H bond angle be decreased to about 102 degrees or that both be adjusted to some intermediate value. However, it seems more likely that in the presence of the positive Si atom the C-H distance would increase. Also the H-C-H angle in ethane is somewhat larger than tetrahedral (H-1) and by analogy we might expect that any change in this angle in other compounds containing methyl groups would be in the same direction. Thus it seems reasonable, in the absence of positive evidence to the contrary, to assume that the bond distances and angles of the methyl group are as postulated previously. We must then look elsewhere for a way to make theory agree with experiment.

By the simple expedient of ignoring the second moment data and relying on intuition it becomes possible to postulate that the methyl group is rotating only about the Si-C bond. The barrier to such rotation or tunneling of the methyl group should be low because the Si-C bond and Si-Cl bonds are considerably longer than the corresponding C-C and C-Cl bonds in methyl chloroform and thus the barrier produced by the chlorine atoms should be reduced.

A series of derivative curves were computed using this latest assumption and several values of β/α between 0.25 and 0.40. The closest correlation was obtained when β/α 0.36. This curve is represented by the dashed line in Figure II. The points of discrepancy are the tails of the curve and the minima at $\pm$2.8 gauss. However the spacings of both the

central and side peaks are quite close. The absence of the long tails accounts for the very low values of the second moments calculated from the experimental curve.

As we shall see when we discuss methoxytrichlorosilane, we cannot assume that the tails of the curve were lost in the background noise on the recorded trace, since the tails are visible in the curves obtained from methoxytrichlorosilane. However, it seems probable that there is some low-frequency motion of the molecule about axes perpendicular to the Si-C bond, since methyltrichlorosilane is a nearly symmetrical molecule. Such motion, if of sufficiently low frequency, might cause the observed decrease in the second moment as well as the loss of the tails of the derivative curve without otherwise affecting the line shape appreciably.

It is also quite possible that our assumption of a Gaussian broadening function to account for intermolecular interactions is not a good approximation. Pake and Purcell (P-7) have pointed out that this type of function is based on the assumption that there are a large number of near neighbors about each absorbing nucleus which add to the strong external field. It would seem likely that this assumption would be less valid when the broadening from such neighbors is small, as in the present case, and would be an increasingly better approximation as β increases.

3. Methoxytrichlorosilane. The observed derivative curve is shown in Figure III. The theoretical curve, represented by the dashed line, was computed assuming rotation of the methyl group about the C-C bond and a broadening factor β/α of 0.36. It can be seen that theory and experiment agree more closely than in the previous case.

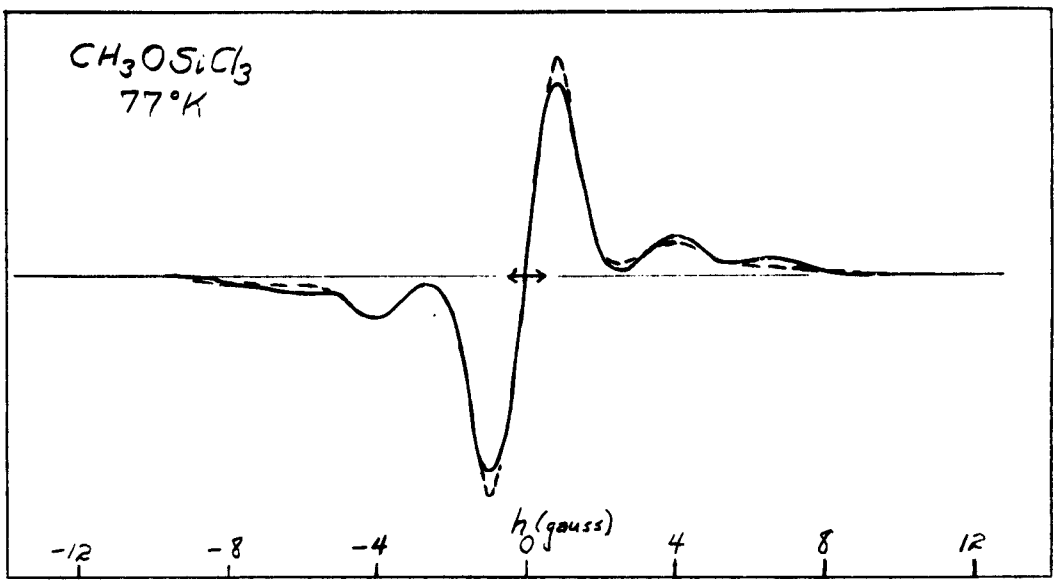

Figure III: Line Shape Derivative Curve for Methoxytrichlorosilane

The experimental second moment is 7.3 gauss^2, which is corrected to 6.3 gauss^2 when the intermolecular broadening is subtracted. The theoretical second moment for rotation about the C-O bond is one-fourth the rigid lattice second moment, or 5.5 gauss^2. The agreement is not remarkable, unless perhaps in comparison to the previous case. However, the experimental second moment is controlled largely by the long, low-amplitude tails in which the experimental error is likely to be large. Thus the assumption of rotation of the methyl group about the C-O axis seems to be well supported by the data.

It is interesting to note that there is apparently less residual motion in methoxytrichlorosilane than in methyltrichlorosilane at 77°K. On the basis of the Roth-Harker theory it might be expected that the Si-O bond would be somewhat flexible and permit the methyl group to "waggle". This is apparently not the case, at least at the temperature of these observations.

C. Dimethyldichlorosilane

The replacement of one of the chlorine atoms of methyltrichlorosilane by a methyl group produces a marked change in the proton line shape of the sample. This is illustrated by the experimental derivative curve for dimethyldichlorosilane shown in Figure IV.

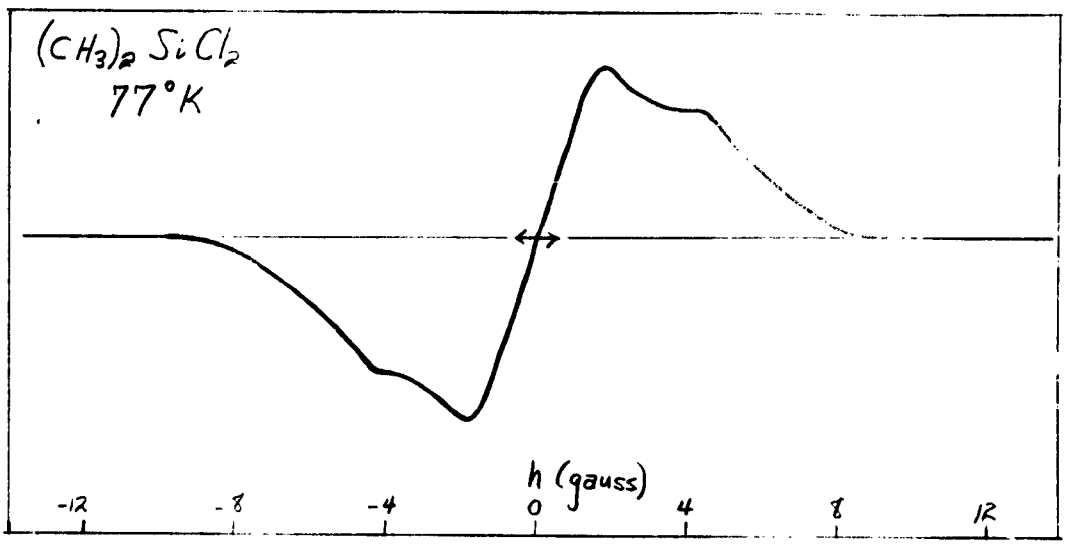

Figure IV: Line Shape Derivative Curve for Dimethyldichlorosilane.

Qualitatively, the derivative curve is about as one would expect. The line has been broadened and the fine structure largely masked by the addition of the second methyl group. This can be considered as a combination of two effects, the interaction between the two methyl groups in the same molecule and the reduced shielding of the methyl groups by the chlorine atoms.

The second moment computed from the experimental curves has an average value of 6.9 $gauss^2$, which is significantly higher than the second moments of the methyl- and methoxytrichlorosilane. However, the broadening parameter β has increased to a value of approximately 2.4 gauss, and the removal of its contribution to the second moment yields an experimental

estimate of the intramolecular second moment of 4.0 gauss^2. The theoretical intramolecular second moment can be computed from the electron diffraction data (L-1) with the assumption that the methyl group has the same configuration as previously assumed. Again we shall neglect the chlorine contribution. There are three possible configurations of the methyl groups with respect to each other, one staggered and two eclipsed with the staggered configuration having the least potential energy. For a C-Si bond distance of 1.83Å and a tetrahedral C-Si-C bond angle, equation (2-6), Part II, yields a rigid lattice second moment of 23.0 gauss^2 for the staggered configuration and 23.1 23.4 gauss^2 for the two eclipsed configurations. Thus $\langle \Delta H_2^2 \rangle_{EXP} / \langle \Delta H_2^2 \rangle_{RIGID} =$ 0.17 -0.174, which is less than that predicted for rotation of the methyl groups about the C-Si bond. We have assumed that the interactions between the methyl groups are decreased in the same proportion as the intra-group interactions, in accord with Andrew's calculations (A-2).

Attempts were made to fit the experimental curve in the same manner as described above for methyltrichlorosilane. The result was again unsatisfactory, for the same reasons. The assumption of double rotation yields a theoretical derivative curve without any indications of fine structure, while the theoretical curve for rotation of the molecule about an arbitrary has very slight indications of side peaks at spacings considerably less than those of the experimental curve. In this case the theoretical curve for the assumption of methyl group rotation or tunneling.is equally unsatisfactory, the side peaks of the theoretical curve being reduced to mere inflections of the curve although these are at approximately the desired spacing. There is, of course, the possibility that the molecule is rotating as a whole about one of the C-Si bonds, in which case the line shape will be composed of the

curve for methyl group rotation plus the curve for rotation of the other methyl group such that $\in$ is one-half the tetrahedral angle. Visual correlation of these two curves indicated that this combination would yield no better fit than the previous attempts. There is thus considerable ambiguity in the interpretation of the line shape of dimethyldichlorosilane. However, the conclusions reached with regard to methyltrichlorosilane suggest that the most reasonable interpretation of the data is that the methyl groups are tunneling about the C-Si bond with some residual motion of the whole molecule at a very low frequency. It can be seen from Figures II and IV that this interpretation of the data is at least consistent. In both cases we must assume that there is some low frequency rotation of the molecule as a whole, and that this motion is sufficient to reduce the second moment and accentuate the fine structure of the experimental derivative curve without, however, appreciably affecting the spacings of the maxima.

D. The Trimethyl Compounds

1. Trimethylchlorosilane. The presence of the third methyl group in trimethylchlorosilane increases the intermolecular broadening and the interactions between methyl groups on the same silicon atom to such an extent that the line structure is completely masked. This is shown by the experimental derivative curve in Figure V.

The second moment, after correction for intermolecular broadening, is found to be 5.2 gauss^2, which is only slightly less than the value expected for tunneling of the methyl groups. On the assumption that such tunneling is the predominant type of motion theoretical derivative curves were calculated for the two broadening factors $\beta/\alpha = 0.8$ and 1.0, and these were compared with the experimental curve. It was

found that the latter compared well in overall form with either of the curves, and that the peak of the experimental derivative curve at 2.6 gauss fell between the values of 2.1 and 3.2 gauss for the theoretical curves for θ/α = 0.8 and 1.0 respectively. Thus the approximate estimate of .85 is consistent with the theoretical curves.

Once again the tail of the experimental curve cuts off more abruptly than theory would indicate. This can be interpreted as before as indicating the existence of some low frequency motion of the molecule as a whole, which is consistent with the slightly low value of the second moment.

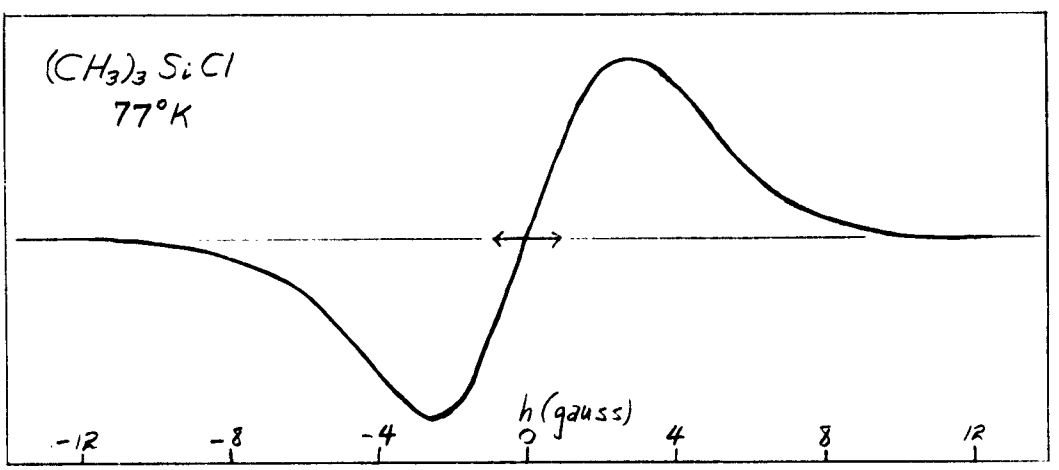

Figure VI Line Shape Derivative Curve for Trimethylchlorosilane

2. Hexamethyldisiloxane. The derivative curve for this compound is shown in Figure VI.

The comparison between the theoretical and experimental curves may be summarized as follows. Evaluations of θ/α from the experimental curve led to an estimate of 0.95 for the broadening factor. This is consistent with the shape of the two theoretical curves mentioned in the previous section with regard to the location of the peak of the experimental curve. However, the tail of the experimental curve falls off more

abruptly than the theoretical curve would indicate. At the same time the corrected experimental second moment has the very low value of 3.0 gauss^2, which is about the same as that computed for methyltrichlorosilane. Thus there must be considerable motion in addition to the tunneling of the methyl groups. The assumption that the molecule is rotating as a whole about an axis perpendicular to the Si-C bond yields a theoretical derivative curve in which the tail falls off faster than that of the experimental curve, if we assume that β/α has the value 1.3. Thus we once again have a case in which a good correlation of theory and experiment is not obtainable on the basis of the specific types of motion postulated.

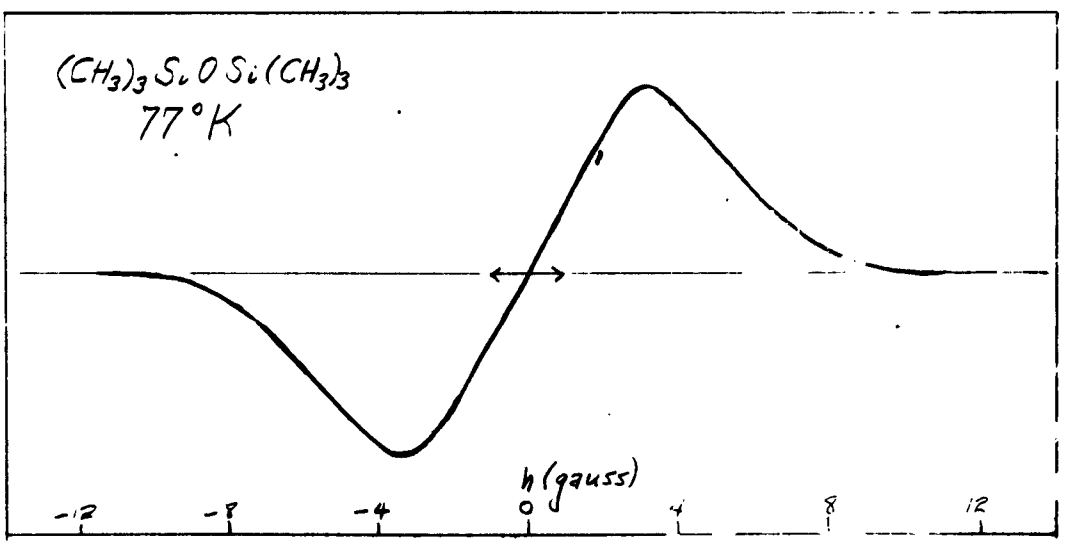

Figure VI: Line Shape Derivative Curve for Hexamethyldisiloxane.

There is still the possibility that there is rotational oscillation of the methyl groups in addition to tunneling about the C-Si bond. In terms of the second moment data this would require that γ be at least 40 degrees. The line shape is of no use in determining whether rotational oscillation is taking place, except for the negative evidence that the observed derivative curve cannot be fitted by theoretical curves on the basis of rotation alone. However, other structural evidence suggests that rotational oscillation is

not impossible. The Si-O-Si bond angle has been estimated by both electron diffraction and dipole moment studies (R-1), and has been variously determined to be anywhere from 140 to 180 degrees. The latter value was determined from the dipole moment in the gas phase (O-1). The large value of this angle compared to that found in organic ethers, as well as the considerable dispersion in the results, suggests that there is considerable flexibility of the Si-O bonds; this may be considered as an indication of rotational oscillation about an axis perpendicular to the Si-Si axis in the molecule. However, it must be admitted that this is a highly speculative conclusion, in the absence of further evidence.

E. The Cyclic Siloxanes

Three of the cyclic siloxanes have been investigated in this research, hexamethylcyclotrisiloxane (trimer), octamethylcyclotetrasiloxane (tetramer), and decamethylcyclopentasiloxane (pentamer). Because of the similarity of their absorption lines they will be considered together. Before considering the nuclear resonance data, let us review the structural information obtained by other methods.

The structure of the cyclic trimer has been determined by both electron diffraction (A-3) and x-ray diffraction (P-8). In addition we may consider the x-ray diffraction studies on octamethylspiropentasiloxane by Roth and Harker (R-3) since this compound may be considered to consist of two trimer rings with a common silicon atom (see Figure 1-4, Part I). The results are summarized in Table I.

All investigators have concluded that the ring is planar, with the carbon atoms arranged symmetrically above and below the plane of the ring. The silicon-oxygen bond distance is considerably less than the sum

of the covalent radii indicating that there is considerable ionic character in the silicon-oxygen bond. There is some disagreement about the Si-C bond distance. The electron diffraction data for the trimer, which was obtained from the vapor, and the x-ray data on the spirosiloxane yield a value which is less than the sum of the covalent radii (1.94Å), whereas the x-ray investigation of the trimer determines this distance as being significantly greater than the sum of the covalent radii. The explanation of this discrepancy is not known.

	E.D. trimer	X-ray trimer	X-ray, spiro-pentasiloxane
Si-O , Å	1.66 ± .04	1.6[illegible] ± .04	1.64 ± .03
Si-C , Å	1.88 ± .04	1.9[illegible] ± .0[illegible]	1.88 ± .03
O-Si-O	115 ± 5°	1[illegible]4 ± [illegible]°	110 ± 4°
Si-O-Si	135 ± 5°	1[illegible]6 ± [illegible]°	130 ± 4°
C-Si-C	112 ± 6°	1[illegible] ± [illegible]°	110 ± 4°

It is significant that each of the [illegible]e led to the conclusion that the thermal motion of the [illegible] larger than normal. The conclusions of Roth and Harker [illegible] already [illegible]d (Part I). With regard to the trimer, [illegible]ll and [illegible] thermal motion of about 0.09Å as compared to the normal value of 0.04Å. [illegible]d Peyronel found it necessary to include [illegible] in his x-ray diffraction studies which [illegible] s of Roth and Harker.

Finally it should be pointed out that no transitions were found in the trimer by the [illegible] were extended to the temperature of liquid oxygen.

The detailed x-ray investigation of the cyclic tetramer is now in the process of preparation. However, preliminary results indicate that there is a transition at -16°C. The x-ray data indicate that

above the transition point there is angular precession of the methyl groups similar to that proposed by Roth and Harker but that there is no precession below the transition point. Hoffman has determined the dielectric constant of the tetramer in the region of the transition point (H-2). He finds a break in the dielectric constant curve at -16.30°C, which he explains as due to a change in volume of the sample. The change in volume is in turn assumed to be caused by the onset of molecular rotation. Returning to the x-ray investigation, the preliminary studies indicate that the ring in the tetramer molecule is nearly planar. The silicon atoms are all coplanar, and the oxygen atoms are slightly above or below the plane or both. This would indicate that the Si-O-Si bond angle is somewhat less than 160°C.

The structure of the cyclic pentamer has not yet been determined. From the tentative structure of the tetramer we may assume that the various bond distances and angles will be about the same as those in the tetramer, so the ring will be more puckered. It does not necessarily follow that the silicon atoms will be coplanar.

The nuclear resonance data for the cyclic siloxanes are shown in Figures VII, VIII, and IX. The line shape derivative curves at 77°K are all very similar; within the limits of the experimental error they may be considered as identical. The spacing between the maxima is somewhat larger for the tetramer curve than for the others, and the second moment is also larger. However, this could easily be caused by a difference in the field inhomogeneity because the location of the coil in the magnet gap could not be set exactly. The second moments before and after correction for intermolecular broadening are given in Table II.

Compound			
Trimer	9.4 gauss^2	2.9 gauss	5.2 gauss^2
Tetramer	10.2 gauss^2	3.1 gauss	5.4 gauss^2
Pentamer	9.7 gauss^2	2.9 gauss	5.5 gauss^2

Table II

The corrected values of Table II are to be compared with the value 5.45 gauss^2, which is the theoretical second moment to be expected for an isolated methyl group tunneling about the C-Si bond. The agreement is surprisingly good. Furthermore, the line shape computed on the basis of such motion and using the broadening factor $\beta/\alpha = 0.80$ ($\beta = 2.95$ gauss) agrees equally well with the experimental curves, the deviations being too minute to be visible when the line shape is plotted to the scale of the figures. Thus we may confidently say that the only motion within the cyclic siloxanes at 77°K is rotation or tunneling of the methyl groups about the C-Si bonds.

The temperature dependence of the line widths obtained from these compounds is also shown in the figures. These were obtained by chilling the sample to 77°K and sweeping the oscillator frequency back and forth across the absorption line as the sample warmed up in the Dewar flask. The line width is taken to be the distance, in gauss, between the maximum and minimum of the derivative curve, in conformity with the usual practice.

Considering the pentamer first (Figure IX) we find that the line width decreases from 5.1 to 4.3 gauss between 77°K and 170°K. This can be attributed to low frequency motion of the molecule or, possibly, rotational oscillation of the methyl groups with an amplitude of perhaps 5-10 degrees. Such a conclusion is purely speculative. It is certain that some additional motion is present to cause the observed decrease in the line width, but it

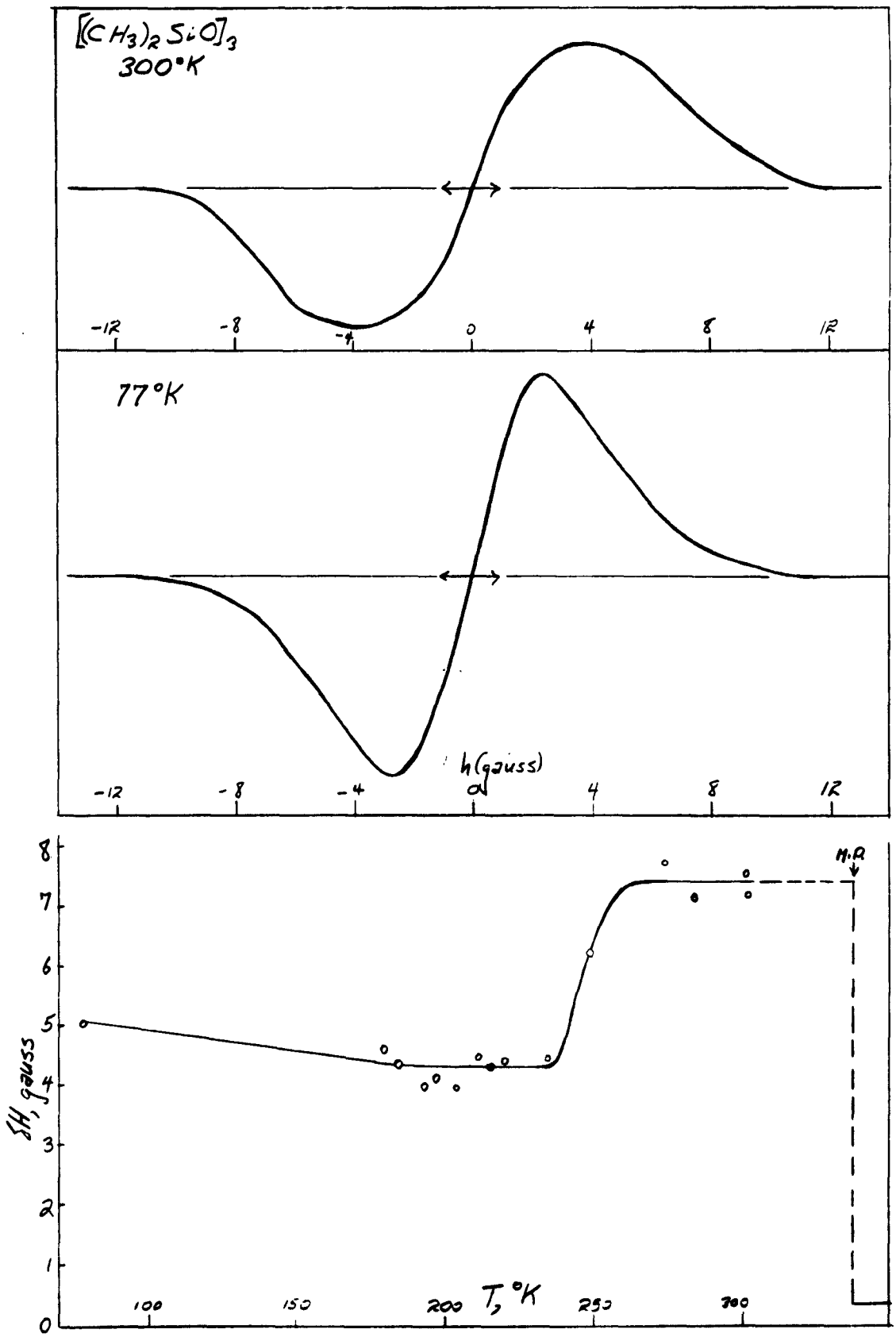

Figure VII: Line Shape Derivative Curve and Line Width vs. Temperature for Hexamethylcyclotrisiloxane.

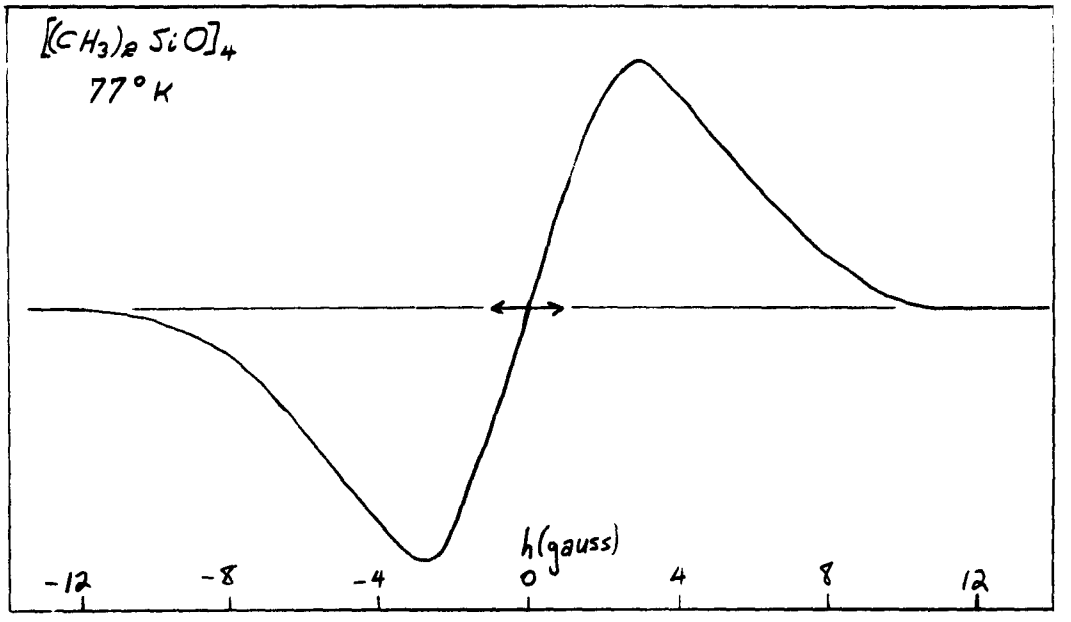

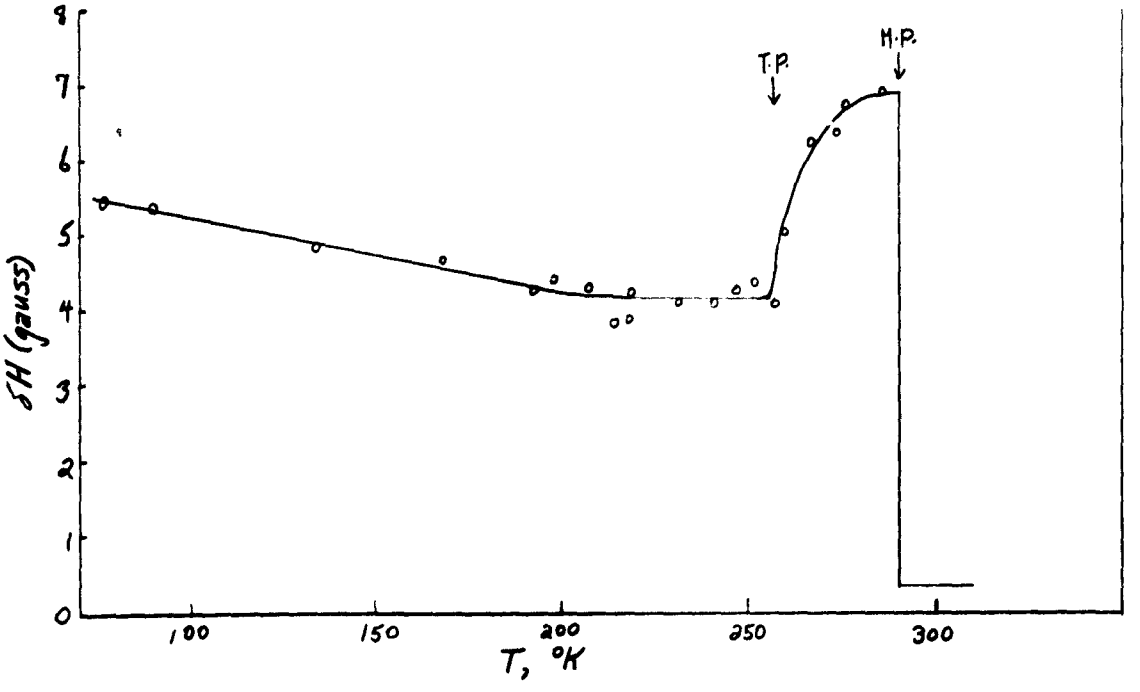

Figure VIII: Line Shape Derivative Curve and Line Width vs. Temperature for Octamethylcyclotetrasiloxane

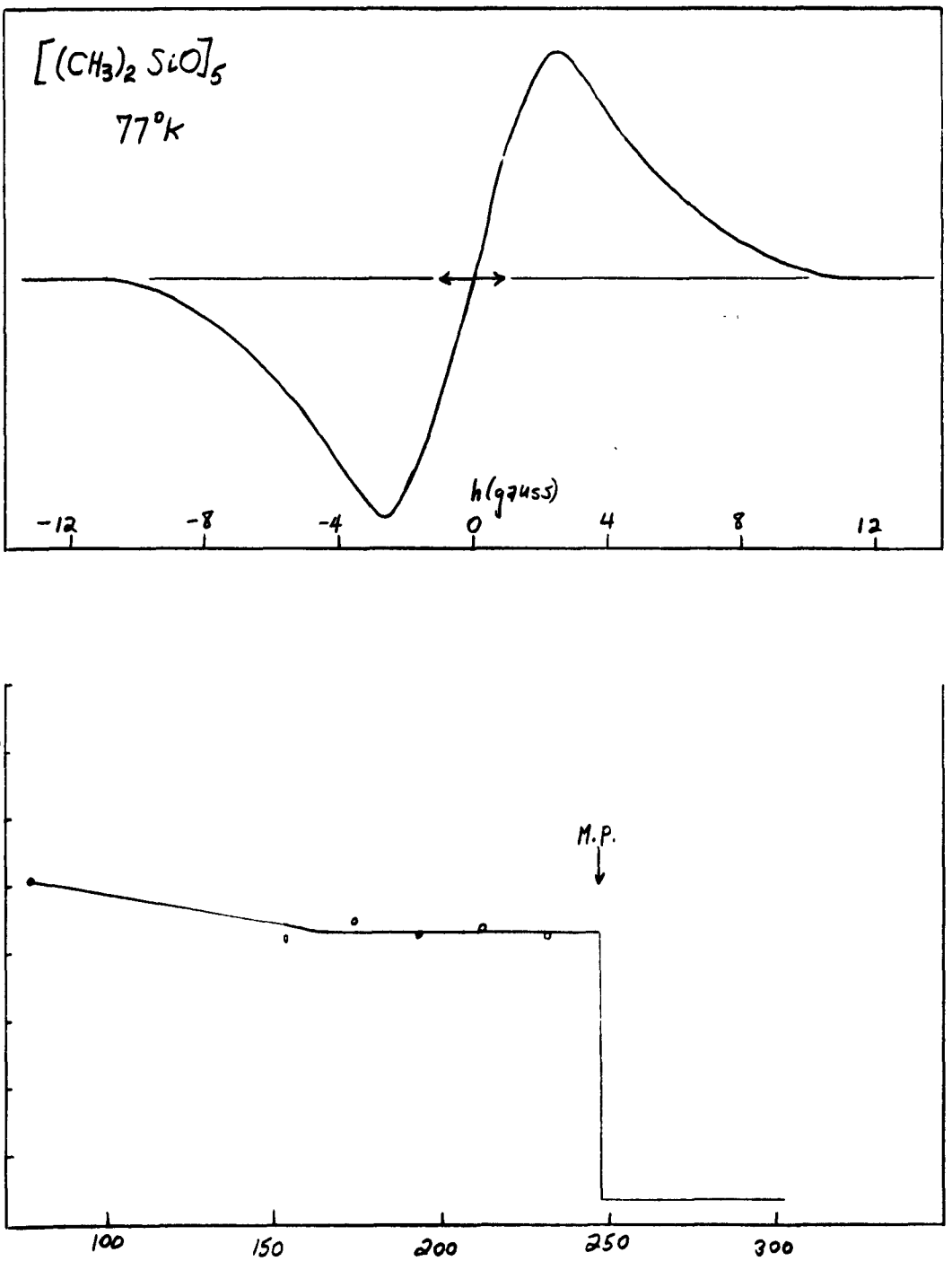

Figure IX: Line Shape Derivative Curve and Line Width vs. Temperature for Decamethylcyclopentasiloxane

is probable that such motion is at very low frequencies. From 170°K to the melting point of the compound at 247°K (-26°C) the line width apparently remains constant. At the melting point the line width decreases sharply to a value determined by the magnetic field inhomogeneity. This is quite normal behavior for a compound which is not spherically symmetrical and which thus is not likely to rotate appreciably in the solid state. On the other hand the cyclic trimer and tetramer yield temperature dependence curves which are startling, to say the least.

Below 240°K, the temperature dependence of the line widths of the trimer and tetramer samples is analogous to that of the pentamer. There is a gradual decrease in the line width between 77°K and about 200°K after which the line width remains constant over about a 40 degree range. However, the sudden increase in the line width observed in both samples is unique. There seems to be only one other case of this type reported. Alpert (A-4) has reported a similar occurrence in his investigation of hydrogen selenide, but considers that the presence of HCl as an impurity in the sample may be the cause of the anomaly. There is little possibility that impurities could be the cause in the present research. The samples had been redistilled before their use, and in the case of the trimer two different samples have been used.

The increase in line width of the cyclic tetramer occurs at about -16°C, which is also a transition temperature for this material. It must therefore be associated with the transition, and must involve either a restriction of the motion that is already present at lower temperatures or a marked increase in the intermolecular broadening. The increase in volume at the transition point which has been observed by Hoffmann seems to rule out the possibility that the interactions between the methyl groups of different tetramer molecules could be increased, so we consider that the

increase in the line width is due to some cause which is purely intramolecular.

The Roth-Harker theory offers a possible explanation of the experimental results. Let us assume that above the transition temperature of the tetramer the methyl groups swing back and forth about the Si-O bonds. They will be restricted in this motion by the methyl groups attached to the other silicon atoms in the same molecule, because any such flopping will decrease the distance between some pair of methyl groups. Thus the time average distance between the methyl groups in the same molecule will be decreased. This will tend to increase the interactions between them. Furthermore, these increased interactions might well increase the barrier to tunneling of the methyl groups about the C-Si bonds, thus restricting this motion in favor of the swinging of the methyl groups. Both effects would produce a broader line and a larger second moment.

The same explanation would apply to the cyclic trimer. The broadening is more marked for this compound because of the greater temperature range between the increase in the line width and the melting point. The line shape and second moment have been determined for the trimer at room temperature. The second moment is 12.1 gauss^2 which is considerably larger than the value determined at 77°K. No attempt has been made to fit the line shape with a theoretical curve because the computed derivative curves are too inaccurate for the large value of B/α required to be of real significance.

We have already mentioned that Peyronel found no evidence of a transition in the cyclic trimer between 77°K and room temperature. In view of the marked increase in line width commencing at 238°K (-35°C)

this is somewhat surprising. It would seem advisable to determine the heat capacity and the volume-temperature curves in this range.

F. Silicone Rubber

The line shape derivative curve and the temperature dependence of the line width for the sample of silicone rubber investigated in this research are given in Figure X. The measurements were made on a sample of SE 450 silicone rubber supplied by the General Electric Company which had been cured for 1 hour at 300°F. The line shape at 77°K is very similar to that obtained from the cyclic compounds at the same temperature and could be fit very well by assuming rotation of the methyl about the C-Si bonds, and using a broadening parameter $\sigma = 2.9$ gauss. The experimental second moment is 10.0 gauss^2 which is corrected to 5.8 gauss^2, a value consistent with the assumption made above. The temperature dependence curve differs slightly from those of the cyclic compounds at low temperatures in that there is no decrease in the line width from 77°K to 164°K. At 164°K (-109°C) there is an abrupt drop in the line width from 5.0 gauss to about 2.5 gauss, and the line width then tapers off more gradually until at 210°K it has a value which is about the same as the magnetic field inhomogeneity.

It is interesting to compare these results with the line width vs. temperature curves for natural rubber (M 4) The latter curves are shown in Figure XI. There is some variation in the temperature at which the first knee in the curve appears, this temperature increasing as the cure time of the sample increases. However, the sharp break in the curve occurs at about 220°K in all cases. This is about 60° higher than the break in the curve for silicone rubber and the line width decreases much more slowly than is the case with silicone rubber. Furthermore, the line width

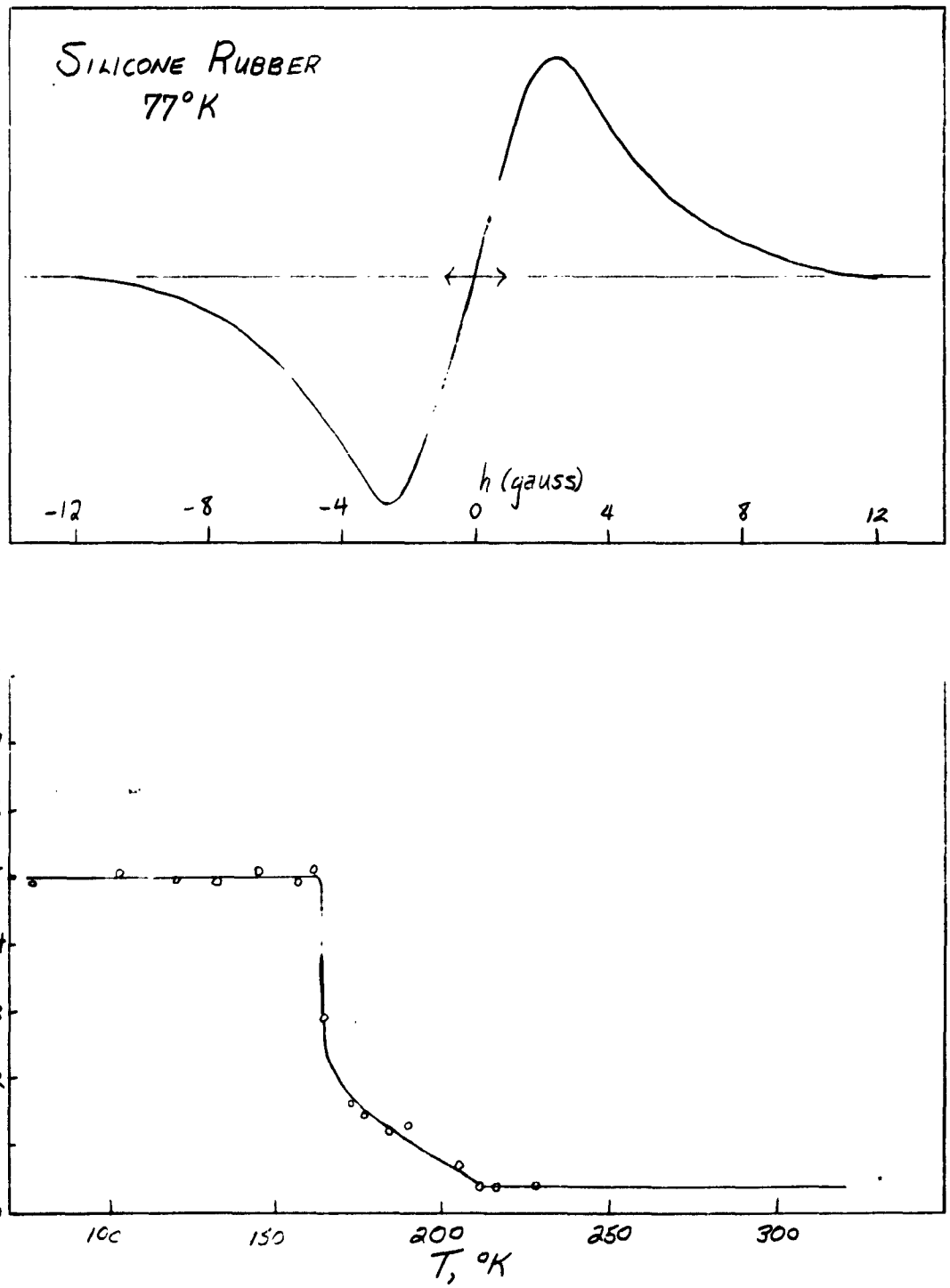

Figure X: Line Shape Derivative Curve and Line Width vs. Temperature for Silicone Rubber

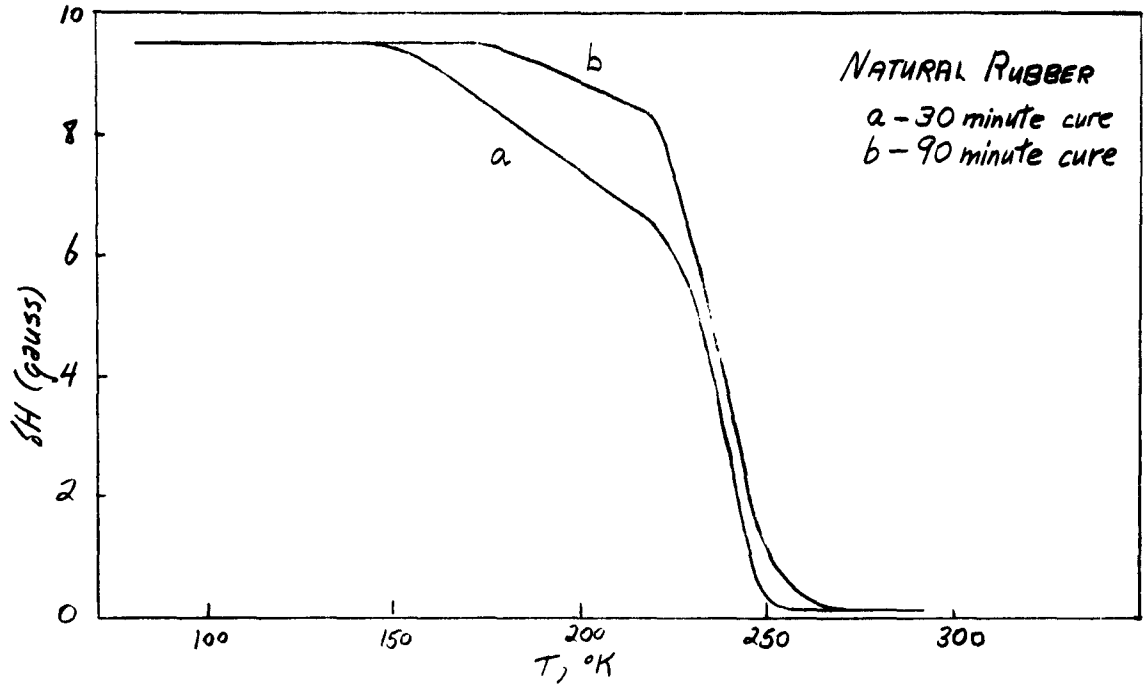

Figure XI: Line Width vs. Temperature for Natural Rubber

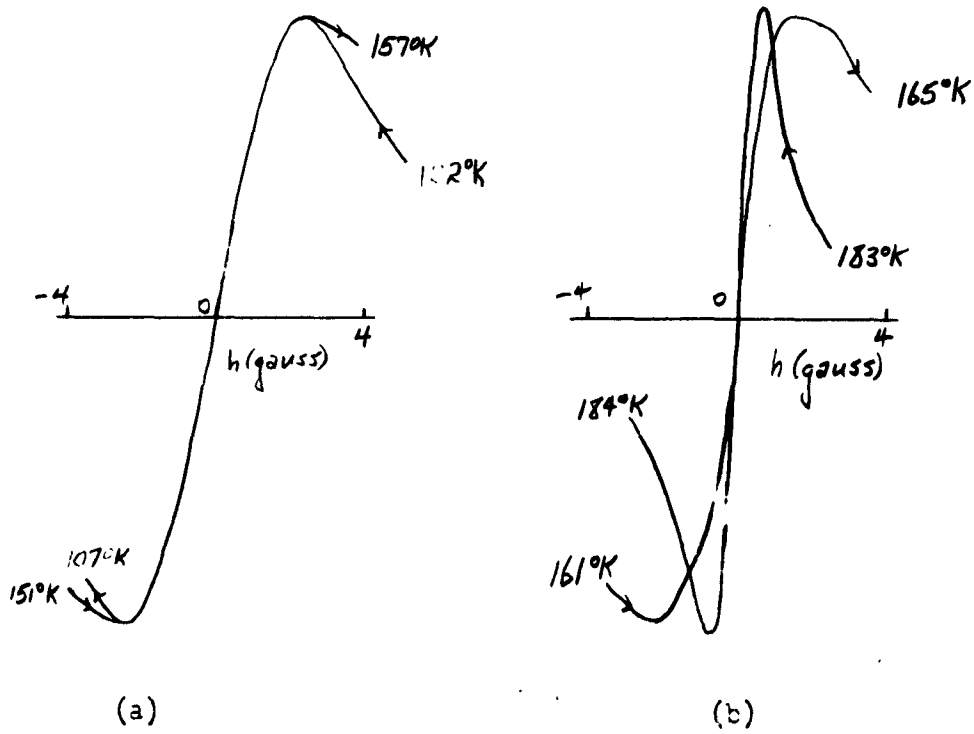

Figure XII: Line Shape Derivative Curves for Silicone Rubber at Several Temperatures.

in natural rubber has reached its rigid lattice value at temperatures of 150°K and less, whereas we have seen that the line width in silicone rubber is still narrower than the rigid lattice value at 77°K.

The segments of the derivative curve which were obtained as the sample warmed up from 77°K showed an interesting and apparently real effect, which is illustrated in Figure XII (a). The sample warmed up about 13° during the time required to sweep through enough of the line width to record the peaks of the derivative curve. The segments of each curve were then plotted as shown in the figure, the amplitude of each being adjusted to have the same peak height. It was noticed that as the temperature increases the tail of the derivative curve falls off less sharply than it does at lower temperatures. The figure shows only the lowest temperature curve and the curve obtained just below the break in the temperature dependence curve, but the other curves obtained at intermediate temperatures show the same effect in amounts which increase with increasing temperature. This indicates that there is a slight increase in the second moment of the line as the temperature increases, although the line width is not appreciably affected. The explanation of this effect would seem to be that there is some rotational oscillation of the methyl groups which, if the polymer molecules are closely packed, would increase the interactions between methyl groups on different chains. The sudden decrease in the line width would then indicate that the molecules begin to rotate freely. If this explanation is valid, we should expect to observe a change in the volume of the sample, sufficient to permit the methyl groups to rotate. Sternberg has attempted to find such a volume change by dilatometric methods, but the results have been inconclusive. No definite break was observed in plot of volume vs. time as the sample warmed. However, there were indications that the slope of the curve changes at about

168°K (-105° C). The simultaneous determination of the temperature of the sample as a function of time also showed a change in the slope of the curve at about 168°K, and this was also observed in the temperature-time curve obtained during the measurement of the temperature dependence on the line width. Both the volume-temperature, and temperature-time curves thus seem to support the explanation given, the temperature-time curve showing a more noticeable effect.

Above 164°K, the segments of the derivative curves show that there is a more gradual decrease in the line width, and at the same time the tails of the curves decrease until a very narrow line, such as is expected from liquids, is observed at 210°K. This is illustrated in Figure XII (b). The line shapes can be explained qualitatively on the basis that they are combinations of two curves, a narrow, liquid-like curve, and a broad curve similar to that observed below 164°K. This would indicate that the molecules do not commence rotating simultaneously. It is suggested that this effect may be due to the fact that there are polymer molecules of widely varying molecular weights. A determination of the temperature dependence of the line widths of a series of more homogeneous fractions should offer a test of this suggestion.

G. Summary and Suggestions

The results obtained in this research indicate there is an unusual degree of motion of the protons in organosilicon compounds, as compared to organic compounds of similar structure. At 77°K this seems to take the form of rotation or tunneling of the methyl groups about the C-Si bonds. The methylchlorosilanes and hexamethyldisiloxane also give evidence that there is also low frequency rotation of the molecule about

some other axis through the center of mass, which is probably due to the near spherical symmetry of these molecules.

We have found it necessary to assume that the methyl groups in the compounds studied have the same bond distances and angles that exist in methane. It is not possible to check the validity of this assumption from the experimental data at the temperatures obtainable with the present apparatus, because the observed motion of the methyl groups persists to the lowest obtainable temperatures. However, it should be possible to obtain detailed information concerning the configuration of the methyl groups at temperatures sufficiently low to freeze out all motion in the sample, because at such temperatures, the line shape will be determined only by the proton-proton distance. There might also be some possibility of obtaining more precise data about both the methyl group configuration and the motion of the protons if studies are made with single crystals of the sample, and at the same time to check the validity of the assumption of a Gaussian broadening function. However, the experimental difficulties involved in preparing single crystals of the substances used in this research might well prove prohibitive.

The cyclic siloxanes offer many interesting possibilities for further study. The anomalous behavior of the temperature dependence of the line widths should be examined more closely in the region where the change in width occurs. This would require the use of a cryostat so that the line width could be examined at fixed temperatures near the transition. Relaxation time studies should also prove valuable because of the dependence of the relaxation time on the motion of the nuclei. Finally the other cyclic siloxanes might well be included in any further work.

The study of single crystals of the cyclic siloxanes should cast some light on the nature of the change that takes place when the line widths increase, because of the less complex nature of the theoretical line shapes. Preparation of the samples would be difficult, but considerably simpler than in the case of the other molecules discussed. The cyclic trimer, in particular, may be prepared in the single crystal form by sublimation at room temperature (P-8).

The results of this investigation of silicone rubber must be considered in connection with the two theories concerning the nature of the siloxanes that have been discussed in the Introduction. The most important fact to be considered is the existence of considerable motion in this material at temperatures above 164°K. This motion cannot be restricted to a particular axis or plane, because of the very narrow line width obtained at higher temperatures. Such line widths imply considerable random motion such as is usually considered characteristic of the liquid state. It seems likely that in the solid rubber there is not only rotation of the methyl groups about the chain axis but also some flexing of the chain, which would imply some deformation of the Si-O-Si angles. This is quite similar to the motion postulated by Roth and Harker.

On the other hand there seems to be no necessity to assume that the coiling postulated by Pauling and Zisman actually occurs. At the same time the evidence does not exclude the possibility. Our conclusions can best be summarized by saying that it is quite possible that the coiling-uncoiling hypothesis applies to the siloxanes, but this hypothesis alone is not sufficient to explain the narrowing of the line width which has been observed.

A recent article on the structure of the polysiloxanes (F-2) contains the suggestion that the unusual properties of these materials may be explained by assuming that some of the molecules of the linear polysiloxanes are actually not linear but are composed of several large rings interlocked with each other like the links of a chain. Thus, such a polymer molecule which contains 10,000 $-[(CH_3)_2SiO]-$ units could actually be a series of 100 rings, each with 100 $-[(CH_3)_2SiO]-$ units. Such molecules would then act as plasticizers for the rest of the polymer. The present results do not give any evidence either for or against this hypothesis. However, it should be noted that according to Frisch, Martin, and Mark, the rings involved in such structures would have to contain at least twenty $-[(CH_3)_2SiO]-$ units, whereas the largest cyclic siloxane isolated thus far is the heptamer, and only trace amounts of material which could be larger cyclic compounds has ever been found in the hydrolysis mixture used in the preparation of silicone rubber gum.

Further studies of silicone rubber and other silicone polymers could take almost innumerable forms. In terms of nuclear resonance studies alone, there are many possibilities. The effect of plasticizers, time of cure, swelling by both oils and organic solvents, and vulcanization warrant investigation, as well as studies of the silicone rubber gum in toto or after fractionation into more homogeneous molecular weight ranges. Such studies have already been made on both natural and synthetic rubber (M-5).

The investigation of the temperature dependence of the relaxation time would seem to be particularly interesting, especially in the region around the break in the line width vs. temperature curve; and more refined measurements of the heat capacity and the volume as a function of temperatures are warranted.

V. BIBLIOGRAPHY

(A-1) E. R. Andrew and R. Bersohn, J. Chem. Phys. 18, 159 (1950)

(A-2) E. R. Andrew, J. Chem. Phys. 18, 607 (1950)

(A-3) Aggarwall and Bauer, J. Chem. Phys. 18, 42 (1950)

(A-4) N. L. Alpert, Phys. Rev. 75, 398 (1949)

(B-1) Bluestein, J. Am. Chem. Soc. 70, 3068 (1948)

(B-2) N. Bloembergen, "Nuclear Magnetic Relaxation", [illegible], Leiden, 1948.

(B-3) Bloembergen, Purcell, and Pound, Phys. Rev. 73, 679 (1948)

(B-4) F. Bloch, Phys. Rev. 70, 474 (1946)

(C-1) Cruft Electronics Staff, "Electronic Circuits and Tubes", p. 106, McGraw-Hill Co., New York, 1947.

(E-1) Eyring, Walter, and Kimball, "Quantum Chemistry", p. 41ff., John Wiley and Sons, New York, 1944.

(F-1) Fox, Taylor, and Zisman Ind. Eng. Chem. 39, 1401 (1947)

(F-2) Frisch, Martin, and Mark, Monatsh. Chem. 84, 250 (1953)

(G-1) H. S. Gutowsky, Thesis, Harvard, 1948.

(G-2) Gutowsky, Kistiakowsky, Pake, and Purcell, J. Chem. Phys. 17, 972 (1949)

(G-3) Gutowsky and Pake, J. Chem. Phys. 18, 162 (1950)

(H-1) G. Herzberg, "Infrared and Raman Spectra of Polyatomic Molecules", D. Van Nostrand Co., New York, 1945.

(H-2) J. D. Hoffmann J. Am. Chem. Soc., in press.

(L-1) Livingston and Brockway, J. Am. Chem. Soc. [illegible]

(M-1) Majorana, Nuovo Cimento 9, 43 (1932)

(M-2) Meyer and Gutowsky, J. Phys. Chem. 57, 481 (1953)

(M-3) Margenau and Murphy, "The Mathematics of Physics and Chemistry", p. 456, D. Van Nostrand Co., New York, 1945.

(M-4) L. Meyer, Thesis, University of Illinois, 1952.

(M-5) F. McCaffrey, Thesis, Notre Dame University, 1952.

(O-1) R. C. Osthoff, private communication, March 1953, concerning work of C. P. Smyth, Princeton University.

(O-2) R. C. Osthoff, private communication concerning lecture by I. Fankuchen, Brooklyn Polytechnic Institute.

(P-1) L. Pauling, "General Chemistry", p. 5, Freeman and Company, San Francisco, 1947.

(P-2) L. Pauling, private communications to E. G. Rochow, July 26 and Aug. 20 1951.

(P-3) G. E. Pake, Amer. J. Phys. 18 438-452 and 473-486, (1950)

(P-4) Purcell, Science 107, 431 (1948)

(P-5) Pound and Knight, Rev. Sci. Inst. 21, 219 (1950)

(P-6) G. E. Pake, J. Chem. Phys. 16, 327 (1948)

(P-7) Pake and Purcell, Phys. Rev. 74, 1184 (1948)

(P-8) G. Peyronel, "Crystal Structure of Hexamethylcyclotrisiloxane", ONR Report, Brooklyn Polytechnic Institute.

(R-1) E. G. Rochow, "Chemistry of the Silicones", chap. 7, John Wiley and Sons, New York, 1951.

(R-2) A. Roth, J. Am. Chem. Soc. 69, 474 (1947)

(R-3) Roth and Harker, Acta Cryst. 1, 34 (1948)

(R-4) N. F. Ramsey, Phys. Rev. 78, 695 (1950)

(S-1) Sommer, Mitch, and Goldberg, J. Am. Chem. Soc. 71, 2746 (1949)

(S-2) S. Seely, "Electron-Tube Circuits", Chap. 3, McGraw-Hill Co., New York, 1950

(S-3) J. C. Sternberg, private communication.

(S-4) Steinfink, Brooklyn Polytechnic Institute, report in preparation.

(V-1) J. H. Van Vleck, Phys. Rev. 74, 1168 (1948)

(W-1) G. D. Watkins, Thesis, Harvard, 1952.

(W-2) G. D. Watkins, private communication.

(W-3) J. C. Williams, private communication.

(W-4) R. L. Weber, "Temperature Measurement and Control", p. 402, The Blakiston Co., Philadelphia, 1941.